Implementation of a Fixed Bed Solid Fuel Combustor for the Purpose of Macroalgal Biomass

Co-firing Studies

By

Brian Gregory Gessler

Submitted to the graduate degree program in the Department of Mechanical Engineering and the

Graduate Faculty of the University of Kansas in partial fulfillment of the requirements for the

degree of Master of Science.

_____

Chair: Dr. Christopher Depcik

_____

Dr. Edward Peltier

_____

Dr. Ronald Dougherty

Defended: August 30th, 2017

The Thesis Committee for Brian Gessler certifies that this is the approved version of the

following thesis:

Implementation of a Fixed Bed Solid Fuel Combustor for the Purpose of Macroalgal Biomass

Co-firing Studies

By

Brian Gregory Gessler

_____

Chair: Dr. Christopher Depcik

Accepted: _____, 2017

Abstract

Coal-fired power plants represent the majority share of fossil fuel based electricity generation facilities. Due to their numerous negative environmental impacts, however, they are targeted for reduction and eventual replacement. Algal biomass is a promising third generation biofuel that could reduce coal usage through co-firing in the near future and possibly replace coal in the more distant future. Unlike another popular co-combustion biomass, woody biomass, little is known about direct algae firing and co-firing. As a result, a solid fuel combustor is created and instrumented with the intent of burning pelleted mixtures of pine, macroalgae, and coal in order to determine algae's properties as a direct firing and co-firing fuel. In keeping with this vision, a normalization study is conducted using various mixtures of pine and algae, finding that increasing algae content yielded higher exhaust temperatures with more nitrogen oxides and sulfur oxides emissions than pine. Emissions of carbon dioxide are reduced with increasing algae content, however. A normalization study is also proposed using coal-biomass fuel blends, but technical issues required that a separate accelerant study be made. It is found that 10 mL of petroleum distillate added to the fuel just before attempting ignition greatly improved the combustion characteristics of the coal-containing pellets. However, increased air flow rates from the biomass mixtures are also required to begin shifting the coal-containing mixture to thorough and complete combustion. The adjustments to the air flow rates provided to the burner prompted further modifications of the setup and the experimental procedures to ensure the safety and sustainability of the experimentation. An optimization study is also begun, yielding a simple but accurate mass burned calculator that can be used to augment and improve further experiments. Tangent to this optimization study is a flow validation study which ultimately failed in its intended goal of validating the Alicat reported air flow rates. Despite its difficulties, however,

this study provided significant insight regarding the sizing and design of the pipe diameters and

lengths employed in a Pitot-tube based system.

Acknowledgements

It is rare for work of the scope and scale as described within to be a sole venture. Throughout the course of designing and conducting the experiments that forms the basis of this work, several individuals or organizations provided support for this endeavor. First, Dr. Christopher Depcik, who provided the opportunity to study the growing field of alternative fuels and combustion, and who guided these projects and the individuals involved with a depth of knowledge, passion, and capability rare in anyone. Dr. Edward Peltier is likewise instrumental in ensuring that resources and attention needed for these projects is given. Arkan Jalal helped to ensure that our supply of fuel is always ready for testing and helped to set up and conduct numerous combustion tests. Jonathan Mattson is always free with guidance and advice and aided the operation of the experimental set up in nearly every test. The Research Experiences for Teachers program provided funding for peripherals and maintenance supplies for two summers of work, during which their teachers participated in nearly every aspect of the normalization study contained within this thesis. Wes Ellison, Charles Gabel, and Ash Shadrick all gave advice regarding the construction or modification of experimental set ups. Charles and Ash additionally helped to construct and modify the solid fuel burner used for the majority of the work while Wes loaned the lab a manometer on several occasions to aid in a flow rate validation study. Two KU alumni, Bob Apprill and Logan Coen, helped in the design, construction, and implementation of the original combustor, most of which carried over to this current work. Chenaniah Langness, a former graduate student, is instrumental during the design and early implementation period with the planning, wiring, and utilities work for the combustor. Of course, a big "thank you" should also be given to my family, especially my parents Bill and Susan, and my many brothers and my sister for all of their support and encouragement during these three years.

Last is a final acknowledgement and dedication to Dr. Val Smith, whose own research and expertise, and that of his lab, laid the groundwork for the work described within.

Tables of Contents

Contents

Table of Figures

Table of Tables

Nomenclature

° - degree (angle)

°C - degrees Celsius

°F – degrees Fahrenheit

" - inches

$/MWhr - Dollars (US) per megawatt-hour

%Algae – fuel algae content in percent by weight

%C – percent composition of carbon (by weight)

%H – percent composition of hydrogen (by weight)

%mass – percent by mass

%Misc – percent composition of inorganics, trace elements, and other materials (by weight)

%N – percent composition of nitrogen (by weight)

%O – percent composition of oxygen (by weight)

%vol - percent by volume

%wt - percent by weight

a – moles of nitrogen in one mole of fuel (mol)

A_C – cross-sectional area of the pipe at the Pitot tube measuring point (ft^2)

$A_{C,equivalent}$ – Equivalent cross-sectional area of air flow at the Pitot tube measuring point (ft^2)

atm – atmosphere (pressure unit)

b – moles of CO_2 produced via stoichiometric combustion of one mole of fuel (mol)

$C_{adjusted}$ - mass per volume content of CO_2 adjusted for ambient conditions at time = 1 sec (gm of species i per m^3 of exhaust mixture)

C_{CO_2} – mass per volume content of CO_2 at time = 1 sec (gm of CO_2 per m^3 of exhaust mixture)

$C_{CO_2,basline}$ - mass per volume content of CO_2 due to compressed air flow-through at time = 1 sec (gm of species i per m^3 of exhaust mixture)

$C_{i,adjusted}$ - mass per volume content of species i adjusted for ambient conditions (gm of species i per m^3 of exhaust mixture)

$C_{i,baseline}$ - mass per volume content of species i due to compressed air flow-through at data point j (gm of species i per m^3 of exhaust mixture)

C_i- mass per volume content of species i at data point j (gm of species i per m^3 of exhaust mixture)

c - moles of H_2O produced via stoichiometric combustion of one mole of fuel (mol)

cm^3 m^{-3} - cubic centimeters per cubic meters (alternate form of ppm for gaseous emissions)

C – carbon

CH – methylidyne radical

CHON – Carbon Hydrogen Oxygen and Nitrogen

CO - carbon monoxide

CO_2 - carbon dioxide

D – diameter of the pipe at the Pitot tube measurement point (ft)

DAQ – Data Acquisition unit

DIN - Deutsches Institut für Normung (German Institute for Standardization)

d – moles of N_2 produced via stoichiometric combustion of one mole of fuel (mol)

EHS – Environmental Health and Safety

EIA - Energy information Administration

f – mole fraction of reacting air in a combustion reaction (-)

ft - feet

ft^2 – square feet

ft^3 – cubic feet

$ft\ min^{-1}$ – feet per minute

$ft^3\ min^{-1}$ – cubic feet per minute

FTIR - Fourier Infrared Spectroscopy unit

g – mole fraction of atmospheric air reacted in a lean-regime combustion reaction (-)

GHG - greenhouse gas

gm – grams

$gm\ mol^{-1}$ – grams per mole

H_2O – water vapor

HCN – hydrogen cyanide

HHV – Higher Heating Value

H_v – heat of vaporization of water ($kJ\ kg^{-1}$)

$\bar{h}^0_{f,CO_2}$ - molar heat of formation of gaseous CO_2 ($kJ\ kmol^{-1}$)

$\bar{h}^0_{f,fuel}$ - molar heat of formation of the fuel ($kJ\ kmol^{-1}$)

$\overline{h^0_{f,i}}$ - molar heat of formation of species i ($kJ\ kmol^{-1}$)

$\bar{h}^0_{f,H_2O_g}$ - molar heat of formation of water vapor ($kJ\ kmol^{-1}$)

$\bar{h}^0_{f,O_2}$ - molar heat of formation of gaseous molecular oxygen ($kJ\ kmol^{-1}$)

$\bar{h}^0_{f,N_2}$ - molar heat of formation of gaseous molecular nitrogen ($kJ\ kmol^{-1}$)

i - current emission species of interest

j – current time step of interest (sec)

$J\ kmol^{-1}\ K^{-1}$ - Joules per mole-Kelvin

k - current data point of interest in Appendix C

K - Kelvin

kg - kilograms

kg kmol^{-1} - kilograms per kilo-mole

kg m^{-3} - kilograms per cubic meter

kg s^{-1} - kilograms per second

kJ kg^{-1} – kilo-Joules per kilogram

kJ mol^{-1} – kilo-Joules per mole

kJ kmol^{-1} - kilo-Joules per kilo-mole

kmol – kilo-moles

kPa - kilo-Pascal

KU – University of Kansas

kWh – kilowatt-hours

L - Liter

LCOE - levelized cost of electricity ($/MWhr)

LED – Light Emitting Diode

LHV – Lower Heating Value (kJ kg^{-1})

Lpm - liters per minute

m_{burned} – mass of fuel burned during a test in appendix C(kg)

m_C – mass of carbon emitted as a product of combustion during an individual test (gm)

m_C – mass of carbon in combustion reaction (Appendix C) (kg)

m_H - mass of hydrogen in combustion reaction (Appendix C) (kg)

m_N - mass of nitrogen in combustion reaction (Appendix C) (kg)

m_O - mass of oxygen in combustion reaction (Appendix C) (kg)

$m_{\text{C from CO}_2}$ – mass of carbon emitted as CO_2 in an individual test (gm)

$m_{CO_2,total}$ – mass of CO_2 emitted during an individual test (gm)

m_f – mass of fuel burned during an individual test (gm)

m_{fuel} - average mass of fuel in a fuel basket during a single test (gm)

m_i – mass of species i emitted (gm)

$\dot{m}_{air}$ – mass flow rate of air through combustor (gm s^{-1})

$\dot{m}_{CO_2}$ – mass flowrate of CO_2 at time = 1 s (gm s^{-1})

$\dot{m}_{fuel}$ – mass flow rate of fuel during combustion (kg s^{-1})

$\dot{m}_{fuel,k}$ - mass flow rate of fuel during combustion at time point k (kg s^{-1})

$\dot{m}_{fuel,k+1}$ - mass flow rate of fuel during combustion at time point $k + 1$ (kg s^{-1})

$m_{H2O,out}$ – mass of water produced through combustion (gm)

$\dot{m}_i$ - mass flow rate of species i (gm s^{-1})

$\dot{m}_{i,j}$ - mass flow rate of species i at data point j (gm s^{-1})

$\dot{m}_{i,j+1}$ - mass flow rate of species i one data point past data point j (gm s^{-1})

M_{air} - molar mass of air (kg mol^{-1})

M_C – molar mass of carbon (kg kmol^{-1})

M_{CO_2} – molar mass of CO_2 (kg kmol^{-1})

M_{fuel} – molar mass of fuel (kg kmol^{-1})

M_H – molar mass of hydrogen (kg kmol^{-1})

M_i - molar mass of species i (kg mol^{-1})

$M_{mixture}$- molar mass of the total exhaust mixture (kg mol^{-1})

M_N – molar mass of nitrogen (kg kmol^{-1})

M_O – molar mass of oxygen (kg kmol^{-1})

m - mass of gas (kg)

m^2 – square meters

m^3 - cubic meters

m^3 s^{-1} - cubic meters per second

min – minutes

MJ kg^{-1} – mega-Joules per kilogram

mL - milliliters

mm - millimeter

MWhr - megawatt-hour

n - number of moles of a gas in Eq. (8) (kmol)

n_f – number of moles of fuel (-)

$\bar{n}_i$ – mole fraction of species i

$\dot{n}_{air}$ – molar flow rate of air through the combustor (mol s^{-1})

$\dot{n}_{fuel}$ - molar flow rate of fuel during combustion (mol s^{-1})

NH_3 – ammonia

N_2 – molecular nitrogen

N_2O – Nitrous Oxide

NI – National instruments

NO – Nitric Oxide

NO_2 – Nitrogen dioxide

NO_x - nitrogen oxides

NPT – Nominal Pipe Threaded

O_2 - molecular oxygen

OH - hydroxyl

P - gas pressure (Pa)

P – Products of combustion reaction (Appendix C)

P_d – dynamic pressure of the air flow across the Pitot tube (Pa)

P_s – static flow pressure of the air flow across the Pitot tube (Pa)

P_{gas} – air pressure from outlet of Alicat flow controller (psia)

Pa – Pascals

PM – particulate matter

PPE – Personal Protective Equipment

ppm - parts per million

ppm (w) – parts per million weight basis

ppm s^{-1} – part per million per second

psi - pounds per square inch

psia - pounds per square inch, absolute

psig – pounds per square inch, gauge

PVC – polyvinyl chloride

$\overline{Q}_{HV}$ - molar heating value of the combusted fuel (kJ mol^{-1})

Q_{HHV} – higher heating value of the fuel (kJ kg^{-1})

$Q_{LHV,fuel}$ – lower heating value of the fuel (kJ kg^{-1})

$Q_{release}$ – total energy released through combustion of fuel during a single test (kJ)

R – reactants of combustion reaction (Appendix C)

$\bar{R}$ - universal gas constant (J kmol^{-1} K^{-1})

s – seconds

Sch – Schedule (system of standardized pipe wall thicknesses)

sec - seconds

sLpm - standard liters per minute

SO_x - sulfur oxides

STP - Standard Temperature and Pressure

t – time (sec)

T - gas temperature (K)

T_{gas} – air temperature from Alicat flow controller (K)

THC – Total Hydrocarbons

t_{max} – maximum time point (sec)

US – United States

USB – Universal Serial Bus

V - gas volume (m^3)

$v_{airflow}$ – flow velocity of the Alicat air flow as measured by a Pitot-static tube (m s^{-1})

$v_{airflow,Imp}$ - flow velocity of the Alicat air flow as measured by a Pitot-static tube (ft min^{-1})

$\dot{V}_{air}$ - volume flow rate of air (Lpm or m^3 s^{-1})

$\dot{V}_{Alicat,Imp.}$ – actual flow air from Alicat flow controller (ft^3 min^{-1})

$\dot{V}_{Alicat,Lpm}$ - actual flow rate of air from Alicat flow controller for Eq. (17) (Lpm)

$\dot{V}_{Lpm}$ - actual flow rate of air from Alicat flow controller (Lpm)

$\dot{V}_{measured}$ – volume flow rate of air provided by the Alicat, as measured by the Pitot tube (ft^3 min^{-1})

$\dot{V}_{sLpm}$ - normalized air flow rate (sLpm)

VDC – Voltage (Direct Current)

w_C – weight fraction of carbon in an emission species

WC – inches Water Column

x – moles of carbon per moles of a fuel (mol)

x_i – mole fraction of species i from Appendix C (-)

x_{CO} - mole fraction of CO produced via a lean combustion reaction (-)

x_{CO_2} – mole fraction of CO_2 produced via a lean combustion reaction (-)

x_{H_2O} - mole fraction of H_2O produced via a lean combustion reaction (-)

x_{N_2} - mole fraction of N_2 produced via a lean combustion reaction (-)

x_{NO} - mole fraction of NO produced via a lean combustion reaction (-)

x_{N_2O} - mole fraction of N_2O produced via a lean combustion reaction (-)

x_{NO_2} - mole fraction of NO_2 produced via a lean combustion reaction (-)

x_{O_2} - mole fraction of O_2 produced via a lean combustion reaction (-)

x_{THC} - mole fraction of THC produced via a lean combustion reaction (-)

X_{air,O_2} – mole fraction of O_2 in air (-)

X_{air,N_2} – mole fraction N_2 in air (-)

X_C – mole fraction of carbon (-)

X_H – mole fraction of hydrogen (-)

X_i – Mole fraction of species i (-)

X_N – mole fraction of nitrogen (-)

X_{N_2} – Mole fraction of molecular nitrogen (-)

X_O – mole fraction of oxygen (-)

y – moles of hydrogen per moles of a fuel (mol)

y_{algae} – total algae mass in mixture (gm)

$y_{ash,algae}$ - ash mass fraction in algae (-)

$y_{ash,mixture}$ – total estimated ash mass in the fuel mixture (gm)

$y_{ash,pine}$ – ash mass fraction in pine (-)

y_{pine} – total mass of pine in a mixture (gm)

$y_{C\ in\ CO_2}$ – weight fraction of carbon in CO_2 (-)

Y_{CO_2} – mass fraction of CO_2 (-)

Y_i - mass fraction of species i (-)

z – moles of oxygen per moles of a fuel (mol)

Δt – change in time between successive data points (sec)

π – pi, or the ratio between a circle's diameter and circumference

ρ - density of a gas (kg m^{-3})

ρ_{air} – density of air (gm m^{-3})

$\rho_{mixture}$ – density of the exhaust mixture (kg m^{-3})

φ_{CO_2} – volume fraction of CO_2 (-)

φ_i - volume fraction of species i (-)

Chapter 1 – Introduction

The United States (US) consumed an average of 11107.64 Megawatt-hours (MWhr) of electricity per day in 2016 [1]. Furthermore, recent predictions by the Energy Information Agency (EIA) indicate that annual energy consumption of the US will likely increase, potentially by as much as 12% in 2018 [1, 2]. Roughly 65% of the electricity produced per day during 2016 in the US is generated through fossil fuels sources (specifically petroleum, natural gas, and coal) with 30.5% of the total consumption attributed to coal sources [1, 2]. However, these traditional sources of energy are expected to become environmentally unfeasible to extract and use by the year 2050 [3-6]. Additionally, there are many concerns regarding the numerous harmful emissions produced by fossil fuels, especially in large scale power generation applications.

Coal powered energy generation is of particular interest in this regard because of its relatively large share among electric power sources and its respectively severe environmental impacts as compared to other fuel sources, including other fossil fuels [7-13]. The environmental concerns of using coal for power generation are well founded. Compared to other hydrocarbon-based fuels, coal tends to be rich in sulfur, silicates, and many heavy elements; e.g., mercury and arsenic [8, 10]. When burned, sulfur will produce sulfur oxides (SO_x), known greenhouse gases (GHGs), while contributing significantly to acid rain formation [14, 15]. Mercury, arsenic, uranium, and other heavy metal emissions from coal fueled boilers can additionally seep into soil and leach into nearby crops or water supplies, subsequently poisoning local ecosystems and human populations over extended periods if not controlled [8-12]. Coal ash must also be captured and properly treated, as radioactive minerals (namely thorium and uranium), several heavy elements, and multiple carcinogens tend to concentrate in the ash during combustion [9, 11]. Even coal mining provides a lengthy list of adverse environmental and health problems from

river and soil pollution and acidification to Coalworker's pneumoconiosis, also commonly known as Black Lung [7, 8].

Each of these issues presents compelling arguments for coal's eventual replacement. Contemporary arguments against coal usage, however, more prominently cite the large amount of carbon emissions formed by coal combustion as a primary concern. Like the sulfur in coal, carbon is normally emitted as an oxide, chiefly as carbon dioxide (CO_2), with carbon monoxide (CO) and hydrocarbon emissions possible in regions with lower oxygen concentrations. Both are emitted in great amounts during the combustion of any fossil fuel, but coal is a particularly prolific producer. Carbon monoxide is a colorless and odorless gas capable of causing asphyxiation in large enough concentrations. While less directly harmful to people, CO_2 is the largest contributor to global warming by virtue of the volume produced annually [14]. In specific, CO_2 emissions generated through the usage of fossil fuel combustion has been linked to a 0.66°C increase in Earth's average air temperature from 1900 to 2005 with a total temperature rise of 2°C predicted by 2050 without significant changes in energy sourcing [16]. This rise in temperature and its subsequent effects on the world's varied environments has led to significant efforts in industrialized nations to reduce and eventually eliminate fossil fuel usage in all energy sectors.

Thus, significant public attention has been given to renewable sources of energy. Among these, solar, wind, and hydroelectric initially appear to be the most attractive. However, each of these non-combustion energy sources has significant technical, logistic, or economic drawbacks [17-21]. Solar thermal power plants, for example, possess significantly higher levelized cost of electricity (LCOE) compared to other methods. This LCOE is a metric of the total cost per unit of energy for a fuel type. As a levelized (or alternatively, normalized) metric, LCOE attempts to

account for the cost of fuel, plant construction, subsidies, and other factors in order to accurately represent the total cost of electricity generation for a particular energy source. EIA predicted the LCOE of several electric plant types for 2022 (accounting for new plants with the most modern technology to be built for every plant type), calculating an average cost of 184.4 $/MWhr for solar thermal plants as compared to 52.2 $/MWhr for onshore wind power, 66.2 $/MWhr for hydroelectric energy, and a best case of 123.2 $/MWhr for coal plants with 90% carbon sequestration systems [22]. Additionally, solar, hydroelectric, and wind power sources can only produce significant amounts of electricity under certain conditions. Solar energy is obviously limited to producing electricity during daytime with clear, cloudless skies, making implementation of solar facilities in more extreme latitudes difficult. Solar thermal facilities additionally generate peak power during midday, long before peak demand occurs in the evening [20]. Wind energy has similar problems to solar in that peak electricity generation hours often do not coincide with peak demand hours [21]. Additionally, wind powered electrical generators are only efficient and effective in regions with suitable conditions [17, 21]. Hydroelectric power is also severely limited in terms of suitable locations as it requires flowing water to generate power. Installations of some hydroelectric facilities also have significant effects on the geography of the surroundings and the water flow downstream of the facilities, often with negative consequences [18, 19].

As a result, even when discussing a limited subset of renewable energy, the need for multiple sources of renewable energy is apparent. The three discussed sources would have difficulty replacing current fossil fuel power generation alone; hence, additional sources of renewable energy are needed. Preferably, these sources would also be closer in price to current fossil fuel supplies and use similar systems and technology as the fossil fuel plants. In this area,

solid biomass has been significantly considered as a potential substitute for coal in power generation facilities [5]. Biomass is renewable since it is made from biological feedstocks that can be continuously grown or produced [23, 24]. Additionally, since these biological sources affix carbon dioxide from the air to form the carbon based portions of their structures, biomasses are considered carbon neutral [24-26]. Thus, there is theoretically no cap on biomass supplies and biomass combustion will effectively not increase the concentration of carbon-based GHGs in the atmosphere. These advantages may mean total replacement of coal in solid fuel electrical power plants with biomass by 2050 [27-29]. However, currently and for the immediate future, only a portion of the coal (typically 15% but never more than 20% by thermal energy) used in solid fuel boilers will be replaced by biomass in a co-combustion set up due to economic and technical constraints [25, 26, 30].

Usage of biomass as a substitute for coal in contemporary power plants is limited in part because of the reduced availability of biomass, but also because of some performance issues related to biomass's general composition [24-26]. Biomass tends to have a higher moisture content than coal, effectively reducing its available heating value [24, 26]. Additionally, biomass has a proclivity toward higher ash content and greater alkaline content as compared to coal [24, 30]. Thus, the ash production of biomass combustion is usually similar to low grade coal, and the high alkaline content of the ash leads to ash melting [24]. Combined other trace elements commonly found in biomass, these depositions can lead to increased corrosion and other reliability issues in boiler systems that co-fire biomass and coal contrasted to those that burned purely coal, if proper measures are not taken [24, 30]. Despite this limitation, woody biomass is currently popular in Europe and the US for co-combustion with coal since it is readily available and relatively easy to store and process as compared to other biomass sources. Moreover, it can

often be added directly to a coal fuel stream for straight co-combustion; hence, simplifying the modifications necessary for industrial implementation [24-26, 31, 32]. However, the amount of woody biomass needed to replace fossil fuel power generation in its entirety is such that the world's forests would be depleted within nine years since biomass requires time to grow and replenish exploited populations [33, 34]. Thus, additional or replacement sources of solid biofuels are needed to effectively reduce the amount of coal utilized in the power generation industry.

Woody biomass is considered to be a second generation biofuel [35-37]. First generation biofuels are generally defined as liquid fuels derived from a crop plant source and are made up primarily of ethanol, biodiesels, and plant-derived oils [36, 37]. The most widely used fuels of this generation include corn-derived ethanol and biodiesels made from potential food crops. Thus, even though first generation fuel sources have typically comparable performance to traditional fossil fuel sources, they are significantly disadvantaged by their inherent fuel versus food competition [35, 36]. Additionally, these fuels are not easily adapted to the solid fuel based systems employed in coal fired power plants or in any solid fuel application due to their liquid nature.

Second generation biofuels (which include woody biomasses despite having been used all around the globe for centuries as a heating source) are a more physically diverse group of fuels than the first generation [36, 37]. The hallmark of this generation of biofuels is their source. Second generation biofuels are produced from agricultural and certain industrial wastes, as well as lignocellulosic sources [35-39]. In this manner, second generation biofuels avoid the primary downside of their first generation cousins, the food versus fuel conflict, by using resources that are inedible by humans and by farm animals. Additionally, waste-derived second generation

fuels reduce landfill and other waste build up by burning these materials; thereby, reducing the solid volume of the waste significantly [38, 39]. This positive interaction has led to the continued investigation of second generation biofuel sources as a method to simultaneously reduce significant and logistically demanding sources of waste while also replacing portions of fossil fuel demands [38, 39]. The most pressing negative issue for second generation fuels is their availability, namely, that they are dependent on the size of the industry supplying the waste or lignocellulosic material. Woody biomass is additionally limited for energy generation since it competes with or relies on pulp, lumber, and domestic heating industries for usage, although many plants do utilize waste fragments from these industries instead of raw feedstock [26, 31, 32, 40].

Third generation biofuels attempt to expand upon the success of second generation fuels (namely the avoidance of the fuel versus food competition) while also circumventing the dependency that these fuels have on other industries. For these reasons, third generation biofuel research focuses largely on algal biofuels [41, 42]. While a multibillion dollar industry relies on algae for food, cosmetics, and medicines in northeastern Asia, algae (macroalgae in particular) are significantly underutilized in the US [36, 43, 44]. Thus, there are no industries competing with the energy industry for algae utilization. Additionally, algae do not require arable land in order to develop, growing instead in any sufficiently sized and non-polluted water source [36, 45, 46]. However, this water source does not need to be potable, further removing algae from food versus fuel competition. Furthermore, algae's aquatic nature allows it to be grown in densely packed, three dimensional "clouds" that increase algae's effective biomass yield by up to 30% over terrestrial biomasses [46]. These features combined make algae an attractive option for

renewable fuel investigation, but there are several downsides that have prevented algae's immediate implementation in industry.

First and foremost of these downsides is algae's composition. All algae is rich in nitrogen, inorganics, and sulfur as compared to most terrestrial biomasses [46]. In addition, algae tends towards higher ash and silicate content contrasted to woody biomass [46]. Where woody biomasses typically have ash contents (by % weight) of 0.5% to 2%, macroalgae species regularly have ash contents above 3.5% and up to 46% [46]. As an aquatic plant species, algae also possesses an innately higher moisture content versus terrestrial biomasses. This makes it more difficult to store, process, and, combined with algae's high ash content, reduces its heating value significantly as compared to drier fuel sources (such as woody biomasses and coal) [36, 46]. Thus, there are concerns that algae will not have the energy content that can effectively replace woody biomass or coal in power generation. Moreover, there are apprehensions that the emissions generated by algal combustion will cause its usage in industry to produce undesired emissions outside of federally mandated levels.

In particular, the abundance of fuel-bound nitrogen and sulfur in some species of algae may predispose it toward producing potentially prohibitive amounts of nitrogen oxides (NO_x) and SO_x. Nitrogen oxides are highly regulated in the US as they are potent greenhouse gases while also being key precursors to smog and acid rain formation [14]. Sulfur oxides are dangerous asphyxiates and are associated with acid rain that destroys plant life and alters the pH levels of local water sources, as described previously. Thus, the potential of algae to form greater levels of these emissions is a significant concern that must be addressed and investigated. However, little examination into the co-firing of algal biomass in air has been previously

reported, creating a gap in knowledge that needs to be filled before discussion can be furthered [36, 43, 45, 46]. Specifically, macroalgae co-firing is underrepresented in literature [46].

Thus, a custom solid fuel combustor is designed and fabricated at the University of Kansas for comparing solid macroalgae to woody biomass (i.e., pine) as a fuel source, followed by further comparisons between coal/pine and coal/algae mixtures. The combustor itself is shown in Fig. 1 and can be broken into three main segments for easier description. The first is the control and sensor systems, which also includes the air flow inlet. This section includes 11 type-K thermocouples and sampling probes for an AVL Fourier Transform Spectroscopy (FTIR) unit and an AVL Smoke Meter. The final piece of instrumentation is an Alicat MCR-500sLpm mass flow controller that both regulates and reports the air flow to the combustor's fuel bed. The
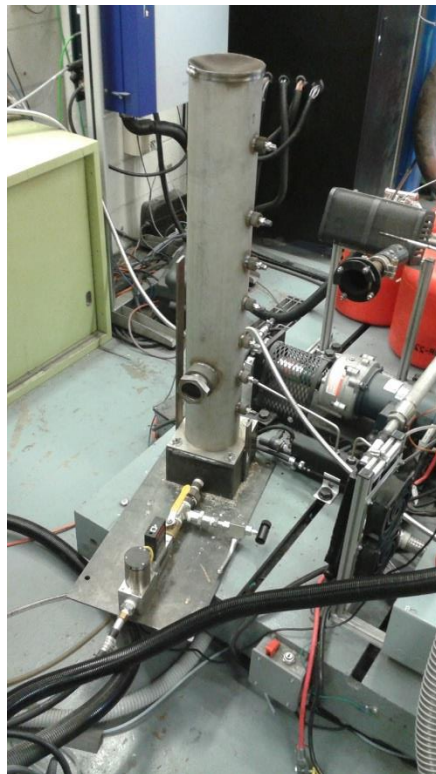
Figure 1 The fixed bed solid fuel combustor and flow controller without its wire harness.

flow controller can be seen near the bottom of Fig. 1 where it rests on the combustor base and connects into the bottom of the combustor. Data are collected from the instruments by multiple LabVIEW programs created in-house along with AVL's own Smoke Meter collection and control software. The LabVIEW program responsible for collecting thermocouple and flow meter data also controls the flow rate supplied by the Alicat flow controller via a National Instruments NI-9265 control module in a NI CompactDAQ chassis. AVL's own proprietary software is responsible for controlling the FTIR collection and cleaning routines. The air flow is supplied to the flow controller by a 95 psi compressed air line from the building's compressed air supply system and is sent into the next major section of the burner via a series of threaded pipe connections, as seen in Fig. 1. These connections include a globe value for completely choking flow in the event of an emergency, and also a tee that connects the compressed air line to a second gate valve and a tank of compressed CO_2. During an emergency in which stopping combustion is required, the air flow is first cut off with the first globe valve. Then, the CO_2 tank is tapped and its connecting globe valve is opened, allowing CO_2 to flow into the combustor, starving combustion reactions of oxygen and stifling the oxidation event.

These combustion reactions occur in the fuel bed, which is constructed of Type 304 stainless steel. The fuel bed forms the top half of the second major section of the combustor: the combustor base. Air from the flow control enters the base at the plenum. A rectangular box made of mild carbon steel, the plenum is a space for the turbulent, relatively high pressure flow from the Alicat flow meter to normalize at a pressure closer to atmospheric conditions before reaching the combustion bed. The plenum also includes integral threaded bolts that fit though matching holes drilled into the base of the combustion bed, allowing ishers and nuts to secure the bed to the rest of the base. Other features of the base include a plate on the bottom of the plenum to

hold the flow controller off the ground and a wire mesh separator between the plenum and the fuel bed to prevent ash and other small material from falling into the plenum chamber. As previously stated, combustion occurs in the fuel bed, and the hot gases produced by this process are carried upward by the air flow into the final section: the combustor tube.

Fabricated from type 304 stainless steel, the combustor tube prevents potentially harmful combustion emissions from leaking into the test cell before being siphoned off by the cell's exhaust system. This tube also provides several compression fitting mounting points for the thermocouples and AVL sampling probes mentioned previously. The combustor tube rests in grooves machined into the base plate of the fuel bed and is secured by a glow plug, which threads into a nut welded on the side of the fuel bed. The nut is concentric with a drilled hole, allowing the glow plug to penetrate into the fuel bed and double as the ignition source of the combustor. A layered mesh cap is secured to the top of the combustor tube to prevent hot sparks and embers from being carried into the exhaust system where they may be able to ignite the system's liner. The combustor setup and the experimental procedures used with the setup are described in further detail in later sections of this work. In particular, copies of the official experimental procedure documents are included in Appendix A.

Initial experiments involving the solid fuel combustor revealed potential inaccuracies in the Alicat flow controller and its associated control software. Thus, as described in Chapter 2, a Pitot tube flow validation set up is constructed and utilized to measure the flow from the Alicat flow controller. This setup begins with the Alicat flow controller threaded into a series of gradually widening tubes. At the end of these tubes is a Dwyer Model 160-8 Pitot-static tube, which connects with a Dwyer Series 477 manometer. The manometer reads the differential flow pressure produced by the flow controller, and further calculations allow conversion of this

pressure reading to a volumetric flow rate. Comparison between the calculated manometer flow rates and the Alicat reported flow rates is located in Chapter 2.

At this point, the instrumentation and procedures of the combustor allow for the accurate collection of a multiple gaseous emission species in addition to particulates, exhaust temperatures, and flow measurements. In Chapter 3, these various measurements are used first to normalize the combustion rates between a pure white pine fuel mixture and two mixtures of white pine and algae. This analysis involves using multiple carbon emission measurements and MATLAB programs to calculate the total combustion times and total energy release during the combustion of the pelletized fuel mixture. The peaks of the total carbon curves, as well as the combustion times and the energy released, are compared to establish the air flow rates necessary to normalize the pine/algae fuel mixtures to a baseline pure pine test. From there, normalized emissions data for similar pine and algae blends are then used to compare the combustion characteristics and emissions produced by the pine and macroalgae used. Conclusions regarding the combustion characteristics and products of algae as compared to pine are then presented.

Chapter 4 repeats the analysis process, elucidated and exemplified in Chapter 3, using coal and biomass mixtures instead of pure pine and pine/algae fuels. Pine and coal are significantly different both chemically and physically. As can be seen in Chapter 3, these differences dramatically influence the combustion properties of the pelleted fuels. Thus, it is important that tests with coal/pine and coal/algae mixtures be conducted to uncover the influences of coal's physical and chemical. However, during early phases of the normalization process for coal fuel blends, it is discovered that the glow plug ignition system used in the experimental setup is insufficient to reliably achieve light-off. Thus, an additional study is conducted to determine the amount of accelerant needed to reliably achieve the start of

combustion. After the accelerant study results are presented at the end of Chapter 4, just before concluding remarks.

Finally, Chapter 5 presents a summary of the results found in Chapter 2 through Chapter 4 in addition to conclusions drawn from these results. These points are not made in detail (that is left to the more detailed descriptions in the individual chapters) but rather serves as a relatively brief, high-level summary of the major information and talking points presented earlier in the thesis. This chapter additionally includes planned and suggested paths for future investigation into algal biomass co-combustion and related topics.

Chapter 2 - Analysis procedure for co-combustion optimization and air flow rate validation study

2.1 Abstract

Combustion optimization is a process often performed in order to improve the completeness of a particular fuel's combustion in a given set up. Thus, it is desirable to determine a method to optimize the combustion of the numerous fuel blends proposed for testing in the solid fuel combustor setup so that each blend can be compared under its most ideal conditions. To that end, a method based on measuring the mass burned during a combustion test is proposed as a first step in an optimization procedure for the solid fuel combustor. Initial difficulties in creating the model for this process prompts an additional flow rate validation study for the Alicat flow controller. This study utilizes the proven combination of a Pitot-static tube and manometer setup but also presents its own technical difficulties. In the end, the issues surrounding the mass burned calculator are resolved, resulting in a simple and fast method of accurate mass burned estimation, regardless of the fuel blend used. The technical problems of the flow validation setup prohibited accurate results from being obtained with the setup itself. However, the Alicat reported flow rates are found to be accurate utilizing an alternate method that did not depend on the flow validation setup. Although the validation set up proved ultimately unable to accurate measure the flow from the Alicat flow meter, its design, construction, and modification resulted in a significant amount of knowledge regarding the implementation of Pitot-style tubes in flow validation capacities is learned.

2.2 Introduction

Optimization is a nebulous term, defined by Merriam-Webster as "an act, process, or methodology of making something (such as a design, system, or decision) as fully perfect,

functional, or effective as possible or as the mathematical procedures (such as finding the maximum of a function) involved in this [process]" [47]. Thus, it is important to determine what effectiveness means for a design or process, and what criteria can be used to determine the level of effectiveness. For solid fuel combustion, the effectiveness of this system is determined primarily by the completeness of combustion; i.e., the amount of fuel reacted to form stoichiometric products [48-50]. In specific, having a greater level of complete combustion typically results in a larger energy release and higher overall efficiencies [48-50]. In comparison to optimization, normalized combustion of the various biomass and coal/biomass fuel mixtures, as seen in Chapters 3 and 4, is useful in comparing the combustion characteristics of each mixture. However, it is equally important that each mixture's combustion should also be optimized in order to determine its best possible performance and the practicality of achieving this performance.

The optimization tests presented in this Chapter can be performed using the same experimental set up as the normalization tests in Chapters 3 and 4. The combustor used in these tests is a fixed bed design (as described in detail in Chapter 1 and 3) made largely from 304 stainless steel and mild carbon steel with attachment points for an air flow controller, several thermocouples, an AVL Smoke Meter probe, and an AVL Fourier Transform Infrared Spectroscopy (FTIR) probe. Since the optimization definition for solid fuel combustion relies on a known chemical Equation formulation, it is logical that an optimization process can be formed around this chemical expression along with the fuel composition data collected from high temperature combustion studies and the emissions data measured by the FTIR during combustion tests. In practice, this concept proved to be initially difficult to implement. These difficulties are revealed later to simply be calculation errors made early in the model that significantly affected

the final result. The original hypothesis, however, is that there are errors in the control and reporting systems of the Alicat air flow controller that caused the reported flow rates to be incorrect.

Because of this, a flow rate validation study is proposed. It are noted that flow rate validation is still a good practice, particularly in a system as dependent on oxygen content and mixing as the combustion set up. This validation study involved the construction of a new experimental setup that would connect directly to the Alicat flow controller. Air from the controller would enter this setup, a series of in-line tubes with expanding diameters plus adapters to fit them together, into a Pitot-static tube. Pitot-static tubes have been used for decades to measure the flow rate in ducts and similar systems via the pressure difference between flow kinetic pressure and flow static pressure [51-53]. Additionally, Pitot-tubes are relatively simple to use, requiring only proper alignment and an appropriate manometer to function [51-53].

Hence, the focus of this Chapter involves presenting the logic, methods, and results of both the attempted optimization study and the flow validation study while extrapolating conclusions from these results. First, the logic and methods used in the attempted optimization inquiry are presented in detail followed by the experimental setup and procedure used for the flow validation analysis. Afterwards, the results of the optimization study are presented and discussed, with emphasis on why the results are seen as inaccurate. The results of the flow validation study are then presented and discussed before the major points of this Chapter are summarized and future work is described.

2.3 Methods
2.3.1 Combustion Optimization

The optimization process begins with the emission data gathered from the AVL FTIR. These data are in terms of parts per million (ppm) with the exception of molecular oxygen (O_2), which is in volume percentage (%vol). Both ppm and %vol (in the case of the FTIR's data collections) are variants of volume fractions, with ppm being Equivalent to $cm^3\,m^{-3}$ and %vol simply being the volume fraction multiplied by one hundred. Thus, both types of emission data are first converted to volume fractions via Eqs (1) and (2) for ppm and %vol measurements, respectively:

$$\varphi_i = \text{ppm}_i \left(\frac{m^3}{(10^2)^3 cm^3} \right) = \frac{cm^3}{m^3} \left(\frac{m^3}{(10^2)^3 cm^3} \right) = \frac{m^3 \text{ of species } i}{m^3 \text{ of mixture}} \qquad (1)$$

$$\varphi_i = \frac{\%vol}{100} \qquad (2)$$

where φ_i is the volume fraction (which will be considered to be in terms m^3 of emission species per m^3 of the total mixture) of emission species i. Because all of the emission species can be considered ideal gases, these volume fractions can then be directly converted to mole fractions (kmol of species i per kmol of total mixture) with a conversion factor of one. The mass fraction of these species can then be found through these mole fractions via:

$$Y_i = \varphi_i \frac{M_i}{M_{mixture}} \qquad (3)$$

with Y_i representing the mass fraction of species i in kg of species i per kg of mixture, M_i is the molar mass of species i in kg $kmol^{-1}$, and $M_{mixture}$ is the molar mass of the total mixture in kg $kmol^{-1}$. The value of $M_{mixture}$ changes at each time point since it depends on the instantaneous composition of the mixture:

$$M_{mixture} = \sum X_i M_i \qquad (4)$$

where X_i is the mole fraction of species i and M_i is the molar mass of species i in kg $kmol^{-1}$. In order to use Eq. (4) accurately requires that the mole fraction of molecular nitrogen be known at each data point. This value is not directly measured by the FTIR but can be calculated through the unity condition for the sum of mole fractions in a mixture:

$$\sum X_i = 1 \qquad (5)$$

Solving Eq. (5) for the mole fraction of N_2 yields:

$$X_{N_2} = 1 - \sum X_{i \neq N_2} \tag{6}$$

where $X_{i \neq N_2}$ represent mole fractions for emission species that are not N_2, in kg kmol^{-1}. Solving Eq. (4) at each time step allows for Eq. (3) to be solved for the mass fraction of each emission species at every time point.

Combining the mass fraction of a species with the density of the overall mixture produces a mass content per volume of mixture via:

$$C_i = Y_i \rho \tag{7}$$

with C_i as the content of species i (in kg of species i per m^3 of total mixture) and ρ representing the density of the mixture at the FTIR sample line temperature and pressure. For reference, the FTIR sampling lines are kept at a steady temperature of 191°C and pressure of 86 kPa. Gas density is found using the ideal gas law, normally written as:

$$PV = n\bar{R}T \tag{8}$$

where P is the FTIR sample line gas pressure in Pa, V is the gas volume in m^3, n is the number of moles of gas present in kmol, $\bar{R}$ is the universal gas constant in J kmol^{-1}K^{-1}, and T is the FTIR sample line gas temperature in K. The volume is then written in terms of mass and density:

$$V = \frac{m}{\rho} \tag{9}$$

so that Eq. (9) can be substituted into Eq. (8), and the resulting equation rearranged to form:

$$P = \rho \frac{n\bar{R}T}{m} \tag{10}$$

Since neither the mass nor the moles of any of the emission species are known at this step, it is convenient to combine them into a molar mass term, M (in terms of kg kmol^{-1}), which can be readily found or determined for any of the exhaust stream components. Substituting Eq. (4) into Eq. (10) and isolating the density term finds:

$$\rho = \frac{PM_{mixture}}{\bar{R}T} \tag{11}$$

which allows the density of the mixture to be found. These densities are then used in Eq. (7) to solve for the mass per volume content of each species in the overall mixture at each time step.

Before further conversions are made on the mass per volume content of each species, these values should first be adjusted to account for the content due the compressed atmospheric air flow from the Alicat flow controller. This baseline content for each species is calculated as the arithmetic mean of the first thirty-five data points for that species:

$$C_{i,baseline} = \frac{\sum_{j=1}^{35} C_{i,j}}{35} \tag{12}$$

where j is an integer denoting the data point being reference at the current step in the summation and $C_{i,j}$ is the instantaneous mass per volume of emission species i at data point j. The first thirty-five data points are used for this estimate since they occur while the glow plug is still heating the fuel. Thus, the content measurements at these times are entirely due to compressed air flowing through the combustor. Note that if the result of Eq. (12) is negative, it is replaced with a baseline value of 0 kg m^{-3}. Adjusted contents for all emission species at all times are then calculated by subtracting corresponding $C_{i,baseline}$ from the calculated total content at every time point. Before continuing, the adjusted content values are checked for negative values similar to the baseline values mentioned. Any negative values are replaced with zeros during this step.

With the content of every species determined via Eq. (7), the next step is to convert this measurement to a mass flow rate of each species. To accomplish this, the volumetric flow rate of the overall exhaust mixture is required. As a simplification, it is assumed that the volume flow rate of the combustion products is significantly less than the volume flow rate of the air provided by the Alicat flow meter. Thus, the exhaust volume flow rate can be approximated by the air flow rate provided by the Alicat. The mass flow rate of each emission species can then be calculated via:

$$\dot{m}_i = C_{i,adjusted}\dot{V}_{air} \tag{13}$$

where $\dot{m}_i$ is the mass flow rate of emission species i in kg s^{-1}, $C_{i,adjusted}$ is the adjusted content value for species i in kg m^{-3}, and $\dot{V}_{air}$ is the volume flow rate of air supplied by the Alicat flow controller in m^3 s^{-1}.

The air volume flow rate must be converted from the standard liters per minute (sLpm) unit reported by the Alicat flow controller. This flow rate description normalizes the actual flow rate from the controller to standard temperature and pressure (STP) conditions using the expression:

$$\dot{V}_{sLpm} = \dot{V}_{Lpm}\left(\frac{294.26\ K}{T_{gas}}\right)\left(\frac{P_{gas}}{14.696\ psia}\right) \tag{14}$$

with the sLpm measurement represented by $\dot{V}_{sLpm}$, the actual liters per minute (Lpm) measurement given by $\dot{V}_{Lpm}$, and T_{gas} and P_{gas} representing the flow temperature in K and flow pressure in psia, respectively.

Thus, by rewriting Eq. (14) as:

$$\dot{V}_{Lpm} = \dot{V}_{sLpm}\left(\frac{T_{gas}}{294.26\ K}\right)\left(\frac{14.696\ psia}{P_{gas}}\right) \tag{15}$$

the actual volume flow rate of air in Lpm can be determined at any time step. Since the air flow rate is held constant during individual tests, all $\dot{V}$ variables can be treated as constants during this calculation procedure. The Lpm flow rate can be converted into the needed $m^3\,s^{-1}$ flow rate via the conversion:

$$\dot{V}_{air} = \dot{V}_{Lpm}\left(\frac{10^3\ m^3}{1\ L}\right)\left(\frac{1\ min}{60\ s}\right) \tag{16}$$

Solving Eq. (16) for the steady air flow rate and Eq. (7) for every emission species' content at every time point then allows for Eq. (13) to be solved for the mass flow rate due to fuel combustion of every species at every time point.

From this point, the total mass emission of each species can be found by integrating the mass flow rates over all time points. Since the emissions data are presented as individual data points and not a single Equation, this integration can be estimated using the trapezoidal rule:

$$m_i = \int_0^{t_{max}} \dot{m}_i dt \cong \sum_{n=0}^{t_{max}-1} \frac{1}{2}\left(\dot{m}_{i,n} + \dot{m}_{i,n+1}\right)\Delta t \tag{17}$$

where t_{max} is the final data point time in seconds, $\dot{m}_i$ is the adjusted mass flow rate of species i, n is the current time step, $\dot{m}_{i,n}$ and $\dot{m}_{i,n+1}$ are the adjusted mass flow rates for species i at the current and former time step, respectively, and Δt is the size of the time step in seconds. The result of Eq. (17) is then the total mass emission of species i, m_i, in kg which is converted into grams.

Once the total mass emission of all emission species are found, the weight fractions of carbon for each of the carbon containing emission species can be applied to the results from Eq. (17). This determines the amount of carbon emitted as a result of combustion. Using the fuel mass fraction composition data found in Chapter 3, the total carbon mass emission is then used to calculate the total mass of fuel burned via:

$$m_f = \frac{m_C}{w_{C,f}}$$
(18)

where m_f is the mass of fuel burned in gm, $w_{C,f}$ is the fuel's carbon mass fraction, and m_C is the mass of carbon emitted in gm as determined from the preceding process. Note that a sample calculation for the entire process outlined in this section can be found in Appendix B. The result of Eq. (18) is expected to be less than the measured total mass of the fuel placed in the combustion bed, as some of this mass is expected to be converted to ash or other particulates which would not be measured by the FTIR. The original results of this study produced m_f results that are inaccurate. Eventually, the error in logic causing the inaccuracies is uncovered, resulting in the findings discussed in the Results section.

Originally, however, it is reasoned that the most likely source of major error is the Alicat flow controller. The other major piece of measuring equipment, the FTIR, is a proven suite of instrumentation that had been in use for years and is properly calibrated before all. Therefore, if one of the inputs to the fuel burned model are incorrect, it is most likely the Alicat. Thus, a flow validation study is proposed to manually ascertain and check several parameters leaving the Alicat flow meter. Several potential errors in the assumptions regarding the flow temperature and pressure are found and corrected, improving the accuracy of the results. Not all discrepancies in the model's results are eliminated after the corrections, although the remaining discrepancies are less significant in terms of magnitude. Additionally, it is not possible to eliminate all sources of error in this model. In particular, the trapezoidal estimation process for the mass flow rate integral, although necessary for the model to function, is not exact. Thus, the value of this integral will never be completely accurate and so neither will the model's final result.

Additionally, despite the FTIR is not perfectly accurate, despite the numerous procedures and systems in place to prevent statistically significant inaccuracies. This is best visualized by noting the negative emission measurement values recorded in a data file from the FTIR emissions program. Logically, either an emission species will be present (producing a positive number in the measurement) or it will be absent, recording a zero value for that measurement. Thus, a negative emission value is logically impossible. Even if such negative values are removed from data sets before an analysis, the influence of the inaccuracies that produced them cannot be entirely removed. Despite these issues, the results of the final study show that the model is still relatively accurate and certainly useful even if its inaccuracies cannot be fully corrected.

2.3.2 Flow Rate Validation

The flow rate validation experimental set up is pictured in Fig. 2. It consists primarily of the Alicat MCR-500sLpm flow controller and several PVC pipes that increase in diameter from ¾" Schedule 40 near the flow controller to 3" Schedule 40 at the opposite end. The ¾" PVC is
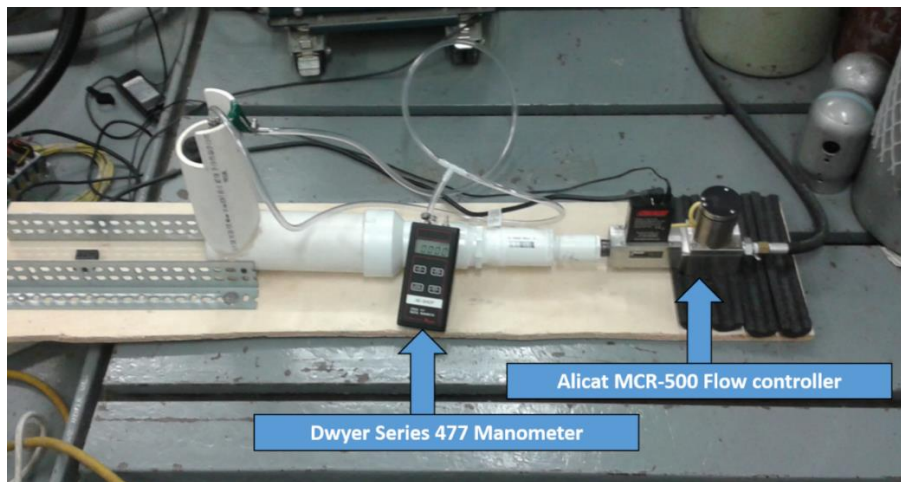
Figure 2 The flow rate validation experimental set up with the Alicat flow meter and Dwyer manometer attached.

connected to the Alicat via a threaded ¾ in Nominal Pipe Thread (NPT) steel pipe nipple of the

same size, and PVC adapters are used to connect the individual pipes sections as they increase in

diameter. The adapters and pipe sections are secured to each other with hot melt adhesive and the

connections are further covered with pipe sealing tape to ensure that no air flow escapes via a

gap in the connections. The end of the 3" diameter section is covered by a Plexiglas plate that

Figure 3 The Plexiglas restrictor plate attached to the end of the flow validation set up.

Figure 4 Clear plastic tubing attached to a tee. The top two tubes attach to the static and total pressure ports of the Pitot-static tube while the bottom tube sends this combined reading to the Dwyer manometer.

has five ¼" diameter holes punched in it, as seen in Fig. 3. This plate acts a flow choke,

providing back pressure to the set up to increase the measurability of the flow, since it is found

that there is too little pressure to produce results without the plate.

The pipe section attached to the top of the 3" pipe section is designed to hold a Dwyer

Model 160-8 5/16" Pitot-static tube in position and properly aligned at an insertion point 1.5"

upstream of the Plexiglas plate in the 3" pipe section. Dynamic and static pressure ports in the

Pitot-static tube connect to a Dwyer Series 477 1 in WC manometer. Note that Pitot-static tubes

normally connect with the dynamic flow pressure port going to the high pressure side of a

manometer while the static flow pressure port goes to the low pressure side of the manometer.

However, as seen in Figs. 2 and 4, the current design sends the flow from the two Pitot tube ports

to a tee before the combined flow is sent to the high pressure side of the manometer while the

low pressure port of the manometer remains open to the atmosphere. The back pressure in the set

up is over 14.696 psia (1 atm), but tee style connection allows the manometer to read the

pressure difference in psig. This setup therefore averts the need for a manometer with a 400 in

WC range or greater, which would be far more expensive than the 1 in WC manometer.

The Alicat flow controller is set up and controlled in largely the same manner as during

the normalization studies. A National Instruments CompactDAQ chassis still holds the NI 9625

control module that interfaces with the flow controller. Commands from the in-house LabVIEW

program used during combustion tests to control and monitor the Alicat are relayed to the DAQ

and into the flow controller via a USB connection from the DAQ to a laptop loaded with the

LabVIEW program. The major differences from the combustion tests are that the thermocouples

are not used in this study, so their readings in the LabVIEW program are ignored, and the Alicat

itself connects to the PVC pipes as described above rather than feeding into metal piping to the plenum as described for combustion testing in Chapter 1.

The flow validation procedure begins by first connecting the various components of the set up together, as described above and as shown in Fig. 1. The 12VDC power supply that powers the CompactDAQ and the power supply for the Alicat flow controller are then powered on by connecting a surge protector protecting both supplies to a wall outlet in the test cell. A laptop loaded with the LabVIEW control program is also activated and the LabVIEW program started. The 1 in WC manometer is then turned on and zeroed to ensure accurate readings. The LabVIEW program is used to turn the flow controller on and send through a moderate amount of flow (100 to 150 sLpm). At this time, the setup is scrutinized for leaks along the length of the tube by listening for sounds other than air flowing through the restrictor plate and by placing a hand near each seam in the piping to feel for escaping air. If leaks are found, they are patched with pipe sealing tape or a similar material. Once the setup is no longer leaking, the flow is stopped and the manometer is re-zeroed.

Next, the LabVIEW program is used to adjust the flow setting on the Alicat from 50 sLpm to 350 sLpm in increments of 20 sLpm. At each setting, roughly 8 seconds is allowed to pass for the Alicat to adjust to the setting and for the manometer to reach a steady reading. That reading is then recorded, and the Alicat flow setting adjusted to the next desired mark through the LabVIEW control program. Once values for 50 sLpm through 350 sLpm have been recorded, the Alicat is set to 0 sLpm flow and the manometer is re-zeroed. The described flow rate sweep is then repeated two more times (re-zeroing the manometer between these sweeps) so that every flow setting from 50 sLpm to 350 sLpm has three associated manometer readings.

The manometer readings are then averaged for each flow setting using an arithmetic mean. This averaged pressure differential will function as a single reading for the calculations needed to compare the measured volumetric flow rate from the Pitot-static tube to the set flow rate from the Alicat controller. Reported sLpm flow rates form the Alicat flow controller are converted into Lpm readings using Eq. (13) above and then to ft^3 min^{-1} readings using:

$$\dot{V}_{Alicat,Imp.} = \dot{V}_{Alicat,Lpm} \left(\frac{0.0353147 \text{ ft}^3}{\text{L}} \right) \tag{19}$$

In Eq. (19), $\dot{V}_{Alicat,Imp.}$ is the volumetric flow rate set on the Alicat controller in ft^3 min^{-1}, and $\dot{V}_{Alicat,Lpm}$ is the Lpm flow rate of the Alicat as found using Eq. (15).

The Pitot tube and manometer setup outputs the pressure differential between the flow static and dynamic pressures in kPa. This pressure differential is then converted into a flow velocity using:

$$v_{airflow} = \sqrt{\frac{2(P_d - P_s)}{\rho}} \tag{20}$$

where $v_{airflow}$ is the air flow velocity in m s^{-1}, P_d is the dynamic pressure in Pa, P_s is the static pressure in Pa, and ρ is the density of the air in kg m^{-3}. Similar to the set flow rate, the result of Eq. (20) are converted to ft min^{-1} for easier calculations in future steps and for easier comparison. This conversion is simply:

$$v_{airflow,Imp} = v_{airflow} \times \frac{3.28084 \text{ ft}}{\text{m}} \times \frac{60 \text{ s}}{\text{min}} \tag{21}$$

resulting in $v_{airflow,Imp}$, or the flow velocity in terms of ft min^{-1}.

Determining the volumetric air flow rate as measured by the Pitot-static tube requires that the cross-sectional area of the setup at the point of measurement is known. The Pitot-static tube is set in a 3" Schedule 40 pipe with a circular cross-section, making its cross-sectional area:

$$A_C = \pi \left(\frac{D}{2} \right)^2 \tag{22}$$

47

where A_C is the cross-sectional area in ft^2 and D is the diameter of the pipe in ft. With the cross-sectional area known through Eq. (22), the air flow rate as measured by the Pitot tube is therefore:

$$\dot{V}_{measured} = v_{airflow,Imp} A_C \qquad (23)$$

with $\dot{V}_{measured}$ representing the measured volumetric flow rate in ft^3 min^{-1}. For further clarity, a sample calculation is provided in Appendix B using the air flow rate procedure described above.

The results of Eq. (19) and Eq. (23) are compared to each other and are roughly equal (accounting for relatively small differences due to rounding error and instrument calibration) if all pieces of the set up are functioning correctly. For reasons that will be elucidated upon in the Results section, the desired equality between Eqs. (19) and (23) is not achieved in the final results. Instead, the final results yielded measured volume flow rates that are several times larger than the set volume flow rates. Differences as large as those found in these results indicate that the entire system is not modeled correctly, as opposed to smaller errors which would have been indicative of the suspected errors in the flow meter. For this extra analysis, the cross-sectional area of the air flow is assumed to be smaller than the cross-sectional area of the piping at the measuring point. Eq. (23) can be rewritten as:

$$A_{C,equivalent} = \frac{\dot{V}_{Alicat,Imp.}}{v_{airflow,Imp}} \qquad (24)$$

where $A_{C,equivalent}$ is the Equivalent cross-sectional area of the flow at the measuring point in ft^2. The result of Eq. (24) is compared to the calculated cross-sectional are of the piping at the measuring point and to the estimated cross-sectional area of the Alicat's outlet (0.05134 ft^2 and 0.0024 ft^2, respectively). Conclusions regarding the set up and the air flow within are made from these comparisons in the Results section.

2.4 Results

2.4.1 Combustion Optimization

The primary results of the mass fuel burned calculations are given in Table 1 along with the average fuel mass of each fuel blend added to the fuel bed for a test). Comparing the results of similar fuel mixtures under different air flow rates has shown that the mass of fuel burned tends to increase with increasing air flow rate. Since it is expected that a higher air flow rate (and therefore oxygen flow rate) to the combustor fuel bed will improve the completeness and rate of combustion, this result makes logical sense. Additionally, it is seen in Table 1 that increasing algae content also increases the final fuel mass burned for the normalized tests. This is also consistent with real world effects since the mass of fuel in a fuel basket increases with increasing algae content (as seen in Table 1) due to algae's increased density and its enhanced binding effects over pure pine mixtures.

Comparing the total mass of fuel burned to the total fuel mass in Table 1 shows that the results of the above study are likely accurate to the real world as well. Starting with the pure pine fuel mixture, its estimated fuel burned mass is 0.2 gm less than the total fuel mass. Compared to pine's ash content range of 0.5% to 2.5% by mass (or 0.1 to 0.5 gm for an average 100% pine test basket), found in Table 2, the deficit between the mass burned estimation and the total fuel mass estimation for the pine test falls well within the expected range assuming complete combustion of non-ash materials. Table 2 additionally provides the approximate ash mass ranges for the all of the biomass fuel blends. The approximation procedures for the pine/algae mixture's ash contents as well as for converting from a %wt to a gm basis are both provided in Appendix B.

Table 1 Estimated mass burned and average fuel mass for multiple biomass fuel blends.

Fuel Mixture	100% pine	90%/10% pine/algae		75%/25% pine/algae	
Average Fuel Mass [gm]	20.5	23.5		27.5	
Air Flow Rate [sLpm]	70 (normalized)	70	67 (normalized)	70	82 (normalized)
Estimated Mass Burned [gm]	20.3	23.8	22.5	15.8	26.3

Table 2 Estimated ash content and ash mass ranges for each fuel blend assuming a sample weighing the average fuel mass from Table 1 [46].

Fuel Mixture	100% pine	90%/10% pine/algae	75%/25% pine/algae
Estimated ash content [%wt]	0.5-2.5%	0.8-6.9%	1.3-13.4%
Estimated ash mass [gm]	0.1-0.5	0.2-1.6	0.4-3.7

The comparisons between the ash estimations and the mass burned estimations for the two pine/algae blends at normalized air flow rates further reinforces the validity of the model, as the deficit between average basket masses and the mass burned estimations fall within the expected ash mass ranges for both tests. Results for the non-normalized pine/algae tests, however, both fall outside the expected range. For the 75%/25% test under 70 sLpm of air flow, the estimated mass burned is 11.7 gm less than the average fuel mass, over twice the theoretical maximum of deficit of 3.7 gm from Table 2. It is theorized, however, that a 70 sLpm air flow rate does not provide a high enough rate of O_2 to the bed to facilitate complete combustion over the entire fuel basket. This conclusion is drawn from the results of the normalization study

mentioned before, and will be explained in detail in Chapter 3. However, if complete combustion cannot be sustained across the entire basket, then it is highly likely that unburned fuel material would remain beneath layers of relatively inert partial combustion products, lowering the mass burned to below optimal conditions.

For 90%/10% mixtures under normalized flow, however, the mass burned estimate is actually greater than the average fuel mass by 0.3 gm, as seen in Table 1. It is possible that the particular test used for this estimation had a higher than average fuel mass, since a total fuel mass of 24 gm to around 25 gm would have projected ash masses consistent with the estimated mass burned figure. Another possible source of error is in the total mixture volume flow rate estimation. As elucidated prior, this value is estimated as being equal to the volume flow rate of air provided by the Alicat flow controller. This assumption may overestimate the volume flow rate of the exhaust during lean combustion, which would decrease the model's accuracy at flow rates above the normalized (or non-optimal) air flow rate. It should also be re-emphasized here that the trapezoid approximation used in the model and the FTIR itself have unavoidable inaccuracies as well which could contribute to this seemingly overly large mass burned figure.

For normalized combustion, however, the mass burned estimation model can be regarded as accurate for the purposes of locating air flow rates for optimal combustion. The discrepancies caused by flowing too much or too little air to the combustion bed (as compared to the projected ash masses for each test) can be used to aid in locating these flow rates as well. It are noted that a second model will be presented as part of Chapter 3 which can additionally function as a mass burned estimation model. The process used for this model allows for further and more detailed analysis, but is more difficult to do in situ during a combustion test. Additionally, its estimate of mass burned appears to be less accurate than the previously described model. Thus, the model

presented in this Chapter functions well as an estimation tool to analyze test results in situ and

make immediate adjustments on subsequent tests. This not only allows more accurate

optimization and flow rate adjustment estimates quickening the optimization process

significantly.

2.4.2 Flow Rate Validation
         The results of the initial flow rate test are given in Table 4, while the results of the final

study are given in Table 5. Note that both tables include the equivalent flow cross-section

calculations found using Eq. (24). Table 3 provides a sampling of sLpm flow rate settings and

the resulting pressure and temperature readings reported by the Alicat alongside the Alicat

reported volume flow rate for the sLpm setting and the calculated volume flow rate for that sLpm

flow rate and the provided pressure and temperature. The calculations in Table 3 utilize Eq. (15)

to determine the volume flow rate from the set sLpm flow rate and the Alicat reported flow

pressure and temperature.

Table 3 Flow data as reported by the Alicat MCR-500 flow controller at several sLpm set flow rates. The calculated volume column uses the reported pressure and temperature with Eq. (15).

Set Flow Rate [sLpm]	Alicat open to atmosphere				Alicat connected to validation setup			
	Alicat Volume Flow Rate [Lpm]	Alicat Flow Pressure [psia]	Alicat Flow Temperature [°C]	Calculated Volume Flow Rate [Lpm]	Alicat Volume Flow Rate [Lpm]	Alicat Flow Pressure [psia]	Alicat Flow Temperature [°C]	Calculated Volume Flow Rate [Lpm]
50	52.1	14.15	24.27	52.5	52.1	14.15	24.32	52.5
100	104.4	14.14	24.41	105.1	104.5	14.15	24.32	105.0
150	156.1	14.14	24.41	157.6	155.0	14.15	24.32	157.5
200	207.1	14.15	24.33	210.0	208.0	14.21	24.32	209.1
250	259.0	14.15	24.33	262.5	258.0	14.24	24.32	260.8

300	310.0	14.18	24.31	314.3	308.0	14.30	24.32	311.7

In Table 3, comparing the reported and calculated flow rates shows good agreement between the reported volume flow rate and the flow rate calculated with the exit conditions. The volume flow rate calculated with the inlet pressure is much greater than the reported flow rate and is thus apparently inaccurate. Since the exit conditions are similar to the ambient atmospheric conditions, it is appropriate to use these values in the estimates calculated in Tables 4 and 5. From Table 4, it is important to note that the 3" diameter pipe section during this test is roughly 1 ft longer than in the final design. Less material is used to seal the connections in this iteration as well, the effects of which can be seen by examining the flow rates calculated from the manometer readings. Specifically, the changes in the Pitot tube measured volume flow rates between sLpm set points are smaller than changes in the sLpm settings and less than the Alicat reported flow rates.

An excellent example of this trend is found from the 330 sLpm set point to the 350 sLpm set point in Table 4. There, the sLpm setting's magnitude changes by roughly 6.1% (from 330 sLpm) with the Alicat reported volume flow rate also increasing by roughly 6.1%. The Pitot-tube measured flow rate only increases by 0.9% between the two points, however. This reduction in measured volume flow rate indicates that there are leaks along the length of the piping, allowing air to escape before reaching the Pitot-static tube and therefore reducing the measured flow pressure and volumetric flow rate.

Between the test represented by Table 4 and the final test represented in Table 5, further hot melt adhesive and pipe sealing tape are used to eliminate the remaining leaks in the set up and the length of the 3" pipe section is reduced by approximately 1 ft to its final length. Shortening the 3" pipe section is consistent with advice given by a subject matter expert

Table 4 Set flow rates and results from the first flow validation test. The flow pressure is assumed to be similar to ambient conditions in the test cell (14.15 psia and 24.3 °C).

Alicat Set Flow Rate [sLpm]	Measured Flow Pressure [kPa]	Alicat Volume Rate [ft^3 min^{-1}]	Measured Volume Flow Rate [ft^3 min^{-1}]	Estimated Cross-section Area [ft^2]
50	0.01067	1.85	43.68	0.002179
70	0.01733	2.60	55.68	0.002393
90	0.02267	3.34	63.67	0.002690
110	0.02933	4.08	72.43	0.002891
130	0.03633	4.82	80.61	0.003069
150	0.04167	5.56	86.33	0.003307
170	0.05033	6.30	94.88	0.003410
190	0.05600	7.04	100.08	0.003613
210	0.06300	7.79	106.15	0.003765
230	0.07000	8.53	111.89	0.003912
250	0.07833	9.27	118.37	0.004020
270	0.08433	10.01	122.82	0.004184
290	0.09100	10.75	127.58	0.004327
310	0.09567	11.49	130.81	0.004511
330	0.1060	12.23	137.69	0.004562
350	0.1080	12.98	138.98	0.004793

Table 5 Set flow rates and results from the second flow validation test. The flow pressure is assumed to be similar to ambient conditions in the test cell (14.15 psia and 24.3 °C).

Alicat Set Flow Rate [sLpm]	Measured Flow Pressure [kPa]	Alicat Volume Rate [ft³ min⁻¹]	Measured Volume Flow Rate [ft³ min⁻¹]	Estimated Cross-section Area [ft²]
50	0.02400	1.85	65.52	0.001453
70	0.04733	2.60	92.01	0.001448
90	0.07733	3.34	117.61	0.001457
110	0.1167	4.08	144.45	0.001449
130	0.1610	4.82	169.69	0.001458
150	0.2160	5.56	196.55	0.001453
170	0.2800	6.30	223.79	0.001446
190	0.3473	7.04	249.24	0.001451
210	0.4260	7.79	276.03	0.001448
230	0.5133	8.53	303.01	0.001445
250	0.6060	9.27	329.22	0.001445
270	0.7040	10.01	354.85	0.001448
290	0.8123	10.75	381.17	0.001448
310	0.9203	11.49	405.72	0.001454
330	1.0373	12.23	430.74	0.001458
350	1.1673	12.98	456.93	0.001458

regarding method of improving the accuracy and reliability of the set up. These modifications

yielded the results in Table 5. Looking at the column displaying the volume flow rate

calculations using the cross-sectional area of the 3" pipe, the clear trend of increasing measured

flow rate with increasing set flow rate indicates that the air leaks are sealed off. However, each

of the Pitot tube measured flow rates in Tables 4 and 5 is also significantly greater than the set

flow rates given by Eq. (15). Thus, Eq. (24) is applied to each set point with the results given in

the right most column of Tables 4 and 5.

All of the estimated areas in Tables 4 and 5 fall between the estimated Alicat outlet area

of 0.0024 ft^2 and the 0.05134 ft^2 cross-sectional area of the 3" pipe. Each flow area estimate in

Table 5 is additionally roughly equal to the other estimates. Conversely, in Table 4, the

Equivalent areas increase with increasing sLpm setting and flow pressure. There also appears to

be an inverse trend in the increase of measured flow rates in Table 4 and the corresponding

Equivalent area (i.e., as the percent change in flow rates between settings decreases, the

Equivalent area increases). Thus, it is theorized that the air flow in both versions of the setup is

still expanding when it reaches the Pitot tube. Using the 50 and 70 sLpm set point readings in

Tables 4 and 5, it can be seen that the Equivalent area generally increases with the distance the

flow has traveled from the Alicat as well, consistent with expanding flow. The trend of

increasing area in Table 4 is additionally likely related to the aforementioned leaks. Air would

leak from the setup before the Pitot-tube carrying air and energy away from the flow, artificially

inflating the Equivalent area since the volume flow rate across the Pitot tube is assumed to be

Equal to the flow rate at the Alicat opening. That is not the case with the setup used for Table 5,

however, since the Alicat flow is no longer split between the setup's piping and the leaks to the

atmosphere. Because it is expanding in this region, the flow will not occupy the full cross-section

of the tube, and potential turbulent effects in the expansion region can also contribute to inaccuracies in the flow pressure readings and cross-sectional area calculations.

The previously mentioned shortening of the overall pipe length is suggested in order to avoid the potential for flow expansion. However, because of the relatively large diameter of the final section, the final shortening may have had the opposite effect, placing the Pitot tube further into the region of expansion instead of before it. Thus, in order to effectively utilize this design methodology, a smaller diameter pipe are used for the measurement. Accordingly, since the current Pitot-static tube would be difficult to fit into a smaller diameter pipe than the current design, a smaller diameter Pitot-static tube or smaller diameter Pitot tube and a static measuring port would be necessary.

Dwyer's literature and website suggest the opposite of the subject matter expert: increase the final pipe diameter and extend the setup so that there is roughly 8 ½ diameter's worth of pipe between the Alicat and the Pitot-Static tube (so for a 3" pipe, roughly 30" of length is suggested) [54, 55]. Such extreme dimensions are not practical given the current test space, so any future flow validation work should take the route suggested by the subject matter expert. The overall set up may need to be redesigned to account for a different style of Pitot tube as well, as the current style may not be practical to produce in a small enough size to enact the more compact design. Do note that Dwyer's advice regarding the relation between the pipe diameter and the pipe length likely still holds for the subject matter expert's advice. However, since the expert's design utilizes a smaller pipe diameter, the pipe length will naturally be shorter in comparison to a design meeting Dwyer's criteria for the current Pitot-static tube.

2.5 Conclusions

Combustion optimization is a crucial process to ensure that a fuel is thoroughly burned in the most effective and efficient manner possible in a setup or application. One method that can be used to ensure that combustion is optimized is to measure the mass of fuel burned using the emissions data measured by the FTIR. Comparing the estimated mass of the fuel burned to the average mass of fuel added to a basket before combustion will give an idea of how must of the fuel's combustible fraction is burned.

The mass burned calculation model presented in this Chapter, although simple compared to similar models presented in a later Chapter, yielded more accurate mass burned estimates and is faster and easier to implement in an in situ environment. Thus, the above model can be used in between individual tests to gain immediate insight into how combustion is being affected by changes. This feedback can then be applied to more immediately, effectively, and accurately make adjustments to the experiment to yield the desired combustion results. In the future, this mass burned model, alongside analysis of individual emissions amounts from FTIR data and combustion models presented in later chapters, can be utilized to optimize the combustion of pure biomass or coal-biomass fuel blends by improving the thoroughness and completeness of the combustion, as well as the energy released by combustion.

Although initially prompted due to programmer error in early versions of the mass burned calculation model, flow rate validation of the Alicat flow meter is a good idea since even small differences in the amount of air provided to the combustion bed have significant effects on the reactions that occur. Pitot-tubes, are not necessarily as straightforward to implement as their simplicity suggests. Nonetheless, the volume flow rates reported by the Alicat are satisfactorily accurate to expected values, and much information regarding design and operation of a Pitot-tube flow validation set up is discovered. If further flow validation studies are needed in the future, it

is recommended that a smaller diameter Pitot tube be used since they are easier to implement in small diameter piping. This, in turn, reduces the required length to produce fully developed flow that will provide accurate, repeatable, and reliable data.

Chapter 3 – Co-combustion of pelleted woody and algal biomass blends in a fixed bed combustor

3.1 Abstract

The power generation industry currently relies heavily upon fossil fuels and is a major source of carbon, nitrogen, and sulfur emissions. Hence, this industry is a target for biofuel applications; however, the sheer amount of fuel required places significant strain on existing biofuel sources. In this area, algae are an underutilized source of biomass with high yield potential, but whose direct combustion is not thoroughly understood. As a result, a custom-built solid fuel combustor is constructed in order to normalize and compare the combustion of algae-containing solid fuel mixtures to pine (a more conventional woody biomass). In general, the algae containing mixtures are found to require less oxygen to combust and produced fewer carbon emissions. Moreover, nitrogen- and sulfur-containing emissions increased with the addition of algae, which agrees with the measured elemental content of the pine and algae. Although significant work still remains in thoroughly understanding algae's combustion properties, the data gathered from these initial experiments provide a solid launching point for further investigation.

3.2 Introduction

Significant effort is currently invested in research for alternative fuels, particularly for power generation. This endeavor is primarily motivated by the dual pressures of increasing worldwide energy demand and a steadily dwindling fossil fuel supply. According to the U.S. Energy Information Agency (EIA), worldwide electricity demand has increased from around 18.6 trillion kilowatt-hours (kWh) in 2010 to nearly 20.3 trillion kWh in 2013 [28]. This trend is mirrored in the increase of world fossil fuel demand for energy production over the last several

years [28]. Fossil fuels, such as coal and oil-based fuels, are additionally projected to "run out" within fifty years at current usage [24]. Moreover, emissions from fossil fuels present numerous concerns, such as greenhouse gases (GHG) and smog formation, along with heavy metal pollution [26, 32, 56]. In this area, coal combustion emissions are viewed as particularly undesirable, in part because of coal's popularity in power generation, and comparatively because of its relatively high concentration of heavy metals, sulfur, nitrogen, and arsenic as compared to other fossil fuels [32, 57]. Thus, much effort is focused on the development of new fuels to replace or reduce the coal used in power plants.

One promising option for new fuels is the rapidly developing field of biomass and biofuels [18, 26, 32, 38, 56]. Biomass refers to any organic matter (typically solid) derived directly from plants or other living sources. In comparison, biofuel is a more general term referring to plant- or animal-derived energy sources that are either directly derived from the original source or from a conversion process [23, 24]. By definition, biomass and biofuels are grown, which means that supplies of these fuels can be replenished as long as there is arable land on which to grow the feedstocks [24]. The ability to grow constantly is what makes biomass renewable and results in its first advantage over fossil fuels. The second advantage is its perceived carbon-neutrality [26, 30, 56]. In short, as biomass grows it pulls the carbon it needs from the atmosphere. This carbon is released as it is burnt, but since the carbon is already in circulation within the environment, (ideally) there is no net change in the amount of carbon in the environment [24-26]. Thus, biomass is often considered to be carbon neutral and can help reduce mankind's net carbon and GHG emissions [26, 30, 56].

The field of biomass and biofuels is often separated into first, second, and third generation fuels. First generation fuels include ethanol, biodiesel, and plant oils [36]. Since crops

such as soybeans and corn are the predominant stocks for first generation biofuel production, these biofuels often compete directly with human food resources. Attempting to avoid this food versus fuel interaction, second generation biofuels are based on lignocellulosic fuels and agricultural wastes [23, 36]. Such stocks generally do not compete with food resources, and can indeed bolster food resources in certain cases by making otherwise unarable land useful to grow food crops [36]. Woody biomass is one of the oldest and most utilized second generation biofuels and is especially popular in South and Southeast Asia [24]. Moreover, woody biomass is growing in use as a co-combustion fuel for many European power plants, with some adoption in the U.S. [30, 58, 59]. Several power plants utilizing coal and wood co-combustion reported lower carbon, nitrogen oxide (NO_x), and sulfur oxide (SO_x) emissions over 100% coal combustion [26, 58, 60]. However, nitrogen and sulfur emissions are somewhat variable due to the varying composition of different wood species [26, 30].

Second generation biofuels are logistically limited and increased demand could make certain fuels unsustainable over long-term use [23]. In particular, woody biomass could be fully depleted in around nine years if used to completely replace coal in power generation [33, 34]. Many other second generation biofuels are waste products and, thus, their supply is dependent on the size of the waste industry. From an economic standpoint, second generation fuels are often significantly more costly than fossil fuels because of logistical issues [26, 31, 58]. Thus, further biomass development has focused on a finding a fuel source with lower utilization and fewer logistical demands.

Investigation of third generation biofuels has focused on aquatic biomasses (micro- and macroalgae), which are not widely utilized as food (in most of the world) and typically have higher volumetric yields than terrestrial biomass [36, 46]. As an example, brown seaweeds (a

macroalgae) averages around 13.1 kilograms (kg) of dry biomass per square meter (m^2) of farming area per year "under cultured conditions" [46]. Sugarcane only produces an average of 10 kg dry biomass per m^2 growth area per year as a comparison [46]. The yield potential of algal biomass is further enhanced by its lack of competition with existing industries and demands. Macroalgae is current only significantly utilized in Asian countries, largely in cosmetics or as a fertilizer, with some usage in the food industry [44]. Microalgae are even less utilized. Both forms of algae have a negligible fuel industries and the non-fuel macroalgae industry is around 100 times as large as microalgae non-fuel industry, in terms of wet tonnage [44]. Furthermore, algae (both macro and micro) can also be grown using resources that are not acceptable for growing food crops, similar to some second generation fuel sources [36, 61]. More precisely, algae do not require potable water to be grown and can be used to clean brackish water or water contaminated with byproducts from certain industrial or power generation effluents [36, 45, 61]. Thus, there is potential for algal fuels to be grown on-site in power generation applications, reducing the economic cost of the fuel by eliminating transportation expenditures [45]. This combination of high yields and ease of growth could make algae a potentially useful fuel source.

However, there are some concerns regarding algae's combustion properties and potential emissions. Most apparently, water content in algal biomass ranges from 80% to 90% by fresh mass, which is greater than even sugar cane's 75% fresh mass water content, the highest of commonly utilized terrestrial biomasses [43, 44, 46]. Previous research shows that biomass combustion is only feasible for biomass with less than 50% water content by weight [43, 46]. Algal biomass additionally has high ash levels, ranging from 4.5% to 46% by dry weight for macroalgae, dependent on the species [46]. Microalgae ash content is similarly variable, but also high, ranging from 7% to 35% by weight [43]. This high ash content is one of the more

thoroughly emphasized detriments to algal combustion. This is due, in part, to the magnitude of the ash content but also because of the severity of the consequences. Firstly, higher ash contents severely reduce the higher heating value of a fuel; hence, algal combustion will generally not release as much energy as other biomass [44, 46]. Secondly, the ash produced by algal combustion, especially with macroalgae, is high in alkali metals [36, 43, 44, 46, 61]. High alkali ash content is associated with thicker, and less porous deposits that are both more difficult to remove than other ashes and more corrosive in vessels under boiler and heater service conditions [24, 30, 44, 46, 61].

The final differences in comparison to woody biomass are algae's typically high content of nitrogen and sulfur along with its make-up containing heavy and alkali metals. This potentially leads to higher emissions of nitrogen and sulfur oxides and increased heavy metal pollution [36, 43, 44, 46]. However, little testing has been conducted in the field of algal direct or co-combustion with other biomasses or fossil fuels [43-46]. Combined with knowledge of the variability of wood and coal combustion products, it is evident that more substantial testing needs to be conducted to verify the impact that fuel-bound substances in algae generate with respect to performance and emissions.

As a result, this current study seeks to expand on macroalgal biomass co-combustion knowledge. Using a custom-made, fixed-bed solid fuel burner, pellets of woody biomass and wood-algae combinations are combusted. A series of thermocouples along with a Fourier Transform Infrared Spectroscopy (FTIR) device and a Smoke Meter are utilized to gather data on the temperature and emissions produced during the combustion process. The ultimate goal of this study is to normalize the combustion rate of all mixtures by comparing peak burn times and total combustion time. An additional goal involves comparing major emission species produced by

the various mixtures, chiefly carbon, NO_x, and SO_x. The purpose-built and properly instrumented burner, combined with proper procedures, will thus add significantly to current macroalgae combustion knowledge.

3.3 Experimental Procedure

The experimental set up is a custom made, solid fuel combustor described in more detail in a previous work with a diagram provided in Fig. 5 [62]. Eleven K-type thermocouples fit into slots machined into the combustion tube, starting just above a glow plug ignitor. The overall experimental procedure involves pellet making, sample construction, lab set up, and the actual testing. The pellet making procedure will not be included here since it is included in the previous effort. Note, however, that the pellet materials and the pellets themselves are dried overnight using drying ovens set at about 60°C. Drying the material reduces the variability in water content
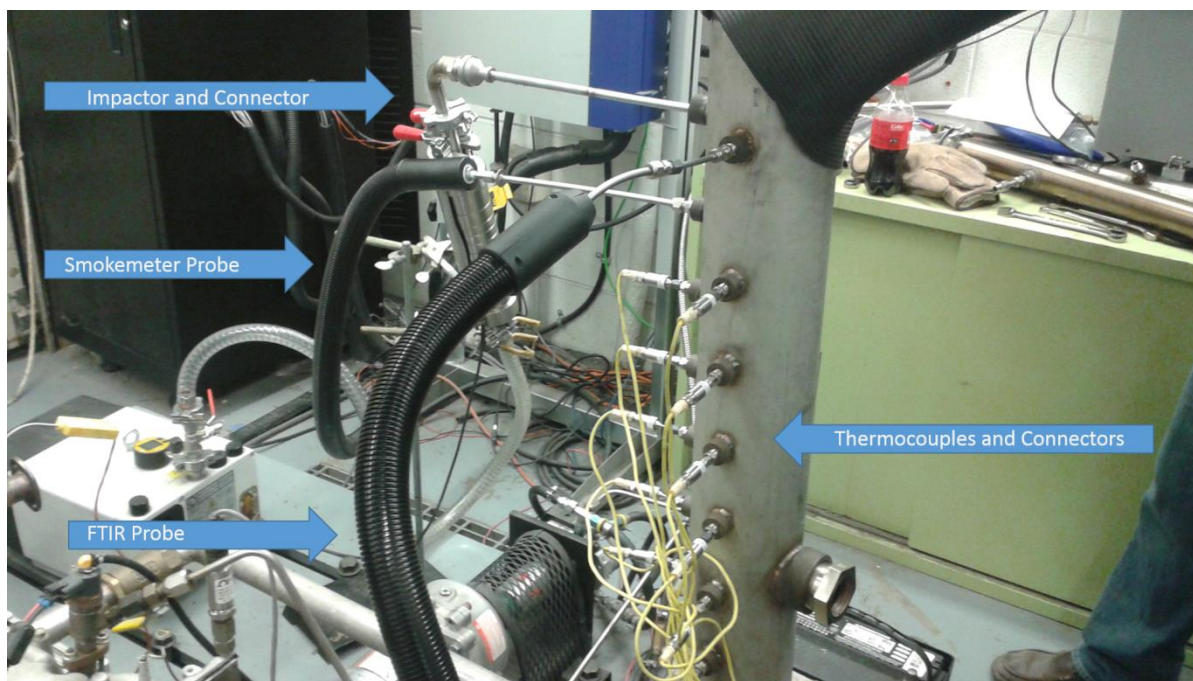
Figure 5 Experimental setup with major sensor attachments labelled.

ensuring repeatability when testing. Pellets produced by the pellet-making process are approximately 9.53 mm in diameter and range in length from approximately 10.32 mm to 23.81 mm. Before each test, pellets of the desired mixtures are loaded sample baskets.

The sample baskets, shown in Fig. 6, are constructed of fine stainless steel wire meshing with approximately 34% open area and form a squat cylinder shape roughly 114.30 mm in diameter and 34.93 mm in height. A "pre-burn" basket, also constructed of a similar wire mesh but made from a single cutout and shaped to fit the fuel bed, is used to hold pre-burn mixtures prior to measured experimentation. Shown in Fig. 7, the pre-burn basket is constructed with larger tolerances as an iterative step toward the current sample basket design, but these tolerances made it less reliable for instrumented tests. For the sample baskets, three tabs attached to the side of the baskets allow them to hang from the lip of the bed chamber, placing the bottom of the basket just underneath the glow plug when the entire combustor is assembled. Pellets are laid into the basket such that circular ends remain perpendicular to the basket bottom, as seen in Fig. 8. Note that no sizeable gaps are left between pellets in the layer. Once one "layer" of pellets is placed, another circular mesh is placed on top of the pellets. A second pellet layer is then placed on this circular mesh (using the same orientation as the first layer) and then covered with a final circular mesh. An example of a fully assembled sample basket is shown in Fig. 6.

As many as six sample baskets are built before every test session and enough scrap material for two pre-burns is additionally produced. Before testing can begin, the measuring instrumentation must be properly attached and calibrated. For an Alicat MCR-500SLPM-D flow controller and the K-type thermocouples, this involves attaching the flow controller or probes in the proper connections, as shown in Fig. 5. The thermocouples and flow controller communicate with a LabVIEW program developed in-house via three National Instruments (NI) Data

Figure 6 (Top) Angled view of a steel mesh sample basket. The mesh circles to the right of the basket are the mesh "separators," meant to reduce the ash lost to the upwards air flow in the combuster. (Bottom) A fully assembled sample basket. Note that the top separator sits nearly flush with the top of the basket sides.

Acquisition (DAQ) modules set in a NI CompactDAQ chassis. The flow controller set-point is adjusted through a NI 9265 module while data from the flow controller and the thermocouples are read by NI 9215 and NI 9213 modules, respectively. The AVL Smoke Meter needs to be

powered on for around fifteen minutes in advance so that it can reach optimum operating

temperature. The AVL FTIR, however, requires a long calibration process that begins roughly

twelve hours in advance of testing with a purge of internal lines using high-purity gaseous

nitrogen. This purge removes any lingering samples from previous tests that could affect the

emissions analysis of current experimentation. Cooling of the FTIR's sample lines via liquid

nitrogen and range calibration of several key parameters is then conducted an hour before

experimentation.

The next step in the experimentation process involves the pre-burns. These pre-burns are

roughly the same volume of material as a normal sample basket, but instead of precisely mixed

pellets, they consist of a mixture of newsprint paper shreds and waste material from the pellet

making procedure. Since pre-burns are meant only to warm up the combustor bed to reduce

Figure 7 The pre-burn basket. The single piece construction makes precision sizing more

difficult, but also increases durability.

Figure 8 A top down view of a pellet layer within a sample basket.

the variation in heat transfer between tests, it is not necessary to tightly control the material within these mixes, and an emphasis is thus placed on preserving stores of testable material. Pre-burns begin by filling the pre-burn basket with material and then securing the basket within the combustor bed by hanging it from the top edge of the stainless steel pipe that makes up the top of the plenum. The slot in the side of the basket is then aligned with the glow plug hole in the side of the pipe, ensuring that the heating element of the glow plug can reach the fuel. Silica fabric insulation is wrapped around the side of the pipe. A hole in the fabric is placed around the nut welded over glow plug hole. The combustor tube is then carefully placed on top of plenum, fitting within the grove machined into the plenum top. To align the tube properly, the glow plug hole drilled into the tube is aligned with the same hole in the plenum's combustor bed. Threading the glow plug through both holes and into the fuel in the basket will secure the tube to the plenum.

With the tube secured, all instrumentation is attached to the correct positions on the tube or plenum. The thermocouples fit through pressure fittings running up combustor tube in two columns. Probes for the FTIR and Smoke Meter are then inserted into compression fittings near the top of the tube. Lastly, wired connections are attached to the Alicat flow meter. One connection provides power from a standard wall outlet while the other, an 8-pin DIN cable, connects the flow controller with the NI DAQ board. A USB connection from the DAQ board is inserted into a computer loaded with a combination control and data collection program for the flow controller and thermocouples. A second computer communicates with the Smoke Meter and FTIR, controlling and gathering data as needed during testing. An exhaust hood is placed over the top of the combustion tube and fans are activated to help pull all exhaust not used for the Smoke Meter and FTIR out of the room and to a dispersal point above the building.

The final preparatory step involves attaching a canister of compressed carbon dioxide (CO_2) gas to the black hook-up shown in Fig. 9. If a test needed to be interrupted for any reason, this canister and the valves between it and the main airline into the plenum would be opened after the flow controller is turned off. This will flood the combustor bed with inert CO_2, stifling any combustion. After all safety systems and instrumentation is in place, the flow controller is activated and set to the desired flow rate. The logging software for the flow controller, thermocouples, and FTIR are activated before a 12 VDC lead-acid car battery is attached via several leads controlled by a switch to the glow plug. Closing the switch completes the circuit to the glow plug, providing enough heat to ignite the pellets. Careful monitoring of the carbon monoxide (CO) emissions measured by the FTIR allows the researchers to pinpoint the moment ignition is achieved. At that time, the switch is closed and the leads removed from the glow plug and the 12 VDC battery. The viewport on the side of the combustor tube is monitored
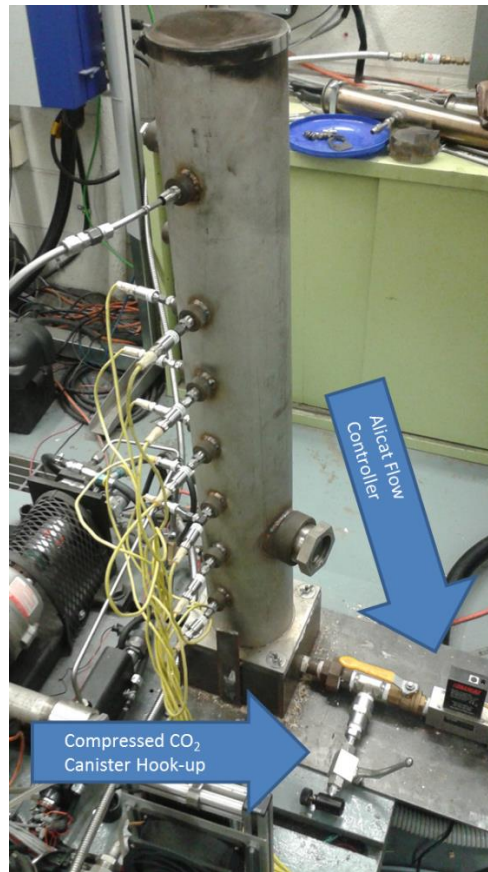
Figure 9 The assembled solid fuel combuster.

and when light from a flame is first seen, the Smoke Meter logging software is activated to gather particulate matter (PM) emissions data.

Once flames can no longer be seen from the viewport, the FTIR readout is once again closely monitored. When carbon emissions reach a near-ambient level, the combustor bed is carefully checked by peering through a slit made between the grate at the top of the combustor tube and the exhaust hood drawing the exhaust out. If flames, embers, or smoldering ash is seen, the exhaust hood is quickly replaced and additional time is allowed before another check. Once no flames, embers, or smoldering material is seen, combustion is assumed ceased, data collection is stopped, and the combustor is disassembled in the reverse of the process described above,

using appropriate personal protection Equipment, such as tongs or insulated gloves as needed. The charge/sample is removed from the combustor bed and the ash is either collected for analysis or placed down a nearby storm drain to prevent re-ignition or ignition of other flammable materials. This burning procedure is then repeated for all pre-burns and sample baskets until testing is concluded.

This method is used to test several distinct mixtures of white pine and macroalgae. The pine is collected as shavings from a local wood shop while the algae samples are dredged from a nearby lake and are, therefore, not a single species. To provide a detailed view of pine and algae combustion and co-combustion, three mixtures (100% pine, 90% pine/10% algae, and 75% pine/25% algae) are pelletized and burned. Table 6 provides the carbon, hydrogen, nitrogen, and oxygen content for each of the mixtures as determined by a high temperature combustion analyzer with the constituents presented on a percent mass basis. The energy content of the algae and pine as pure mixtures, as determined by calorimeter, is also presented in Table 6. Estimations for the energy content of pine/algae mixtures are made by multiplying the fractional content of pine and algae in the mixture with the respective material's energy content. These two values are then summed to produce the total estimated energy content of that mixture. The last column of Table 6 also provides the average mass of fuel in a basket during a test. Since the fuel for each test takes up the same volume, the average basket weight gives an accurate measure of the average fuel density of the pellets for different fuel mixtures. Tables 7 and 8 present the major inorganic and trace element constituents of each mixture. The inorganic constituent data come from ablation studies conducted by a Dr. Peltier's lab, leading to units of percent mass based on a 34% carbon mass content. Dr. Peltier's lab used acid digestion on separate samples from the same batches of fuel to determine the trace element in terms of parts per million (ppm).

Table 6 Carbon, hydrogen, nitrogen, oxygen, and energy content of several pure and mixed fuel types. (* denotes estimated energy contents)

Sample Description	%Algae	Average Composition (% mass basis)					Energy Content	Average Basket Mass
		%C	%H	%N	%O	%Misc.	kJ kg^{-1}	gm
Ground Algae	100	33.4	4.0	2.3	34.7	25.6	8983.94	N/A
75%/25% Pine/Algae Pellet	25	46.5	5.8	0.5	40.8	6.4	16078.14*	27.5
90%/10% Pine/Algae Pellet	10	49.9	6.1	0.2	41.7	2.1	17496.98*	23.5
White Pine Pellet	0	51.4	6.5	<0.1	41.6	0.4	18442.87	20.0

Table 7 Major inorganic constituents of three fuel mixtures.

Pellet Composition	Major inorganic constituents, as % weight (with carbon content of 34%)				
	CaO	MgO	SiO$_2$	FeO	MnO
100% Algae	N/A	1.980	1.320	1.720	5.029
10% Algae, 90% Pine	7.279	0.132	0.132	0.132	0.172
100% Pine	3.705	0.847	0.211	0.132	0.132

Table 8 Trace element composition of several pine/algae blends.

Pellet Composition	Trace elements (in ppm (w), or mg/kg)				
	Cr	Cu	Zn	Sr	Pb
100% Algae	10.8	211.6	2229.0	134.1	493.6
90% Pine	1.9	7.2	284.8	6.5	N/A
100% Pine	0.6	4.4	1761.9	0.1	199.6

Note that the macroalgae tends toward less carbon, hydrogen, and oxygen than the pine used, but has greater amounts of fuel-bound nitrogen and, in general, possesses more inorganic and trace element constituents.

3.4 Results and Discussion

The detailed experimental procedure, combined with two fuels and the combustor set up, allows for burn rate normalization studies and initial comparisons involving pine and algae fuel mixtures. Since quantifying the heat output of a sample is difficult with current instrumentation, the burn rates of the different mixtures are found using the carbon emissions information gathered by the FTIR. Carbon emissions are chosen since its oxides constitute only a small portion of the ambient air while carbon is available in relatively significant amounts in both pine and algae. Thus, emissions of carbon monoxide, carbon dioxide, and hydrocarbons can be used

to estimate the beginning, end, amount, and completeness of combustion, with the final goal of normalizing the combustion behavior of the mixtures.
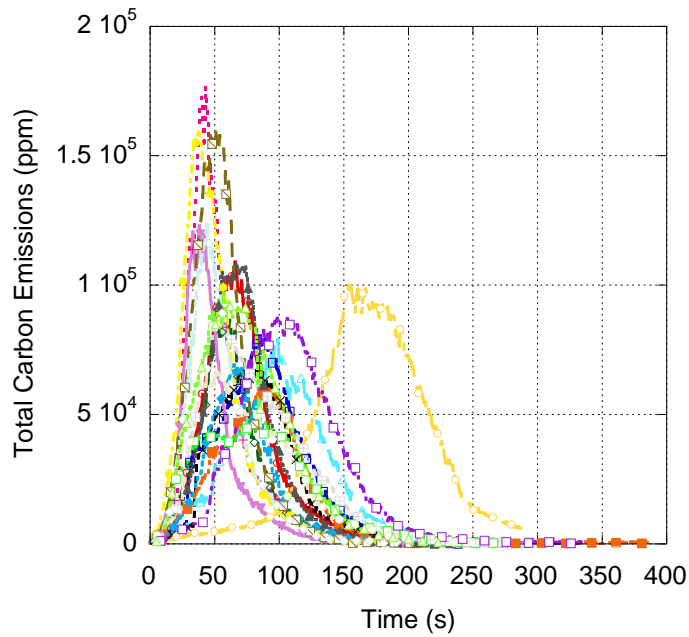
Figure 10 Total carbon emission curves for several 100% pine tests from multiple test dates.

Before proceeding to the primary results of these studies, it is important to discuss an obstacle with the described experimental setup: the difficulty of obtaining numerically consistent results. Combustion is a complicated and non-linear process, and sometimes even small and unavoidable changes in certain systems needed to operate the set up can cause observable and significant alterations to the recorded data. As an example, Fig. 10 displays every recorded total carbon emission curve for 100% pine baskets at a flow rate of 70 sLpm using the experimental procedure described prior.
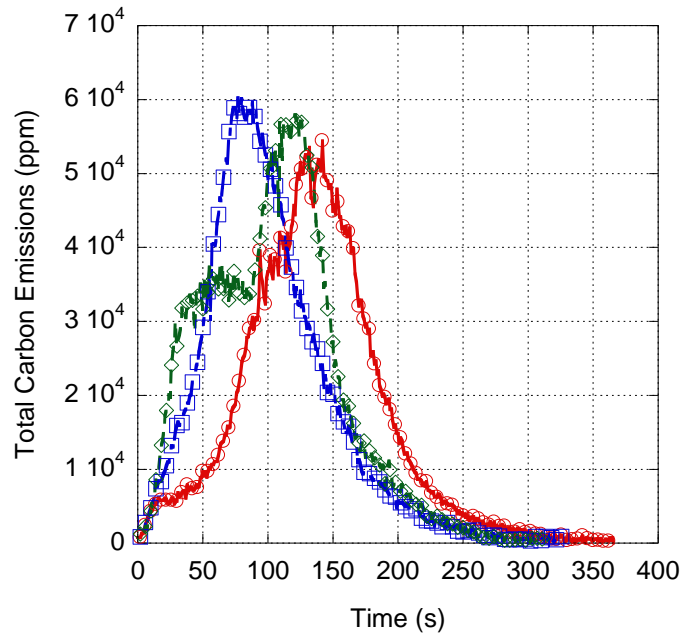
Figure 11 Total carbon emission from three 90%/10% tests at 67 sLpm.
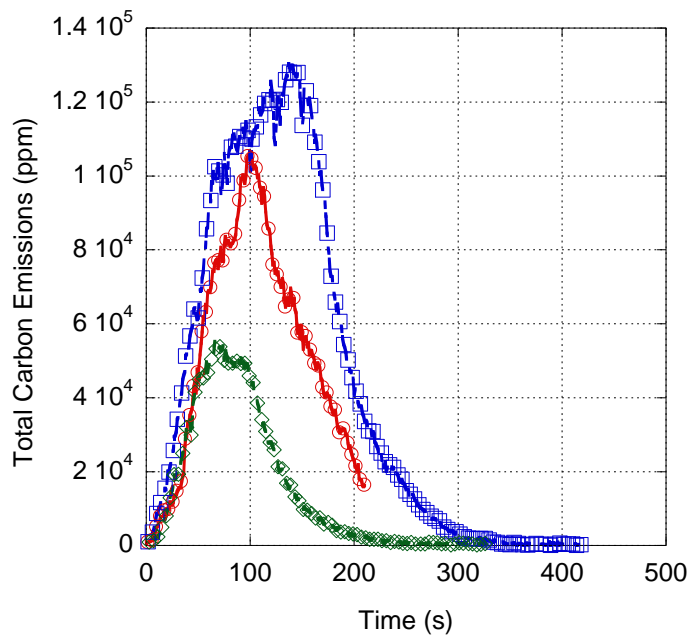
Figure 12 Total carbon emission from three 75%/25% tests at 82 sLpm.

Despite the carefully controlled air flow, fuel composition, pellet orientation, ignition source, etc., it can be seen that the maximum burn rates, total combustion time, and other parameters change in sometimes large degrees between individual pine tests. This is the case even if those tests occurred within minutes of each other. A similar, though less severe, trend is found for 90%/10% and 75%/25% mixtures at comparable flow rates as well, seen in Figures 11 and 12.

Notwithstanding the difficulty in obtaining absolute numerical consistency with the setup, comparing data of mixtures tested in the same session in situ revealed consistent trends between the different mixtures. The figures and analysis in this section are constructed in order
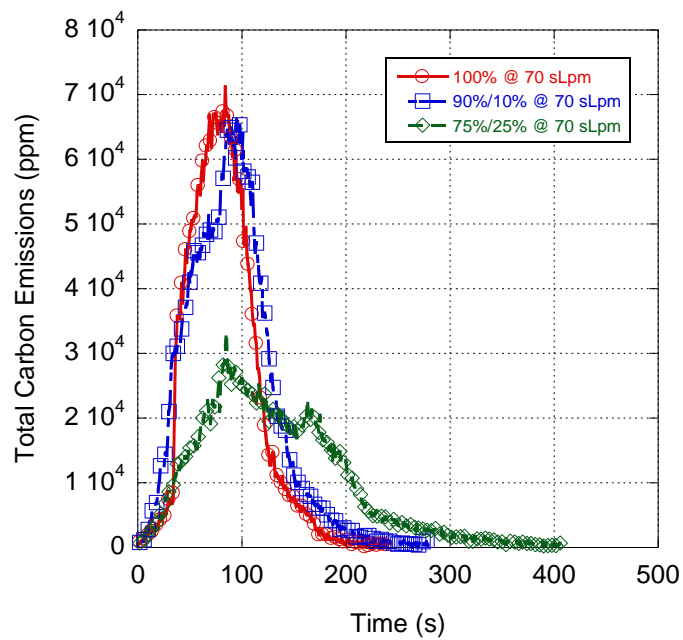
Figure 13 Total carbon emission over time from three pine/algae mixtures with a fixed air flow rate.

to be true to those observed trends, even with the obvious difficulties of such comparisons across multiple test sessions, as illustrated in Figures 10-12.

Normalization requires an understanding of how altered tests compare to the selected baseline. Thus, testing of pure pine pellets and pine/algae mixtures at the same flow rate is necessary to begin the normalization study. A baseline flow rate of 70 sLpm is selected and representative total carbon emission curves for all mixtures at this flow rate are measured and presented in Fig. 13. Using the 100% pine curve as the standard, it is seen that the 75%/25% mixtures reach a peak burn more slowly. While the 90%/10% at first glance appears to also peak later than the 100% mixture, the hindering of the 90%/10% mixture's combustion rate just before it peaks are noted. As elucidated prior, comparing results between test sessions can be difficult and requires additional attention. In this case, despite the decrease in combustion rate, this 90%/10% test at 70 sLpm and other 90%/10% tests at similar flow rates tended to burn more quickly than the 100% pine tests at 70 sLpm that are conducted during the same test sessions as controls. This can be seen in Fig. 14 which contains the 90%/10% total carbon emission curve from Fig. 13, as well as the same curve for each of the pure pine tests conducted in the same session. In Fig. 14, it can be observed that the 90%/10% mixture matches or exceeds the peak combustion time of the 100% pine mixtures at the same flow rate. Additional testing confirms these results, specifically the tendency for 90%/10% at a 70 sLpm flow rate to reach peak combustion slightly sooner than 100% pine with the same flow rate.

Thus, in Fig. 9, it is theorized that the stronger adhesive properties of the algae could augment its combustion with pine. The relative adhesive properties of pine and algae can be seen in Fig. 11, where the 100% pine pellets display a greater porosity and a tendency to fray in comparison to the 75%/25% pellets shown beside them. Added adhesion packs the fuel in the pellets more densely, allowing the flame to potentially propagate more quickly in the 90%/10% mixture than in the 100% mixture. The effect of algae's increased self-adhesion is clearly

overcome by its lower energy content (indicated in Table 6) when larger proportions of algae are used. This is observed in the 75%/25% mixture in Fig. 13, which burns at a slower rate compared to the other two mixtures. Additionally, the fuel composition and extra adhesion of the algal mixtures significantly increases the density of the algae containing pellets. This can be seen
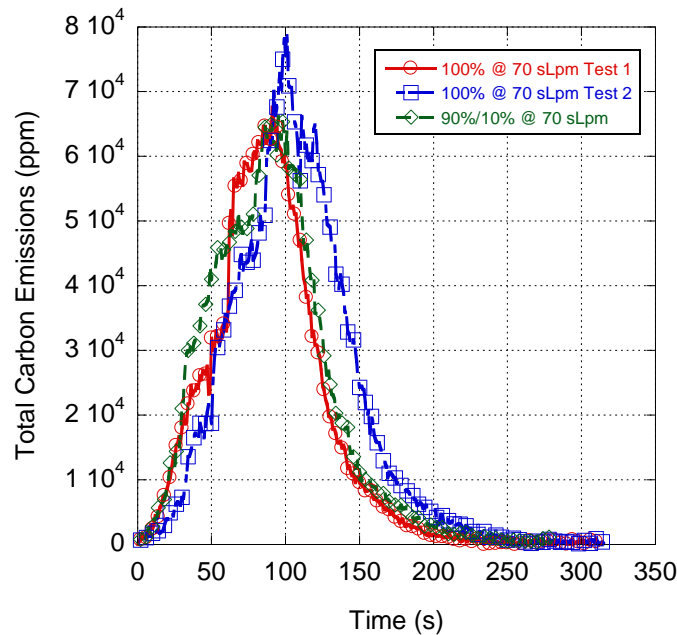
Figure 14 Total carbon emission curves for two mixtures from the same test session as the 90%/10% @ 70 sLpm curve in Fig. 13.

visually in Fig. 15, where fewer gaps observed in the 75%/25% pellets compared to the pure pine pellets shows the increased density of the algae-containing pellets while the lower amount of dust in the 75%/25% bag shows algae's effect on the friability of the pellets. Algae's increased density and adhesive effects can also be seen in the average basket masses included in Table 6, which increase with increasing algae content.

These initial measurements provide an indication for the adjustments needed to normalize the combustion rates. Normalization is achieved by adjusting the air flow rate provided by the Alicat flow meter that directly modulates the oxygen available for combustion. Because the

90%/10% mixture had an accelerated combustion rate compared to 100% pellets, the flow rate is lowered. Fig. 16 shows a flow rate sweep conducted using 90%/10% pellets. Each of these curves is compared to a 70 sLpm curve for 100% pine, as shown in Fig. 17. It is seen that setting the

Figure 15 Pure pine pellets (on the left) exhibit higher friability through an increased number of small pieces and dust than the 75%/25% pine/algae pellets (on the right).

flow rate to 67 sLpm brings the initial slope and the peak of the 90%/10% total carbon emission near the same time point as the 100% peak in total carbon emission. It is unknown why two peaks for the 60 sLpm test are seen; however, its initial rise followed the trend with 70 sLpm and 50 sLpm. Hence, it is possible that the fuel immediately around the glow plug ignited normally, but that the fuel around this ignition point is less densely distributed than normal, lowering the combustion rate until the flame propagated out of this region of lowered density. Similarly, it is seen in the 70 sLpm test that after a period of time, the combustion rate of the 70 sLpm sample

briefly remains constant and then continues rising at a lower slope than before. Again, the exact

mechanics behind this deviation are not known.

Overall, it is generally found that the 90%/10% tests at 70 sLpm exhibited faster

combustion than the 100% pine samples at the same flow rate conducted during the same
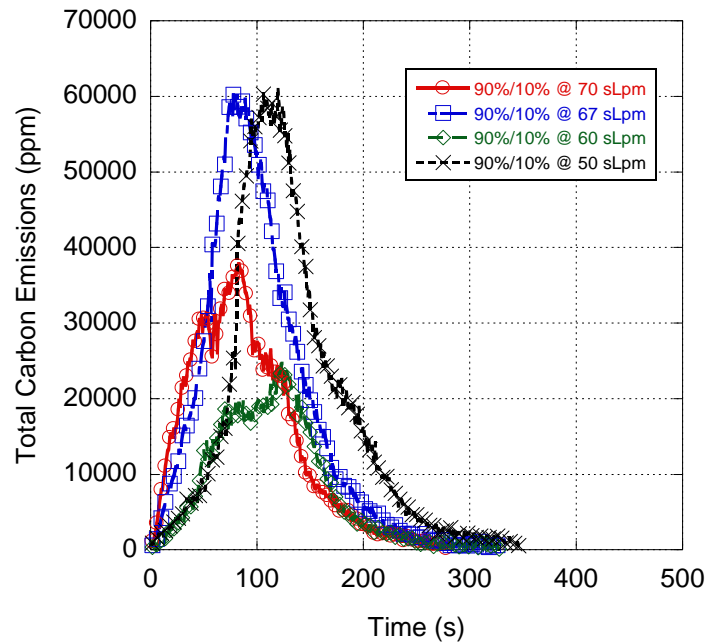
Figure 16 Total carbon emission curves for 90%/10% pine/algae pellets under several flow

rates.

experimental session. Thus, when comparing the curves in Fig. 17, it is important to consider the

initial slope of the total carbon measurements, as well as the peak measurement when

normalizing the various samples. Otherwise, it would be possible to assume that the 70 sLpm test

of the 90%/10% pine/algae mixtures tended to have a later peak combustion time than the 67

sLpm. Such a conclusion is not consistent with the overall trends of the combustion tests.

The flow rate used for the 75%/25% mixture is then adjusted in a similar method to the

90%/10% mixtures. Since its combustion rate is slower as compared to the purely pine mixture,

its flow rate is increased to create a more oxidative environment. A sweep of tested flow rates is

shown in Fig. 18 and generally the combustion rate grew with an increasing flow rate. When
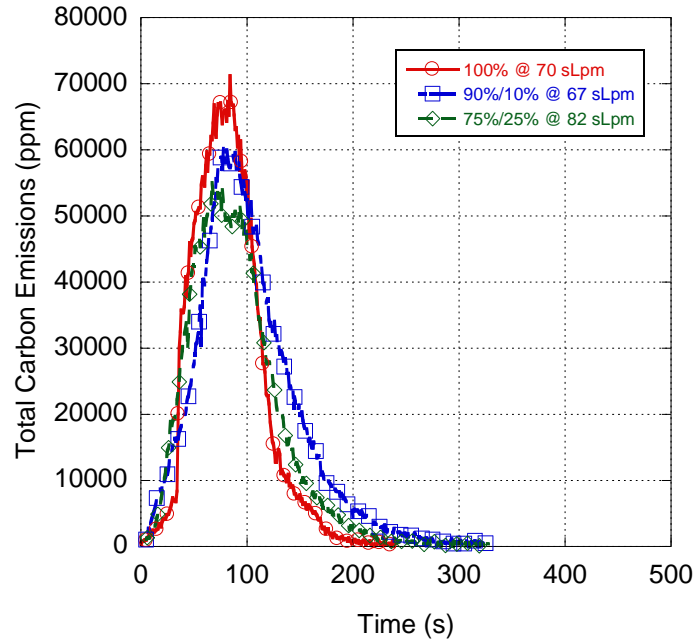
Figure 17 Normalized total carbon emission curves for three pine and algae pellet mixtures.
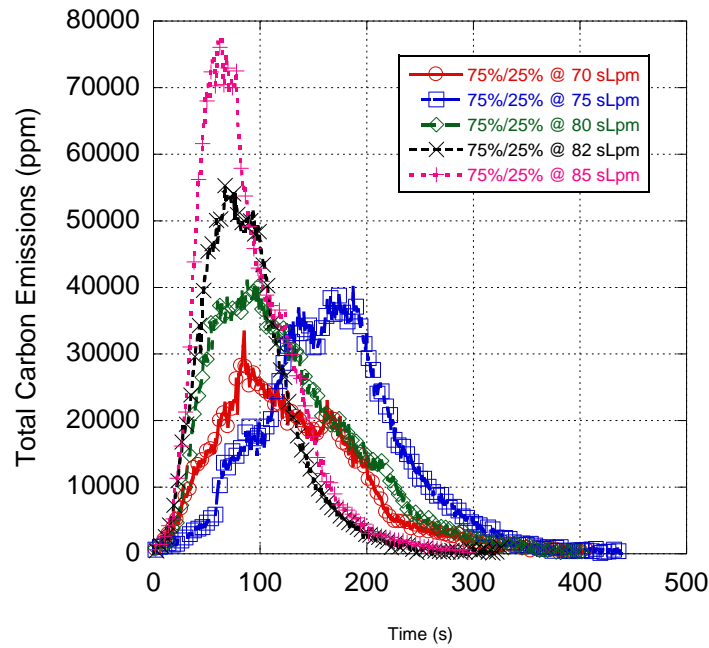
Figure 18 Total carbon emission curves for 75%/25% pine/algae pellets under several flow rates.

The flow rate used for the 75%/25% mixture is then adjusted in a similar method to the 90%/10% mixtures. Since its combustion rate is slower as compared to the purely pine mixture, its flow rate is increased to create a more oxidative environment. A sweep of tested flow rates is shown in Fig. 18 and generally the combustion rate grew with an increasing flow rate. When compared to the 100% and 90%/10% curves at 70 and 67 sLpm (respectively) in Fig. 17, the 82 sLpm curve has an initial slope and peak combustion time that agrees well with both. With the peak combustion time point normalized, the total combustion time is investigated.

Total combustion time normally accounts for fuel warm-up, devolatilization, and char oxidation [18]. These physical parameters are impossible for the current set up to measure directly. There are no thermocouples or other instrumentation in the fuel bed to monitor the fuel temperature, flame initiation or propagation, nor the current reaction state of the fuel within the bed. Thus, combustion time must be calculated solely from the data gathered. To that end, a MATLAB program is created to perform the necessary analysis. To begin, this MATLAB program first imported and then filtered the data. As can be seen in Figs. 10-14 and Figs. 16-18, the emissions measurements sent by the FTIR at a frequency of 1 Hz do not tend to graph smooth lines. Note that 1 Hz is not the sampling frequency of the FTIR itself, but the frequency that it sends data to the in-house data-logging program. This frequency is low because the program's initial usage with the lab's one cylinder compression ignition engine set up, which collects data for significantly longer periods of time and requires a low data collection frequency to avoid memory issues. Because of how the combustion endpoint is determined (to be discussed), the noise present in the measurements will negatively impact the accuracy of analysis and a method of mitigation is, therefore, needed for the data. A simple moving averages filter is

known to be effective at reducing the noise in low frequency signals without significantly influencing the overall trends of the data [63, 64].

The effects of a 5th order moving average filter applied to the data can be seen in Fig. 19. Although the peak combustion time is delayed slightly, the rise and decline in combustion rate remained similar in regards to time. Additionally, the graphs exhibit less noise after the filter, which is clearly exemplified around the 90 second and 200 second marks in Fig. 19. Not only is the sudden spike near peak combustion removed, but a sudden dip in emissions readings on the decline is also smoothed. Lessening the dip in the combustion emissions is especially important as it drastically improves the application of the MATLAB program, as will be elucidated later. First, the physical criteria for determining the start and endpoints of combustion must be discussed.
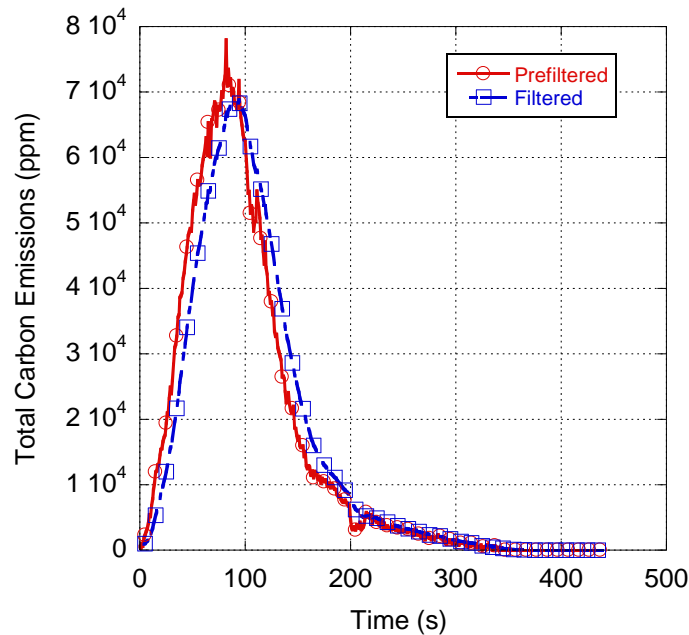
Figure 19 Total carbon emission curve for the normalized 100% pine data before and after a 5th order moving average filter is applied.

To determine these key points of combustion, their physical and mathematical definitions must be considered. The fuel warm-up aspect of the combustion start point is particularly difficult to describe empirically with the current set up. The absence of a temperature probe in the fuel bed, the focused nature of the glow plug ignition system, and the large surface area of the fuel as compared to the glow plug means that the warm-up of the fuel cannot be observed and that the fuel does not warm up as a single mass. Thus, the start of combustion time is considered the "light-off" point of the fuel, or the moment the first fuel pellets begin to combust. In the emissions data, this point is found by noting the time at which the slope of the total carbon emission curve begins to trend upwards. Furthermore, the ambient level of total carbon emission is set to below 1200 ppm. Typically, the ambient total carbon readings remained below 900 ppm, but could occasionally spike to above 1000 ppm for a single sample point, even without fuel in combustion bed. As a result, light-off of the fuel is calculated by finding the time point when the total carbon emission exceeded 1200 ppm with a positive slope and then retreating back toward the start point five data points. This retreat accounts for the warm-up period and initial devolatization periods of the fuel that precede combustion.

Combustion is considered complete when the slope of the total carbon emission curve effectively reaches zero and total carbon emission are similar to the ambient conditions before combustion began. Hence, the slope is defined as being close to zero when its absolute magnitude is less than 40 ppm s^{-1}, since the variance between data points even after the filter is still significant enough to prevent the slopes from falling below this benchmark. Even in Fig. 19 where the filtered curve looks smooth from roughly 200 seconds onward, the point-to-point slopes of the data can be nearly 80-90 ppm/s without significantly impacting the visual smoothness of the curve. Therefore, combustion ended when both the absolute value of the slope

is less than 40 ppm s^{-1} and when the total carbon emission are less than 1200 ppm. The time at the start point is then subtracted from the time at the endpoint to determine the total combustion time of the sample.

Seen in Table 9, the total combustion times of the 100% pine samples at 70 sLpm varied greatly from test to test, even with the amount of fuel held relatively constant. Despite these inconsistencies, Tables 10 and 11 indicate that there is generally a positive relationship between flow rate and total combustion time. In other words, as the flow rate increases, the total combustion time tends to decrease as to be expected with greater oxygen levels. Investigating the trends with algae content at 70 sLpm finds an inverse relationship between the amount of algae in the fuel mixture and the total combustion time. As seen in Table 6, algae have a lower fuel-bound oxygen level along with reduced energy content. Hence, algal-based pellets will burn colder and at a richer fuel-to-air ratio if the air flow rate remains constant resulting in a longer combustion time.

Table 9 Total combustion times calculated for each of the curves shown in Fig. 14 at a flow rate of 70 sLpm. An arithmetic mean is also calculated as the "Average" value of these tests.

Date	23-Nov-15						25-Nov-15		
Total Combustion Time [sec]	215	195	217	181	184	206	163	220	255
Date	30-Nov-15			5-Dec-15			1-June-16		12-July-16
Total Combustion Time [sec]	225	169	230	262	223	234	301	240	204
Date	19-June-16			29-June-16		18-July-16		Average	
Total Combustion Time [sec]	164	281	271	151	188	185	167	213	

Table 10 Total combustion times for several 90/10 pine/algae samples under separate flow rates, corresponding to Fig. 16.

Total Burn Time [sec]			
70 sLpm	67 sLpm	60 sLpm	50 sLpm
240	274	255	341

Table 11 Total combustion times for several 75/25 pine/algae mixtures under varied flow rates, corresponding to Fig. 18.

Total Burn Time [sec]				
70 sLpm	75 sLpm	80 sLpm	82 sLpm	85 sLpm
344	359	347	242	258

Table 12 Total combustion time for several pine/algae fuel mixtures at normalized flow rates, corresponding to the tests in Fig. 17.

Total Burn Time [sec]		
100 Pine 70 sLpm	90/10 67 sLpm	75/25 82 sLpm
206	274	242

Table 12 provides the combustion times for the attempt at normalizing the combustion rates between pellet mixtures. Overall, 100% pine is the fastest; whereas, 90%/10% is the slowest after normalization. Even though the theorized enhanced adhesion of algae may result in a faster light-off, the decrease in O_2 available for combustion (both through the flow rate and more algae) naturally limits the rate of combustion and lengthens the time of combustion. In contrast, increasing the inlet oxygen level (17.1% more oxygen by volume flow rate) for the 75%/25% pellets in order to overcome its lower energy content (12.8% less) results in it burning faster than the 90%/10% pellets.

Another parameter supporting this hypothesis is the maximum recorded temperatures of the 70 sLpm and normalized flow rate tests, shown in Tables 13 and 14, respectively. All of the algae containing mixtures exhibit lower energy content than the pure pine mixture, but also higher peak combustion temperatures as seen in both tables. If the increased adhesion of the algae-containing pellets interacts positively with the glow plug ignition system, it would keep

Table 13 Maximum recorded temperature from thermocouple data and estimated energy release for each pine/algae mixture at a flow rate of 70 sLpm, corresponding to Fig. 13.

Maximum Recorded Temperatures [°C]		
100% Pine	**90%/10%**	**75%/25%**
265.93	388.39	496.33
Estimated Total Energy Release [kJ]		
398.70	413.39	250.22

Table 14 Maximum recorded temperature from thermocouple data and estimated energy release for each pine/algae mixture at normalized flow rates, corresponding to Fig. 17.

Maximum Recorded Temperatures [°C]		
100% Pine @ 70 sLpm	**90%/10% @ 67 sLpm**	**75%/25% @ 82 sLpm**
265.93	460.92	473.01
Estimated Total Energy Release [kJ]		
398.70	392.99	391.49

more fuel near the glow plug's heat and increase the amount of material that lights-off. Then, the increased mass burning all at once would release enough energy to heat the algal mixture's

exhaust stream to a higher temperature than the pure pine exhaust. This increase in light-off material would also naturally speed the initial combustion rate observed; hence, allowing the 90%/10% mixture to match the 100% pine combustion with less air-bound oxygen as shown in Figure 17.

Support for this adhesion theory can also be seen in the estimated total energy release values presented in Tables 13 and 14. These approximations are determined using a MATLAB code for the process as described in Appendix A. At the standard flow rate of 70 sLpm, the 90%/10% test released more energy overall as compared to the pine tests and significantly more than the 75%/25% test. Hence, adhesion due to algae appeared to help the combustion process initially, but eventually the energy content of algae became the overriding factor. Interestingly, the normalized tests indicate a nearly uniform amount of energy released supporting the methodology presented. Decreasing the oxygen flow rate for the 90%/10% pellets reduced its energy release; whereas, increasing the oxygen flow rate for the 75%/25% pellets resulted in a nearly Equivalent energy release.

Of note, the temperature readings may not be as accurate as the energy release calculations. Comparing the 90%/10% maximum temperatures at both 70 sLpm and 67 sLpm indicates that the thermocouples' positioning may have had difficulty in consistently finding the hottest portion of the exhaust stream. Normally, it is expected that a higher air flow rate would produce hotter combustion conditions, as indicated by the 75%/25% measurements in Tables 13 and 14. However, the 90%/10% results in the same tables have the inverse trend showing a potential measure of inconsistency of temperature measurements.

Returning to Tables 6-8 to investigate fuel compositions may also reveal further explanations for the 90%/10% mixture's faster light-off as compared to the pure pine mixtures.

In Table 6, it is seen that algae possesses less fuel-bound oxygen and a lower level of fuel-bound carbon as compared to the pine used. Algae also have a reduced amount of hydrogen but more nitrogen and, in general, more trace and inorganic constituents in their make-up. The larger content of inorganics and trace elements means there is less combustible material (on a per unit mass basis) in the algae than the pine. Furthermore, the comparative reduction of carbon and hydrogen means that less oxygen would be required for complete combustion as well. Increasing the nitrogen content would offset this reduced oxygen demand somewhat, but carbon combusts into carbon dioxide (CO_2) under excess oxygen conditions while nitrogen will react to form predominately nitric oxide (NO) with further reactions required to produce nitrous oxide (N_2O) and nitrogen dioxide (NO_2) [65-69]. Thus, the reduced carbon content (which would require twice the oxygen per atom as compared to nitrogen) has a greater impact on the oxygen demand than the increase in nitrogen content. Therefore, the composition of the algae used indicates that less air bound oxygen would be required compared to the purely pine mixtures, subsequently reducing the flow rate required for algae-containing mixtures to reach complete combustion conditions; hence, faster light-offs. Again, once algae reaches a certain fraction of the pellet, its energy content becomes more dominant during the combustion process.

Another property of algae that helps explain the perceived discrepancies between expected theoretical trends and the experimental findings is that algae pellets are denser. Since the volume of material used during a test is kept relatively Equal from test to test, more mass is available during the 90%/10% tests for combustion (seen in Table 6). The first effect this increased mass would obviously have is to raise the amount of time needed for the algae-containing mixtures to combust since there is more material to be burned, which is consistent with the combustion times in Table 9. The second effect is that this greater mass could grow the

peak combustion temperature observed during the tests, despite algae's lower energy content. Particularly, if the reduced friability of the algae pellets does allow a greater volume of fuel to light-off initially, then a significant amount of additional fuel mass would combust at relatively the same time. This bigger release of energy would raise the combustor's temperature over the pine pellets. Thus, many of algae's negative thermal properties (compared to pine) appear to be offset somewhat by algae's chemical and physical properties, especially in a pelleted fuel application. The tested algae still possesses less than half the energy content of the pine used, however, and such a deficit can only be overcome to a degree.

In addition to conveying combustion rate information, Fig. 17 also shows that algae containing mixtures release less carbon than the pure pine mixture. Given algae's lower carbon content, this result is to be expected. Investigating the total NO_x emissions of the four samples, provided in Fig. 20, appears to follow the nitrogen trends presented in the fuel content data; i.e., NO_x emissions grow with fuel nitrogen level. However, before a definitive conclusion can be made, NO_x formation mechanisms must be explored in more depth.

Previous literature has determined that NO_x is primarily formed via three mechanisms in combustion applications: thermal, prompt, and fuel [67, 70, 71]. Thermal NO_x forms primarily through the combination of atomic oxygen and oxygen radicals with molecular and atomic nitrogen in the flame front [70, 71]. Often referred to as the Zeldovich mechanism, thermal NO_x is heavily dependent on the dissociation of oxygen and nitrogen molecules and is rate limited by high activation energy of 320 kJ mol^{-1} for its initial reaction step [71]. Thus, thermal NO_x is dependent on local temperatures and is found to be the dominant non-fuel NO_x mechanism in lean mixtures, particularly at elevated temperatures [70, 71].
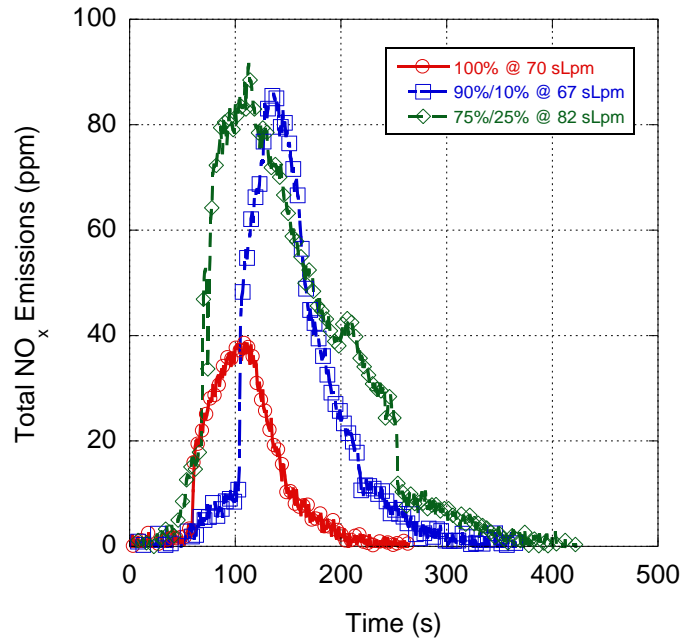
Figure 20 Total NO$_x$ emitted by different pine/algae mixtures under normalized conditions.
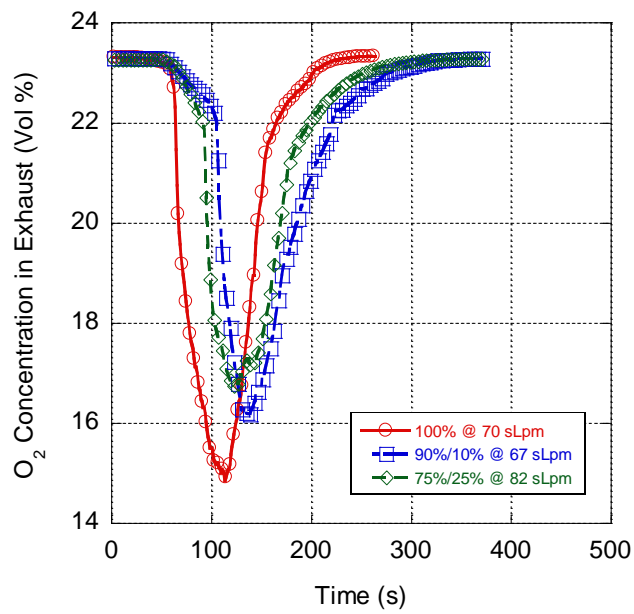
Figure 21 Volume percentage of O$_2$ emissions under normalized conditions.

Prompt, or Fenimore NO_x forms in the pre-flame-front regions of a combustion event, relying on the reaction of hydrocarbon radials (specifically CH) and molecular nitrogen [70, 71]. The prompt NO_x reaction has a lower activation energy than thermal NO_x, but is heavily dependent on the composition of the reacting gases [70, 71]. Since hydrocarbon radicals are most prevalent in more fuel-rich exhaust gases, prompt NO_x favors these conditions, and indeed becomes the primary source of non-fuel NO_x in sufficiently rich mixtures [70].

The final mechanism, fuel NO_x, begins with the formation of hydrogen cyanide (HCN) and ammonia (NH_3), which then reacts with hydroxyl (OH), hydrogen, and oxygen radicals to form NO. Fuel NO_x, similar to prompt NO_x, is strongly dependent on the composition of the gaseous environment, particularly on the amount of existing nitrogen compounds in the oxidizing fluid [67, 70, 71]. Properly interpreting Fig. 20 and algae's effects on the major NO_x mechanisms requires including Table 14, which displays the maximum recorded temperatures during the normalized tests.

Since combustion is lean with excess oxygen under all scenarios (see Figure 21), it can be inferred that prompt NO_x kinetics are negligible for all tests. Investigating combustion temperatures finds that the 75%/25% mixture has the highest values and, therefore, would produce the most thermal NO_x. This is providing that the mixtures are well away from stoichiometry, which appears to be the case in Figure 17 (note: maximum thermal NO_x is generated slightly lean of stoichiometry). Coupling the temperature findings with the greater amount of fuel-borne nitrogen in algae mixtures (found in Table 6) illustrates why the 75%/25% mixture has the greatest amount of NO_x emissions; whereas, the 100% pine mixtures emit a significantly smaller amount due to reduced temperatures and virtually no fuel-borne nitrogen.

Further review of the O_2 emissions in Fig. 21 shows that despite pine's increased mass content of oxygen, it consumes more atmospheric oxygen than the algal containing mixtures. This trend is not unexpected, however, because pine has a greater carbon and hydrogen content; thus, it requires more oxygen to combust completely. Moreover, pine's lower inorganic content is
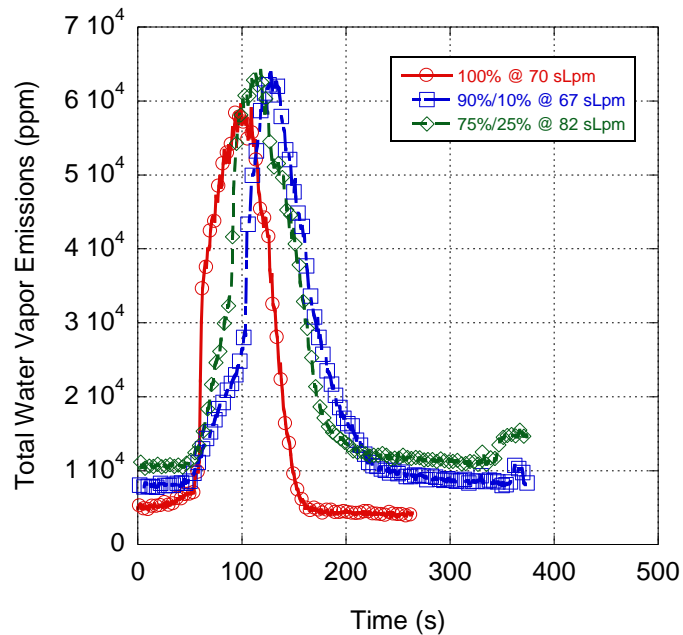
Figure 22 Total H$_2$O emitted during normalized testing of several pine/algae pellet mixtures.

important to mention since these species (e.g., silicates) tend not to combust and, therefore, would not add to overall oxygen consumption.

Even though pine's hydrogen content is greater and it utilizes more atmospheric oxygen, it has a lower water vapor emissions level as indicated in Fig. 22. In this figure, one can see that the 100% pine mixture has a lower ambient H_2O level than any of the algae samples, which lowers the water vapor emissions of the 100% test compared to the algal-containing tests, regardless of the fuel content. Accounting for this reduction would place pine's water vapor emissions near the same level as the other tests. Hence, here it appears that the increase in

hydrogen content of the pine's pellet is balanced by the reduced amount of fuel mass available to be burned. Differences in ambient conditions for SO_x emission are not as significant as H_2O ambient conditions, however, leading to easier comparisons between the SO_x produced by each blend.
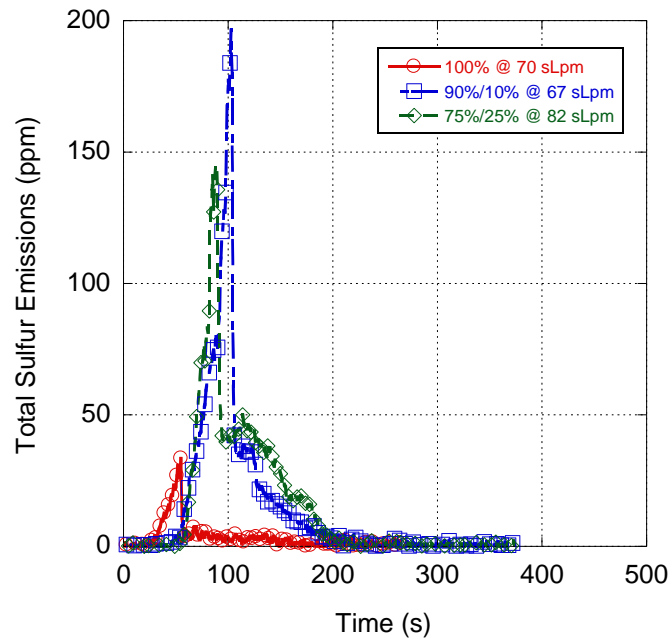
Figure 23 Total SO_x emissions of several pine/algae pellet mixtures under normalized combustion conditions.

As discussed in a previous section, many forms of algae possess a larger mass content of fuel-bound sulfur than woody biomasses. Thus, it is useful to compare the SO_x emissions produced by the three samples. Shown in Fig. 23, the SO_x emissions for the normalized tests show that macroalgae used for this study exhibit a greater fuel sulfur content than pine. Both algae containing mixtures exhibit much higher SO_x emissions peaks and a much greater total amount of SO_x emissions, as evidenced by the area under the individual curves in Fig. 23. However, the exact effect of the fuel bound sulfur and its interaction with other fuel effects is unclear from Fig. 23 since the 90%/10% curve processes a higher maximum SO_x reading than

the 75%/25%, despite the 90%/10% mixture's lower algae content compared to 75%/25%. Thus, more, and more specific testing, are conducted into the sulfur content of algae and its effect on sulfur oxide amounts in algal combustion emissions.

Initial testing conducted with the combustor has revealed significant information about the nature of macroalgal co-combustion with pine. With flow rates now determined to provide a normalized comparison between several pine and algae mixtures, more specific testing will provide even greater insight into algal combustion and co-combustion properties. When combined with additional analyses, such as calorimetry and ablation studies, substantial details of algae's application as a fuel can be determined.

3.5 Conclusion

The numerous environmental and logistical issues of current fossil fuel energy production can be alleviated, at least in part, by the utilization of biomass combustion and co-combustion. First and second generation biofuels are insufficient to meet growing energy demands, but third generation fuels such as macro- and microalgae could augment current biofuel supplies through combustion and co-combustion applications. However, since little is known regarding the specific combustion and co-combustion properties of algal biomass, a custom solid fuel burner is constructed and an experimental procedure developed to consistently burn several varied, pelleted mixtures of white pine and macroalgae. The initial goal of this study is to normalize the peak burn rates and combustion patterns in order to accurately compare each of the mixtures. The normalization studies focused on using comparisons of total carbon emission, total combustion times, and total energy release of various pine/algae fuel mixtures to match the peak combustion rates of algal mixtures to the pure pine fuel.

The normalization studies revealed that the flow rate of air provided to the combustion bed must be decreased slightly for a 90%/10% blend of pine/algae but increased for a 75%/25% mixture in order to align the peak burn times of these mixtures with the peak burn time of a pure pine mixture. The flow rate settings for the different mixtures are affected by the physical properties of the pellets, namely self-adhesion and density, in addition to the chemical makeup and energy content of the fuels. Specifically, the increased self-adhesion of algae allows the 90%/10% mixture to light off more quickly, requiring a decreased flow rate compared to 100% pine. In the 75%/25% mixtures, the lower energy and oxygen content of algae has a stronger influence on light-off and combustion than the self-adhesion of algae, and so air flow rate is increased for these tests. Further evidence for these conclusions is found in the total combustion times recorded for each test, which increase as the total available oxygen in the combustor bed (fuel-bound and air flow) decreases.

This normalization allowed for some initial observations of the emissions produced by each mixture. The pure pine mixture is found to release more carbon during combustion than either of the combinations of pine and algae that are tested, which is in keeping with the white pine's greater carbon content. Water vapor emissions are difficult to interpret due to major differences in the ambient H_2O of the air delivered to the bed during the individual tests. However, it appears that the different mass percentages of hydrogen and oxygen have little effect on the amount of water emitted during combustion of the biomass materials. Recorded NO_x emissions are in keeping with fuel chemical composition. Higher NO_x emissions are recorded for the algal mixtures than the pure pine test, with some variance due to exhaust temperature. The SO_x emissions also increased from the 100% pine to the algal mixtures, indicating a higher fuel sulfur content in the algae compared to pine.

Much work still remains in understanding algal combustion and co-combustion to the degree where it may be pursued for industrial and commercial applications. The above described combustor, pelleted fuel, and developed experimental procedure represents a significant first step towards filling this knowledge gap. Future work performed with this step-up, including tests with coal and coal/biomass mixtures in addition to more in-depth analysis of fuel content and its effect on total emissions, will add a great deal for current knowledge of third generation biofuels.

Chapter 4 – Coal-biomass fuel blend accelerant study

4.1 Abstract

Coal is specifically targeted by many groups for reduction and replacement as a fuel source in the power generation industry. One method of reduction is the co-firing of coal and biomass in a boiler. Woody biomass is popular for this role, but has many logistical shortcomings that could be eliminated by utilizing macroalgae instead. A combustion normalization study is proposed to gain insight regarding the direct co-firing of algae since little is currently known. Difficulties in igniting coal-containing fuel pellets are encountered during the attempted study lead to the proposal of an accelerant study. The accelerant study investigated the applicability of adding a small, measured amount of accelerant is added to the fuel prior to ignition to improve the fuel's combustion characteristics. The amount of accelerant require to meet these goals is found to increase with increasing coal content in the fuel blend, but it is found necessary to additionally increase the air flow rate provided to the bed in order to observe combustion closer to that observed by the purely biomass blends of previous experiments.

4.2 Introduction

Fossil fuels accounted for around 65% of the total energy input into the United States (US) electrical generation industry in 2016 [1]. Of the fossil fuels, coal consumed the majority of this figure, with 30% of the total energy input into the industry [1]. However, fossil fuels are well known producers of several gaseous emissions with severe environmental impacts. In particular, fossil fuels produce large amounts of carbon dioxide (CO_2) and nitrogen oxides (NO_x). Carbon dioxide is a greenhouse gas (GHG), trapping solar energy that enters the atmosphere and is considered to be the largest single contributor to a 0.6°C increase in the average yearly world temperature from 1900 to 2005 [16]. Similarly, nitrogen oxides are GHGs, but are more readily

known as a key precursor to ground-level smog formation and as a contributor to acid rain formation [14].

Coal is one of the dirtier fossil fuels, producing not only large amounts of CO_2 and NO_x relative to other fossil fuels, but also sulfur oxides (SO_x) and several trace element emissions such as mercury, arsenic, and even uranium [7-10]. These additional emissions are tied to acid rain, ground water pollution, and heavy metal poisoning amongst other health and environmental issues [8, 11, 14]. Even the mining and refining of coal can create regional environmental and human health crises if not properly regulated and handled [8, 11, 12]. Like all fossil fuels, coal is a limited resource with a practically finite amount available that some sources indicate will be depleted in as little as 50 years [4, 6, 24].

What is not a matter of conjecture, however, is the negative impact that emissions from fossil fuels power plants have on the atmosphere and annual world temperatures [16]. Currently, it is theorized that anthropogenic global warming must be kept to under a 2°C increase in global average temperature compared to 1900 in order to prevent irreversible damage to the world's environments [16, 27]. At current generation rates, this temperature increase could happen within three decades [34, 56]. Thus, many countries are seeking to reduce their usage of fossil fuels significantly, instead utilizing renewable energy sources that either produce no gaseous emissions during operation or are considered "carbon neutral" [13, 16, 40]. In particular, coal is targeted heavily for reductions with more extreme plans proposing the elimination coal entirely by the 2020s [13, 16, 24, 27, 29].

One proposed replacement for coal is solid biomass [30, 40, 41]. Currently, many plants in Europe and the Americas utilize coal and biomass co-combustion as a cost effective method to offset a portion of their coal usage while additionally reducing emissions of CO_2, NO_x, and SO_x

[30, 40, 60]. At present, biomass replacement of coal is limited to 5-20% (by energy) of the total mixture due to concerns regarding boiler efficiency and plant reliability [30, 60]. In this area, woody biomass is popular for this service because it is available in many regions, it is cheap and easy to store and process, and its energy content is relatively close to that of coal [24, 30, 40]. However, woody biomass as a fuel competes with lumber and pulp industries, and only a certain amount can be harvested during a specified time period for the resource to be considered practically renewable [33-35, 60]. Thus, there is interest in finding a dedicated energy crop that does not interfere with other industries or face food versus fuel competition.

One promising source of renewable solid biomass is macroalgae. Macroalgae is underutilized across the world, with the only significant market being Southeast Asia [46]. Additionally, algae does not compete for crop or forestry land like woody biomass, has superior CO_2 capture properties, does not require potable water, and can even be grown with flue gases from fossil fuel powered boilers [41, 43]. These traits have led to significant interest in both micro- and macroalgae as biofuel sources [5, 72, 73]. Relatively little research has been conducted, however, into algae's potential application in co-combustion systems with coal and air [43, 46]. Compared with woody biomasses, algae tend towards higher ash, moisture, and inorganics content while also possessing larger mass fractions of nitrogen and sulfur [46]. These compositional differences lead to algae possessing a lower heating value than woody biomass while also potentially resulting in increased NO_x and SO_x emissions from algal combustion (as compared to woody biomass). Thus, it is imperative that the co-combustion properties of algae with coal be thoroughly investigated.

As a result, the proposed methodology for an investigation into algae co-combustion is to use a purpose built fixed-bed solid fuel combustor and pelleted fuel mixtures to conduct a

normalization study. A similar method is employed in Chapter 2 to uncover the combustive and emissive properties of wood-algae co-combustion; however, this study focuses on coal-biomass blends, in particular coal-algae and coal-pine mixtures. Before the normalization study could be conducted, it is discovered that the experimental setup could not reliably ignite the coal-containing fuel mixtures. The addition of a small amount of petroleum distillate is proposed as a solution to heat and then ignite the coal pellets, similar to a charcoal grill. As a result, this effort describes the "accelerant studies" conducted to find the amount of lighter fluid necessary to reliably light the coal-containing mixtures for the normalization study.

The process used to determine the amount of petroleum distillates required to ensure light-off is first described in addition to a brief description of the fuels used. The results of the accelerant study are then presented along with a detailed discussion of the results and their practical meaning. A brief conclusion provides a general summary of the experimental procedures and results before providing paths for future investigation.

4.3 Methods

The accelerant study follows the same general combustion test procedure described in Chapter 3 and documented in Appendix A. First, the desired fuel mixtures for each test must be added to the fuel baskets in accordance with the basket-making procedure detailed in Chapter 3. The mixtures used in the accelerant study consistent of varying amounts of sub-bituminous coal from the Wyoming River Basin, white pine shavings from a wood shop, and dried macroalgae harvested from a local lake. Each of these materials is ground into a fine powder before mixing and making pellets. It is important that a consistent volume and orientation of the fuel pellets is added for all tests in an experimental session in order to ensure that a similar cross-section of fuel is exposed to the air flow. Because of the relatively small amount of coal that could be

obtained (in contrast to pine and algae) and the relative difficulty of reducing coal to a suitably small particle size, only about half the volume of coal fuel blends are added to a basket as compared to the biomass blends in Chapter 3. That is, only one layer of pellets is added for tests involving coal-containing fuel as opposed to the baskets with two layers as described for biomass fuel blends.

When constructing the baskets, material for two pre-burn baskets are also be made. Once all of the baskets are constructed, the solid fuel combustion set up is prepared as in Chapter 3 with all instrumentation attachments properly included and the LabVIEW and AVL control programs loaded. As in Chapter 3, the experimental test session begins with the combustion of the two pre-burn baskets made of approximately 50% newspaper clippings and 50% high algae (25-50% by mass) biomass fuel pellets. The pre-burns are designed to heat the combustion bed above a threshold temperature in order to ensure consistent combustion results. The pre-burn procedure begins by inserting the basket into the combustion bed portion of the combustor, then filling the basket with the fuel mixture. Next, the basket is checked for alignment with the glow plug insertion hole before the combustor tube is placed on top of the plenum in the shaped groove on the top plate. A glow plug then inserts into the hole at the bottom of the tube into a similar threaded hole in the combustor bed. This places the tip of the glow plug at the bottom of the fuel basket near the center point of the circular cross-section.

With the glow plug securing the combustor tube to the plenum, all instrumentation connections are checked and made secure before placing the exhaust hood on the top of the combustion tube. The flow rate on the Alicat flow controller is set to 70 sLpm, and a 12 VDC lead-acid car battery is connected to the glow plug so that current flows to the glow plug and its resistive element begins to heat, igniting the fuel in the combustor bed. Once ignition is

confirmed, the wires between the glow plug and the battery are removed to prevent damage to the plug or injury to the researchers. The pre-burn fuel is allowed to combust completely, and the set up is only be disassembled once no embers can be seen within the basket. After the combustor tube is removed, the pre-burn basket is taken outside to a storm drain where the ashes are dumped to prevent re-ignition in a fuel-rich environment. While the pre-burn basket is removed, the top mesh filter of the combustor tube is also removed and taken to the storm drain to remove built up ash. When both parts have been sufficiently cleaned, they are replaced, and the above procedure is repeated for the second pre-burn firing.

When the pre-burns are complete, instead of replacing the pre-burn basket, the first test fuel basket is inserted with the top mesh layer left off. While the ash is dumped, a graduated cylinder is filled with a pre-determined amount of Kingsford petroleum distillate charcoal lighter fluid. Petroleum distillate is a blanket term used to describe several compounds such as mineral spirits, kerosene, and Stoddard solvents in addition to solutions containing these compounds. A material safety data sheet from the lighter fluid manufacturer is provided in Appendix E [74]. Of note, the chemical species in lighter fluid are classified as petroleum naphtha that has a Lower Heating Value of 44.5 MJ kg^{-1} [75]. For the host of tests required for this study, the amount of added lighter fluid is set at 5 mL for the first test of a specific coal-biomass mixture. If necessary, this amount is then increased as needed up to 10 mL in order to ensure complete combustion of the fuel for subsequent tests of the same mixture. As mentioned previously, this lighter fluid addition is needed to ensure proper light-off and total combustion of the coal-containing fuel mixtures.

The petroleum distillates are then spread over the top of the fuel in the sample basket placed in the combustion bed, starting in the center of the basket and moving outwards. Care are

taken to make sure that at least half of the top area of the fuel pellets is covered with lighter fluid. After the lighter fluid is added to the basket, the top mesh layer is replaced and the combustor is reconstructed. After the burner's reassembly, the air flow rate from the Alicat is set and the glow plug is powered on, igniting the lighter fluid and relatively small portions of the solid fuel, with the heat from the lighter fluid igniting the majority of the solid fuel in the combustor bed. Once combustion ceases (or when there are no visible embers in the basket), the combustor is disassembled as with the pre-burn runs. All recorded data for the test is saved, and the set up through disassembly procedures are repeated for each assembled sample basket.

Flow rate settings for individual tests began at 70 sLpm for the initial test of a particular fuel blend, but are adjusted on successive tests once petroleum distillate addition amounts had been determined for the blend. For the accelerant tests, only the set flow rate, the temperature profiles from the thermocouples, and the Smoke Meter measurements are recorded. In part, this is due to the FTIR being under repairs for part of the study. However, careful visual and timed observations are made for each test in order to ensure the study's accuracy and success.

4.4 Results

Similar to the normalization studies, a "baseline" fuel mixture and flow rate setting is chosen for comparison to ensure consistent results and conclusions. For the accelerant study, a 50%/50% (by mass) mixture of sub-bituminous coal and white pine acts as the baseline mixture and 70 sLpm is the chosen flow rate setting. Table 15 presents the light-off and combustion characteristic observations for several coal-biomass fuel mixtures under a baseline petroleum distillate inclusion. Furthermore, the lighter fluid supplements producing the best light-off and

Table 15 Observations of combustion behavior for four coal-biomass fuel mixtures with 70 sLpm air flow rate and 5 mL petroleum distillates addition.

Fuel Composition [%mass]	50%/50% coal/pine	90%10% coal/pine	90%10% coal/algae	50%/37.5%/12.5% pine/coal/algae
Light-off Observations	Fast	Fast	Fast	Fast
Total Combustion Time [min]	4-4.5	10-10.5	10-10.5	5-5.5
Combustion Intensity	• Pellets orange-hot • Smoldering/no flames	• Pellets orange-hot • Smoldering/no flames	• Pellets orange-hot • Smoldering/no flames	• Pellets orange-hot • Smoldering/no flames

Table 16 Observations of combustion behavior for four coal-biomass fuel mixtures under "optimal" accelerant and flow rate conditions.

Fuel Composition [%mass]	50%/50% coal/pine	90%10% coal/pine	90%10% coal/algae	50%/37.5%/12.5% pine/coal/algae
Accelerant Addition [mL]	5 mL	10 mL	10 mL	5 mL
Air Flow Rate [sLpm]	100	250	110	150
Light-off Observations	Fast	Fast	Fast	Fast
Total Combustion Time [min]	3-3.5	4	7-7.5	2.5
Combustion Intensity	• Pellets orange-hot • Smoldering/no flames • Some material ejection upwards	• Pellets orange-hot • Numerous, small, isolated flames • Significant material ejection upwards	• Pellets orange-hot • Limited, small, isolated flames • Some material ejection upwards	• Pellets orange-hot • Small, isolated flames • Some material ejection upwards

combustion characteristics are presented in Table 16. Of primary importance here is the relationship between coal content and lighter fluid addition; namely, a greater coal content requires a more substantial lighter fluid addition necessary to achieve proper light-off and total combustion of the solid fuel mixture. Note, however, that observed light-off of the fuel in the bed appears to be unaffected by the amount of accelerant added. Since the petroleum distillates light off first and subsequently heat the solid fuels to their ignition temperatures, the observed light off during these tests is dependent on the heat transfer rate from the glow plug to the petroleum distillates, which remains relatively constant.

Tables 15 and 16 further show that the fuel mixtures containing 90% coal by mass require 10 mL of petroleum distillates in order to display combustion characteristics closer to the 50%/50% coal/pine baseline case. However, simply adding lighter fluid is not sufficient to induce combustion of the coal-containing fuel pellets. Experimental observations in Chapter 3 found that increasing the airflow rate to the combustion bed has a significant influence on the total burn time and observed combustion characteristics. Table 16 illustrates that increasing the air flow rate shortens the total combustion time and improves the intensity of the combustion of the solid fuel mixtures in this study.

Several discrepancies in the given data and observations (particularly Table 16) require further discussion. Perhaps most notable are the flow rates used in the optimal combustion performance cases, which vary from 100 sLpm for the 50%/50% coal/pine mixture to as great as 250 sLpm for the 90%/10% coal/pine mixture. This variation is due in part to the innate variability of the combustor and its physical limitations, along with coal's significantly different physical properties as compared to the two biomass fuels (especially in pelleted fuel applications). The combustor's variability is thoroughly discussed and demonstrated in Chapter

3, and further elucidation on this subject would not add to this particular discussion. Instead, attention are focused on the more significant contributors in the case of this acceleration study: the limits of the combustor's design and the physical differences between coal and biomass.

As previously stated, a baseline flow rate tense arbitrarily chosen for both the normalization efforts of Chapter 3 and the current acceleration study. The reference flow rate of 70 sLpm is chosen because previous testing demonstrates that this setting produces reasonable combustion results with 100% pine samples while also being a low enough flow rate that combusting particles would not carry up the combustor tube toward the room exhaust system [62]. Such an event is identified as a major safety concern in previous work, and is thus carefully avoided [62]. During the accelerant study, however, it became evident that flow rate settings near 70 sLpm would not be able to produce adequate complete combustion in coal-biomass blends. A higher flow rate setting is needed, but testing with these higher flow rate settings revealed that material ejection from the combustion bed is still a serious concern.

Table 17 Combustion times and observations for 50%/50% coal-pine mixture tests with 5 mL petroleum distillate additions under several flow rates.

Fuel Composition [%mass]	50%/50% coal/pine		
Air Flow Rate [sLpm]	70	100	250
Light-off Observations	Fast	Fast	Fast
Total Combustion Time [min]	4-4.5	3-3.5	6-6.5
Combustion Intensity	• Pellets orange-hot • Smoldering/no flames	• Pellets orange-hot • Smoldering/no flames • Some material ejection upwards	• Pellets orange-hot • Smoldering/no flames • Significant material ejection upwards

This issue came to the forefront during a 150 sLpm test with the 50%/50% coal/pine when a noticeable increase in temperature is noted along the entry of the room exhaust hood. The flow rate is immediately reduced to 90 sLpm to avoid damage to the experimental set up but is increased to 100 sLpm during the next test, producing the 50%/50% data in Table 16 without endangering the facilities. Following this test session, an extra stainless steel wire mesh layer is added to the top of the combustor so that its grain is at a roughly 45° angle to the grain of the first mesh layer. The opening size of the mesh on the top of the combustor is effectively reduced by this change, reducing the size and amount of material that could leave the combustor and enter the exhaust system.

This upgrade allow for application of greater air flow rates during combustion tests without risking ignition of the exhaust system. Further experimentation in this direction yields the 90%/10% coal/algae test in Table 16, which demonstrates the effectiveness of increasing air flow rates to improve the combustion of coal fuel blends. Increasing the air flow rate by 180 sLpm from the baseline setting of 70 sLpm yielded an approximately six minute decrease in total combustion time, as well as visibly improved combustion intensity. Similar, albeit smaller, decreases in total combustion time along with a growth in combustion intensity are seen in the results from Table 2 for the 90%/10% coal/algae and the two lower coal-content blends as compared to their corresponding Table 15 results.

It is interesting to note that the recorded observations for the 250 sLpm flow rate test performed with the 50%/50% coal/pine mixture yields slightly worse performance as compared to both the 100 sLpm and the 70 sLpm tests, as found in Table 17. With 250 sLpm of air flow, the 50%/50% mixture yields a total combustion time of around 6 to 6 ½ minutes. It is theorized that the greater composition of less dense and more friable pine particles in these pellets as

compared to the 90% coal mixtures lead to an increase in material ejections, carrying burning material away from the combustor bed before it could be completely consumed. These ejections, in turn, inhibited flame propagation and reduces the bed temperature to a level less suitable for coal combustion than is occurring in the 90% coal mixture tests. Thus, the benefits of an increased air flow are counteracted in the less dense, high biomass content fuel mixtures. Hence, it appears that coal requires a greater air flow in order to combust completely, and its increased density and relatively secure adhesion enables higher flow rates to be used more safely than with the biomass-only fuel blends.

Note that the reduced flow rate settings of the 90%/10% coal/algae and 50%/37.5%/12.5% blends in Table 16 are not due to poor results, but rather a lack of results. An attempt is made for a 250 sLpm test using the 90%/10% coal/algae pellets after the 90%/10% coal/pine test listed in Table 16. The newly installed double layer mesh at the top of the combustor tube had become choked with soot and ash from previous tests that did not fall out when the baskets are changed. As a result, when the AVL Smoke Meter back-flushed during this test (as it is designed to do after finishing a set of Particulate Matter measurements), the combined blocked exhaust flow and added back flow pushed material from the combustor tube and bed out of the setup from the gap between the plenum and the combustor tube. This included not only exhaust gases, but also some embers and other combusting materials that rendered further testing unsafe. The test is aborted using the emergency stop procedure outlined in Appendix A, preventing injury to the researchers and damage to the setup, but also precluding useable data and observations from being recorded. Since the 250 sLpm test for the 50%/37.5%/12.5% mixture is scheduled to occur after this test, it is cancelled due to these safety concerns. This incident additionally lead to an update of the burner procedure requiring that the

top mesh of the combustor tube be cleaned after every combustion test so that similar exhaust ejections are avoided.

The accelerant study, although relatively limited in scope and analysis capability, provided a significant amount of information to hasten the collection and analysis of practical results from future coal-biomass normalization studies. It is found that a petroleum distillate addition to the combustor bed prior to glow plug ignition is capable of aiding coal light-off and combustion. In order to guarantee adequate results for all fuel mixtures with 50% mass content of coal or greater, the addition of 10 mL of petroleum distillate are evenly distributed on the top of the fuel pellet layer. Beyond its original scope and primary objective, the accelerant study also lead to several additional modifications to the original setup and procedure for the coal-biomass normalization study. Namely, an increased flow rate (150 sLpm or greater) appears to be ideal for ensuring complete combustion of coal. Because of this observation, a small upgrade is added to the combustor in the form of a smaller opening mesh filter at the top of the combustor. This upgrade, in turn, required an update to the burner experimental procedure. Making these discoveries ahead of the normalization study will improve the accuracy of the data collected during those experiments while reducing the total number of experiments, subsequently reducing wasted fuel material.

4.5 Conclusions

Coal combustion in the power generation industry accounts for a significant addition of CO_2 and other GHGs to the atmosphere. These emissions can be curtailed through the usage of biomass as a substitute for a portion of the coal in a process known as co-combustion. Woody biomass is currently popular in this application but macroalgae has considerable potential

advantages that merit its investigation as a potential co-combustion fuel. Few details regarding algal direct co-firing are known, however, prompting the current investigation.

A combustion normalization process similar to one outlined in a previous work is proposed, but issues arose when attempting to ignite coal-containing fuel pellets. Thus, the normalization procedure is modified to allow for a small addition of petroleum distillate to the fuel bed as an accelerant to raise the coal to ignition temperature and incite complete combustion similar to the combustion observed in purely biomass fuel blends. A new study is undertaken to determine the minimum accelerant addition necessary to achieve these goals for all potential blends of coal and biomass.

It is found that the amount of accelerant needed to achieve proper combustion of the carbon in the bed is proportional to the mass content of coal in the fuel blend. As little as 5 mL of accelerant could be added to blends containing 50% or less coal by mass, while the 90% coal mixtures required larger, 10 mL additions. However, in both cases the lighter fluid, although necessary, is not sufficient to incite the same degree of combustion as in the purely biomass tests from Chapter 3. Thus, the air flow rates provided to the combustion bed via the Alicat flow controller are also increased by varying amounts. Increasing the flow rate to 250 sLpm yielded significantly reduced total combustion times for the 90% coal fuel blends. The 50%/50% coal/pine blend experienced as slight decrease in combustion time as well up to around 100 sLpm, but combustion times increases slightly beyond this setting. Currently, it is believed that the pine's more friable nature and reduced density increases the amount of material ejected from the bed by these higher flow rates. These ejections are further theorized to be removed before complete combustion can occur, removing a significant amount of energy from the bed and slowing combustion.

Several weaknesses in the combustor's design are also discovered during this study, leading to a number of small updates in the combustor's design and operation. Overall, the accelerant study provided an extensive amount of information to ensure that the proposed coal-biomass normalization study will proceed uninhibited in the future. Accelerant additions and increased flow rate settings will help ensure that accurate and meaningful data can be collected while wasting a lesser amount of resources than would otherwise be expected. The combustor upgrades and operational changes aid this same goal, but additionally increase the operational safety of the burner. Lastly, observations recorded during this study give a degree of insight into how the physical characteristics of coal will alter the expected combustion trends set by the purely biomass combustion tests.

Chapter 5 – Conclusions and Future Work

Coal is an important component in the United States' current energy portfolio, accounting for nearly half of the total electricity generated from fossil fuels. However, coal also suffers from numerous environmental and health issues with the capacity to emit more GHG per ton than other fossil fuels and the inclusion of multiple heavy metals and carcinogens in its trace elements and inorganics composition. Because of these serious issues, replacements for coal are highly desired, as are shorter term mitigation solutions. Of the numerous potential competitors for coal, solid biomass firing and co-firing has garnered significant attention in recent years as a method to reduce, and potentially eliminate, coal usage.

Woody biomass in particular has proven a popular choice in many countries, especially in Europe and parts of the US. Woody biomass is relatively easy to implement as a co-firing fuel since it is easy to dry and process as compared to other biomass sources. Woody biomass also processes a relatively high energy content among biomass sources. However, woody biomass is utilized by several additional, large industries and increasing the amount of woody biomass used for power generation (to further reduce or eliminate coal usage) when combined with existing demand from other industries could quickly deplete the world's woody biomass. Such an occurrence would cause negative and likely irreparable environmental changes; thus, researchers are looking for underutilized biomass sources that could be used to replace woody biomass in coal-biomass co-firing facilities.

One potential source is macroalgae, which is generally underutilized in nearly all regions of the world. Algae are also relatively easy to grow and possess yield potentials that outpace terrestrial biomasses, without needed potable water or arable land to accomplish these yields. Algae is more difficult to dry and process adequately than woody biomass, however, and its composition tends towards higher nitrogen, sulfur, inorganics, and ash content than woody

114

biomasses, leading to concerns regarding emissions and reliability in algae co-firing facilities. Little research has been conducted into the direct co-firing of algae, however, so these concerns cannot be adequately discussed. As a result, a fixed bed solid fuel combustor is constructed for the purpose of combusting algae-containing fuel mixtures and uncovering the emissions and combustion characteristics of algae co-firing. Gaseous and particulate emissions data is recorded by an AVL FTIR and an AVL Smoke Meter (respectively) while thermocouples recorded exhaust stream temperatures and an Alicat MCR-500sLpm flow controller both altered and reported the normalized flow rate of air to the combustor bed and fuel.

The primary method of investigation is initially proposed to be a normalization study in which the light-off and maximum burn rate times and characteristics of multiple biomass fuel blends are adjusted using the air flow rate to the combustion bed to be similar to a chosen base case. Later, an optimization study, in which the air flow rates are adjusted to provide the most thorough and complete combustion possible for a fuel blend, is additionally proposed. The first step in the proposed study is to determine a method by which to measure the total mass burned during a test, so that this figure could be compared to the total fuel added to the bed to determine the thoroughness of combustion. The resulting method utilized the emissions data provided by the FTIR in addition to several known or directly calculable properties of the emission species to determine the total mass emitted of carbon containing emission species during a burn. The total mass of fuel burned could then be determined using mass fractions of carbon for those species and the carbon mass content of the fuel blend being burned.

The results of this resulting model proved to be reasonably accurate in air flow rate ranges associated with normalized combustion, with non-normalized combustion clearly distinguishable by either a large amount of unburned fuel or a falsely large amount of fuel

burned. Although not as detailed as a second model developed in Chapter 3, this model is slightly more accurate and is easier to use in situ during the combustion tests, which can allow for more rapid and accurate adjustments to subsequent tests. Thus, using this model during future optimization studies of algae-containing fuel blends can potentially reduce the number and length of the testing required to gather accurate and meaningful data.

Although the final results of the model are promising, there are mistakes made initially that lead to the proposal of a flow rate validation study for the Alicat flow controller. Such studies are important in order to ensure the accuracy of experimental data and the health of the flow controller, so despite the final results of the model, this study is considered to be a worthy opportunity. A simple and proven instrument for flow validation is chosen for the experimental setup: the Pitot-static tube. However, implementation of the Pitot-static tube proved to be difficult, and ultimately it is found that the designing experimental set up utilized too large of a final pipe diameter. The diameter of the pipe meant the air flow is still expanding when it met the Pitot tube, resulting in inaccurate measured flow rates. The flow rate of the Alicat is validated through other data reported by the flow controller and calculations made from this data. However, important lessons are learned regarding the design and implementation of Pitot tube flow validation experiments, especially in spaces with little usable volume.

The work completed in Chapter 2 is meant to exist as a tie-in to the original normalization study outlined and discussed in Chapter 3. Here, the solid fuel combustor is used to burn three pelleted mixtures of pine and algae: 100% pine, 90%/10% pine/algae, and 75%/25% pine/algae. The pure pine pellets are selected as a base since the power generation industry has already accepted woody biomass usage for co-firing and because the combustion properties of pine are generally well known and provide a good basis of comparison. The first

step of the normalization study is to adjust to flow rates for each blend in order to normalize the light-off and maximum combustion rate characteristics of each fuel blend to the base case. A flow rate of 70 sLpm is selected as the baseline flow rate for the 100% pine pellets and flow rates of 67 sLpm and 82 sLpm for the 90%/10% and 75%/25% mixtures, respectively, are found to match the baseline case relatively well. The 75%/25% result is expected because of algae's lower energy content and higher inorganics composition compared to pine, the 90%/10% increased flow rate is not expected for the same reasons. The lower normalized flow rate of the 90%/10% mixture is likely due to algae's increased adhesion and density compared to pine, which allowed more fuel to ignite initially than the pure pine's more friable, less dense pellets.

In general, the emissions results from the biomass normalization study are in keeping with expectations based on fuel composition. Carbon containing emissions increased with increasing pine content, while NO_x and SO_x increased with increasing algae content instead. Greatly different ambient H_2O conditions between tests prevents conclusive analysis of the water vapor emissions, however, which are intended as a method to quantify the amount of hydrogen burned during combustion. Additionally, the exhaust streams for the algae-containing tests are, on average, hotter than the exhaust of the purely pine test. Since NO_x formation is highly dependent on temperature and can be formed through dissociation as well as fuel oxidation, some of the difference in NO_x emissions may not be due to the algae's chemical composition.

Before further inquiry in those results could be performed, however, it is desirable to conduct a normalization study on coal-biomass mixtures. During early attempts to gather such data, difficulty is encountered in lighting off the coal-containing pellets. The proposed solution for this issue is to add a small amount of lighter fluid to the fuel just before powering the glow plug ignition system. The amount of lighter fluid needed, however, in addition to other changes

that might be necessary to accommodate the lighter fluid or to further improve the combustion of coal in the setup, is unknown. A study is therefore performed by modifying the normalization procedure in order to determine the amount of lighter fluid require to ignite coal fuel blends.

The study itself quickly found that a 10 mL addition of petroleum distillate lighter fluid is necessary, but not sufficient, to achieve the desired combustion properties in high coal content fuel mixtures. Further experimentation found that coal-biomass blends responded well to air flow rates increased to or above 100 sLpm. However, such high air flow rates had a tendency to eject matter out of the combustion bed and into the exhaust system, creating a potential fire hazard. The open area of the mesh on the top of the combustor tube is reduced to prevent such ejections from damaging the exhaust, but the change also means the mesh needs to be cleaned after every burn to prevent material ejection into the test cell. Overall, the accelerant study left the experimental setup and procedures in good position to complete the proposed coal-biomass normalization study once repairs on other instrumentation are complete.

Much information regarding algae co-firing is gleaned from the experiments reported in this work, but more must be known in order to safely and effectively implement algae-coal co-firing at an industrial scale. The proposed coal-biomass normalization study will add significantly to the knowledge gathered thus far. A potential optimization study for both biomass and coal-biomass fuel blends will also contribute useful information regarding the conditions under which algae co-firing becomes most effective at reducing emissions and/or combusting the fuel most efficiently. Compared to established fossil fuels, knowledge of algal biomass combustion is decades behind, but could reveal an effective and sustainable replacement for one of mankind's largest GHG producers.

References

1. *EIA Annual Energy Outlook 2017*, U.S.D.o. Energy, Editor. 2017, Energy Information Administration.
2. *Short Term Energy Outlook: Electricity Forecast*. 2017 [cited 2017 18 June]; Available from: https://www.eia.gov/outlooks/steo/report/electricity.cfm.
3. van den Berg, M., et al., *Exploring resource efficiency for energy, land and phosphorus use: Implications for resource scarcity and the global environment.* Global Environmental Change, 2016. **36**: p. 21-34.
4. Sener, C. and V. Fthenakis, *Energy policy and financing options to achieve solar energy grid penetration targets: Accounting for external costs.* Renewable and Sustainable Energy Reviews, 2014. **32**: p. 854-868.
5. Giostri, A., M. Binotti, and E. Macchi, *Microalgae cofiring in coal power plants: Innovative system layout and energy analysis.* Renewable Energy, 2016. **95**: p. 449-464.
6. Heede, R. and N. Oreskes, *Potential emissions of CO2 and methane from proved reserves of fossil fuels: An alternative analysis.* Global Environmental Change, 2016. **36**: p. 12-20.
7. Tiwary, R.K., *Environmental Impact of Coal Mining on Water Regime and Its Management.* Water, Air, and Soil Pollution, 2001. **132**(1): p. 185-199.
8. Yudovich, Y.E. and M.P. Ketris, *Mercury in coal: a review.* International Journal of Coal Geology, 2005. **62**(3): p. 107-134.
9. Hvwastendahl, M., *Coal Ash Is More Radioactive Than Nuclear Waste*, in *Scientific American*. 2007, Scientific American: www.scientificamerican.com.
10. Kolker, A.e.a., *Arsenic in Coal*. 2006, U.S. Geological Survey: pubs.usgs.gov.
11. *Radioactive Elements in Coal and Fly Ash: Abundance, Forms, and Environmental Significance*. 1997, U.S. Geological Survey: pubs.usgs.gov.
12. Staudt, J.E., *Control technologies to reduce conventional and hazardous air pollutants from coal-fired power plants.* Report prepared for Northeast States for Coordinated Air Use Management. http://www. nescaum. org/documents/coal-control-technology-nescaum-report-20110330. pdf, 2011.
13. *Connecticut Greenhouse Gas Emissions: Mitigation Options Overview and Reduction Estimates*. 2010, Northeast States for Coordinated Air Use Management: http://www.nescaum.org.
14. Crutzen, P.J. and J. Lelieveld, *Human impacts on atmospheric chemistry.* Annual review of earth and planetary sciences, 2001. **29**(1): p. 17-45.
15. Seguin, A.M., et al., *Elevated biogenic sulphur dioxide concentrations over the North Atlantic.* Atmospheric Environment, 2010. **44**(9): p. 1139-1144.
16. Kalogirou, S.A., *Solar Energy Engineering - Processes and Systems (2nd Edition)*. Elsevier.
17. Eichhorn, M., P. Tafarte, and D. Thrän, *Towards energy landscapes–"Pathfinder for sustainable wind power locations".* Energy, 2017.
18. Fearnside, P.M., *Environmental and social impacts of hydroelectric dams in Brazilian Amazonia: Implications for the aluminum industry.* World Development, 2016. **77**: p. 48-65.
19. Grimardias, D., J. Guillard, and F. Cattanéo, *Drawdown flushing of a hydroelectric reservoir on the Rhône River: Impacts on the fish community and implications for the sediment management.* Journal of Environmental Management, 2017. **197**: p. 239-249.
20. Nguyen, T.T., D.A. Sheppard, and C.E. Buckley, *Lithium imide systems for high temperature heat storage in concentrated solar thermal systems.* Journal of Alloys and Compounds, 2017. **716**: p. 291-298.
21. Villacreses, G., et al., *Wind farms suitability location using geographical information system (GIS), based on multi-criteria decision making (MCDM) methods: The case of continental Ecuador.* Renewable Energy, 2017. **109**: p. 275-286.

22. *Levelilzed Cost and Levelized Avoided Cost of New Generation Resources in the Annual Energy Outlook 2017*. 2017, Energy Information Administration: www.eia.gov.

23. Davis, S.C., K.J. Anderson-Teixeira, and E.H. DeLucia, *Life-cycle analysis and the ecology of biofuels.* Trends in plant science, 2009. **14**(3): p. 140-146.

24. Saidur, R., et al., *A review on biomass as a fuel for boilers.* Renewable and Sustainable Energy Reviews, 2011. **15**(5): p. 2262-2289.

25. Munir, S., W. Nimmo, and B. Gibbs, *Shea meal and cotton stalk as potential fuels for co-combustion with coal.* Bioresource technology, 2010. **101**(19): p. 7614-7623.

26. Robinson, A., J. Rhodes, and D. Keith, *Assessment of potential carbon dioxide reductions due to biomass-coal cofiring in the United States.* Environmental science & technology, 2003. **37**(22): p. 5081-5089.

27. Rockström, J., et al., *A roadmap for rapid decarbonization.* Science, 2017. **355**(6331): p. 1269-1271.

28. Voloshin, R.A., et al., *Review: Biofuel production from plant and algal biomass.* International Journal of Hydrogen Energy, 2016. **41**(39): p. 17257-17273.

29. van den Berg, M., et al., *Exploring resource efficiency for energy, land and phosphorus use: Implications for resource scarcity and the global environment.* Global Environmental Change, 2016. **36**: p. 21-34.

30. Darvell, L., et al., *Combustion properties of some power station biomass fuels.* Fuel, 2010. **89**(10): p. 2881-2890.

31. Hamelinck, C.N., R.A. Suurs, and A.P. Faaij, *International bioenergy transport costs and energy balance.* Biomass and Bioenergy, 2005. **29**(2): p. 114-134.

32. Loeffler, D. and N. Anderson, *Emissions tradeoffs associated with cofiring forest biomass with coal: A case study in Colorado, USA.* Applied Energy, 2014. **113**: p. 67-77.

33. Dolisca, F., et al., *Land tenure, population pressure, and deforestation in Haiti: The case of Forêt des Pins Reserve.* Journal of Forest Economics, 2007. **13**(4): p. 277-289.

34. Kautto, N. and P. Peck, *Regional biomass planning–Helping to realise national renewable energy goals?* Renewable energy, 2012. **46**: p. 23-30.

35. Kosinkova, J., et al., *Measuring the regional availability of biomass for biofuels and the potential for microalgae.* Renewable and Sustainable Energy Reviews, 2015. **49**: p. 1271-1285.

36. Ghadiryanfar, M., et al., *A review of macroalgae production, with potential applications in biofuels and bioenergy.* Renewable and Sustainable Energy Reviews, 2016. **54**: p. 473-481.

37. Bioenergy, I., *From 1st-to 2nd-Generation BioFuel technoloGies.* An overview of current industry and RD&D activities. IEA-OECD, 2008.

38. Kijo-Kleczkowska, A., et al., *Experimental research of sewage sludge with coal and biomass co-combustion, in pellet form.* Waste Management, 2016. **53**: p. 165-181.

39. Kijo-Kleczkowska, A., et al., *Combustion of pelleted sewage sludge with reference to coal and biomass.* Fuel, 2016. **170**: p. 141-160.

40. Demirbaş, A., *Sustainable cofiring of biomass with coal.* Energy Conversion and Management, 2003. **44**(9): p. 1465-1479.

41. Dragone, G., et al., *Third generation biofuels from microalgae.* Current research, technology and education topics in applied microbiology and microbial biotechnology, 2010. **2**: p. 1355-1366.

42. Lee, R.A. and J.-M. Lavoie, *From first-to third-generation biofuels: Challenges of producing a commodity from a biomass of increasing complexity.* Animal Frontiers, 2013. **3**(2): p. 6-11.

43. Milledge, J.J. and S. Heaven, *Methods of energy extraction from microalgal biomass: a review.* Reviews in Environmental Science and Bio/Technology, 2014. **13**(3): p. 301-320.

44.	Milledge, J.J., B.V. Nielsen, and D. Bailey, *High-value products from macroalgae: the potential uses of the invasive brown seaweed, Sargassum muticum.* Reviews in Environmental Science and Bio/Technology, 2015: p. 1-22.

45.	Gao, Y., et al., *Combustion characteristics and air pollutant formation during oxy-fuel co-combustion of microalgae and lignite.* Bioresource technology, 2016. **207**: p. 276-284.

46.	Milledge, J.J., et al., *Macroalgae-derived biofuel: a review of methods of energy extraction from seaweed biomass.* Energies, 2014. **7**(11): p. 7194-7222.

47.	*"Optimization"*. 2017 [cited 2017 4 Aug]; Available from: https://www.merriam-webster.com/dictionary/optimization.

48.	Murr, F., E. Winklhofer, and H. Friedl, *Reducing Emissions and Improving Fuel Economy by Optimized Combustion of Alternative Fuels*. 2011, SAE Technical Paper.

49.	Widmer, N.C., et al., *Combustion optimization for fossil fuel fired boilers*. 2010, Google Patents.

50.	Xiao, H. and A. Valera-Medina, *Chemical Kinetic Mechanism Study on Premixed Combustion of Ammonia/Hydrogen Fuels for Gas Turbine Use.* Journal of Engineering for Gas Turbines and Power, 2017. **139**(8): p. 081504.

51.	González, N.F., J.C. Kindelán, and J.M.L. Martí, *Methodology for instantaneous average exhaust gas mass flow rate measurement.* Flow Measurement and Instrumentation, 2016. **49**: p. 52-62.

52.	Moens, Y.P., et al., *In vitro validation of a Pitot-based flow meter for the measurement of respiratory volume and flow in large animal anaesthesia.* Veterinary anaesthesia and analgesia, 2009. **36**(3): p. 209-219.

53.	Yang, J.-H., et al., *Experimental study on two-dimensional film flow with local measurement methods.* Nuclear Engineering and Design, 2015. **294**: p. 137-151.

54.	*Air Velocity Measurement*. [cited 2017 9 Aug]; Available from: https://www.dwyer-inst.com/Products/AirVelocityIntroduction.cfm.

55.	*Series 160 Stainless Steel Pitot Tubes: Specifications - Installation and Operating Instructions*. [cited 2017 9 Aug]; Available from: http://www.dwyer-inst.com/Product/TestEquipment/PitotTubes/Series160#literature.

56.	Holtmeyer, M.L., B.M. Kumfer, and R.L. Axelbaum, *Effects of biomass particle size during cofiring under air-fired and oxyfuel conditions.* Applied energy, 2012. **93**: p. 606-613.

57.	Zhou, C., et al., *Combustion characteristics and arsenic retention during co-combustion of agricultural biomass and bituminous coal.* Bioresource technology, 2016. **214**: p. 218-224.

58.	Piwowar, A. and M. Dzikuć, *Outline of the economic and technical problems associated with the co-combustion of biomass in Poland.* Renewable and Sustainable Energy Reviews, 2016. **54**: p. 415-420.

59.	Bhattacharya, S., et al., *Potential of biomass fuel conservation in selected Asian countries.* Energy conversion and Management, 1999. **40**(11): p. 1141-1162.

60.	Hughes, E.E. and D.A. Tillman, *Biomass cofiring: status and prospects 1996.* Fuel Processing Technology, 1998. **54**(1–3): p. 127-142.

61.	Posten, C. and G. Schaub, *Microalgae and terrestrial biomass as source for fuels—a process view.* Journal of biotechnology, 2009. **142**(1): p. 64-69.

62.	Apprill, B., et al. *Fixed Bed Solid Fuel Combustor for the Purpose of Testing Solid Biomass Emissions Properties*. in *ASME 2014 International Mechanical Engineering Congress and Exposition*. 2014. American Society of Mechanical Engineers.

63.	Brooker, G., *Introduction to Sensors for Ranging and Imaging*. SciTech Publishing.

64.	Ellis, G., *Control System Design Guide - Using Your Computer to Understand and Diagnose Feedback Controllers (4th Edition)*. Elsevier.

65.	Finesso, R., D. Misul, and E. Spessa, *Estimation of the engine-out NO2/NOx ratio in a EURO VI diesel engine*. 2013, SAE Technical Paper.

66.   Glaude, P., et al., *Kinetic modeling of the mutual oxidation of no and larger alkanes at low temperature.* Energy & fuels, 2005. **19**(5): p. 1839-1849.

67.   Lieuwen, T.C. and V. Yang, *7.3.5 Fuel-Bound Nitrogen*, in *Gas Turbine Emissions*. Cambridge University Press.

68.   Liu, S., et al., *An experimental investigation of NO 2 emission characteristics of a heavy-duty H 2-diesel dual fuel engine.* International journal of hydrogen energy, 2011. **36**(18): p. 12015-12024.

69.   Shah, S.D., et al., *The Oxidation of NO to Yield NO2 in Emissions Testing Sample Bags*. 2007, SAE Technical Paper.

70.   Dean, A.M. and J.W. Bozzelli, *Combustion chemistry of nitrogen*, in *Gas-phase combustion chemistry*. 2000, Springer. p. 125-341.

71.   Irvin, G. and Y. Richard, *Combustion.* 2008.

72.   Arvindnarayan, S., et al., *Algal biomass energy carriers as fuels: an alternative green source.* Journal of the Energy Institute, 2017. **90**(2): p. 300-315.

73.   Assemany, P.P., et al., *Energy potential of algal biomass cultivated in a photobioreactor using effluent from a meat processing plant.* Algal Research, 2016. **17**: p. 53-60.

74.   *Safety Data Sheets: Kingsford Odorless Charcoal Lighter*. Jan 2015 [cited 2017 Aug]; Available from: https://www.thecloroxcompany.com/sds/kingsford-odorless-charcoal-lighter/.

75.   *Technical note: Conversion of fuel data to MWh*.

76.   Krahe, M., *Biochemical engineering.* Ullmann's Encyclopedia of Industrial Chemistry, 2003.

Appendix A – Current Experimental Procedure Documents for Experimental Operations

Burning Procedure

Samples are made ahead of time. See Pellet Making Procedure for details.

Before testing, determine what pellet type the basket will contain. Select a Ziploc bag filled with that pellet type. Then use the most up to date Ash Measurement Procedure and Pellet Layering Procedure to construct the necessary baskets for the proposed test(s).

Note: When handling baskets, especially near the combustion bed, pliers and/or insulated gloves are used to protect the user's hands from burns. This is especially pertinent after a burn has been conducted.

Installing Pre-Burn Charges:

1. Lower the pre-burn basket into the plenum, securing the tabs on the plenum top and rotating the basket so that the side-slot aligns with the glow plug opening.
2. Holding the "lid" open, carefully pour the pre-burn mixture into the pre-burn basket, ensuring that no material overflows from the basket.
3. Secure the basket "lid" using the small tabs on the top of the basket wall.
4. Continue to Step 2 of the section below.

Installing Sample Baskets and Burning Charges/Samples:

1. Lower the wire mesh basket and secure the tabs on the plenum tube. Align the slot in the basket with the threaded hole in the plenum tube.
2. Ensure the silica fabric insulation is wrapped tightly around the plenum tube and does cover the threaded hole in the plenum tube.
    o If the test does not include coal within the fuel mixture, procedure to Step 3.
    o If the test sample contains coal, then 10 mL of charcoal lighter fluid must be added at this point to ensure light-off. Carefully tip and squeeze the bottle of lighter fluid to a small graduated cylinder in the area outside of the formula shop. Continue to add lighter fluid until roughly 10 mL is in the cylinder. Pour this fluid evenly around the fuel in the combustion bed, starting from the center of the bed.
    o Care must be taken when adding lighter fluid to the combustor, especially after a test of relatively slow burning fuels. The fluid has a low heat of combustion and vaporizes quickly; meaning stray embers or even overly hot combustor surfaces may lead to a premature light off. Ensure that all ash has been removed, all embers extinguished, and that the side walls of the combustor bed and the glow plug are relatively cool before adding the lighter fluid.
3. Carefully place combustion tube on base. Insert the glow plug into the bottom most hole in the combustion tube and then thread into the hole in the plenum tube. This will secure the tube. If necessary, rotate the combustion tube to align the holes for the glow plug. The silica fabric insulation may block the inner hole, in which case remove the combustion tube and adjust the insulation.

4. Slide the thermocouples within the appropriate slots in the combustion tube. Note that the thermocouples will not be secured to the tube itself, and will be free to slide during operation.
5. Attach the FTIR and Smoke Meter probes in the top two slots of the combustion tube (regardless of whether emissions measurements will be taken). Take care with the FTIR probe, as it is internally heated, and will be extremely hot. The Smoke Meter probe is also heated, but typically will be cool enough to handle with bare hands.
6. Connect the thermocouples and flow meters to the appropriate computer interfaces. Ensure the DAQ board controlling these instruments is connected to the power supply and receiving power. Make sure the computer reading thermocouples and adjust flow rates to ensure that the flow meter is functioning properly. Reset the flow meter to 0 sLpm when finished.
7. Place protective mesh on top of combustion chamber and secure with bracket.
8. Attach exhaust hose and start the exhaust fan and the room fan.
9. Secure the CO_2 canister to the safety valve. Set the flow rate to the desired number. Begin collecting data from the flow control program (note that it may be required to manually sync this data collection with the emissions-reading program(s) on a separate laptop).
10. Attach the safety switch to the small end of the glow plug and the positive (power) and negative (ground) terminals of a 12VDC lead acid battery. Initiate glow plug by attaching a wire from the base of the glow plug (i.e. the part of the glow plug closest to the hole) to the negative terminal of the 12VDC lead acid battery.
11. Turn off glow plug once combustion begins by removing the connection between the plug and the negative terminal of the battery, and then carefully disassembling the wiring. The onset of combustion is typically characterized by smell, the presence of smoke coming out of the top of the combustor tube, or an exhaust emission reading from the FTIR (if used) of 1200 ppm of CO_2 or higher. Combustion will not be immediately visible, and conflagration will advance very rapidly; do not look down the combustor tube if combustion is thought to have started until the visible flame is gone.
12. If there are any safety concerns during combustion, or if an immediate evacuation of the test cell area is required, flip CO_2 cartridge and open the valve to halt combustion.
13. Once combustion is complete (signified by the extinction of the last visible flame in the biomass char), turn off air flow and let apparatus cool for approximately 30-45 seconds.
14. When cooled, begin disassembling the apparatus (in reverse order of assembly). Use insulated gloves, as the combustor tube will be hot. Removing the thermocouples is not absolutely required, but may make handling the combustor tube easier. At this time, clean the overlapping mesh on the top of the combustor tube and replace once finished.
15. Remove the basket gently and follow the most recent Ash Measurement Procedure for further handling. Also remove the mesh cap on top of the combustor and take it to the storm drain outside of the garage door to tap out any ash caught in the mesh.
16. Repeat Steps 1 through 15 for all desired samples. When all samples have been burned, disconnect all control devices and electrical inputs. Store the thermocouples, flow meter, power supply, and car battery in appropriate areas within the test cell.

If determining emissions:

1. The FTIR must be purged with compressed nitrogen gas for at least 12 hours in advance of testing.
2. Roughly 1 hour before testing, The FTIR must be readied and calibrated for testing. The Smokemeter should also be readied during this time, if needed. Steps 1 and 2 will be completed by one of Dr. Depcik's graduate students.
3. During Step 8 of the Burning Procedure, the FTIR and Smokemeter are connected to a separate, appropriate computer with the control software for both instruments.
4. Data collection for the FTIR are started at the same time as the flow rate and temperature data collection in Step 11 of the Burning Procedure. Smoke meter data collection are set for 30 second measurements, and must be manually started after light-off of the biomass, when flames are visible through the viewport in the combustion tube. No more than 5 Smoke Meter tests are run per sample. Use the same number of Smoke Meter tests per sample during testing. The Smoke Meter can be set up to automatically take consecutive measurements after the first measurement request is made.
5. After the sample has been completely burned, a backflush of the FTIR are performed before disassembly of the test rig (Step 16). DO NOT run the black flush during or after disassembly as it will release hot exhaust gas and soot into the test cell, potentially injuring those within.
6. After the conclusion of the final test, the backflush should immediately be followed by a Purge command of the FTIR. This purge are run before disassembly of the combustor tube.

Basket and Ash Measuring Procedure for Solid Biofuel Testing

This procedure is developed to increase the accuracy and repeatability of the ash mass measurements recorded during testing with the Solid Fuel Combustor located in Learned 1109. All applicable PPE for this room and the Environmental Science Lab in Learned 1116 must be worn at all times in this locations. Review lab-specific trainings available from KU Environmental Health and Safety (EHS) for the exact requirements of these labs.

1) In the Learned 1116, press the On-Off button on the front of the uncovered mass scale on the table near the double doors. Wait several seconds for the scale to turn on and for the reading on the LED screen to stop fluctuating. If the scale's resting value is not zero, press the red Re-Zero button on the front of the scale and then wait several seconds for the reading to zero. Repeat the last step as often as need to reach a zero value while unloaded.
2) Place a sheet of 8.5"x11" sheet of standard printer paper on top of the uncovered scale such that it does not cover the LED screen but also with the center of the sheet near the center of the measuring plate. Carefully place an empty sample basket with its two mesh dividers on top of the sheet of paper, again keeping the center of the basket near the center of the sample.

3) Allow the readings on the LED screen to stop fluctuating before recording the mass of the basket and sheet of paper (around 70.79 g as measured 1-30-17).
4) Remove the basket and mesh dividers from the scale a fill them with fuel pellets of the desired mixture, following standard basket filling procedures.
5) Carefully return the basket and dividers with the fuel pellets to the scale, placing the filled basket near the center of the sample place. Allow the LED screen to adjust and record the new mass reading (This will get near and possibly above 100g for the algae containing mixtures).
6) Repeat Steps 2) through 6) for each sample basket to be used.
7) Follow the Solid Fuel Combustor testing procedure during each basket's test (Note that the printer paper should not be placed in the burner with the basket). After the test, carefully remove basket and dividers from the combustor bed to reduce the ash loss through the mesh bottom. Gently set the basket aside and allow it to cool.
8) Once the basket has cooled, gently replace the printer paper underneath the basket and return it to the Learned 1116 lab (remember your PPE!).
9) Repeat Step 1) to ensure the scale is ready for use. Gently place the paper, basket, dividers, and ash onto the sample plate and wait for the LED display to stop fluctuating before recording the mass.
10) Take the measured basket, paper, dividers, and ash to a clean, open work place with a re-sealable bag. Using a brush or similar tool, carefully remove the ash from the basket, dividers, and paper, brushing it instead into the re-sealable bag. Seal the bag when finished cleaning and secure in a safe location for further testing.
11) Once the ash has been removed, reweigh the paper, basket, and dividers and record the mass.
12) Repeat Steps 8) through 11) for all tested baskets.
13) Return the baskets to their storage location and throw away the paper used for the procedure.

Coal Fuel Mixture Accelerant Testing Goals and Steps

Objectives:

1. Determine if charcoal lighter fluid can be used as an accelerant to light off coal containing fuel mixtures in the Solid Fuel Combustor.
2. If effective, then narrow the amount of lighter fluid needed to a specific amount or range in order to reduce waste and improve result accuracy and repeatability.
3. If able, determine if a meaningful relationship exists between the amount of coal in the fuel mixture and the amount of lighter fluid needed to begin light off.

Procedure:

Part 1: Objectives 1 & 2

All burns should follow the most up-to-date Solid Fuel Combustor Burning Procedure. Carefully review this procedure before testing and ensure that all pertinent safety procedures are flowed during testing.

1. Follow the up-to-date Ash Measuring, Pellet Layering, and Burn Procedures to construct test baskets of 50%/50% pine/coal pellets as well as mix two burn's worth of pre-burn fuel mixture.
2. Conduct the pre-burns as normal and then prepare the first coal sample basket for testing. After inserting the basket as per the Burn Procedure, carefully lift the mesh divider on top of the pellet layer.
3. In the outdoors area immediately outside of the Formula Shop, carefully measure out 5 mL of the charcoal lighting fluid into the graduated cylinder stored with the fluid. Quickly, but carefully, pour the lighter fluid evenly onto the fuel pellets in the combustor bed before replacing the mesh divider.
4. Rebuild the combustor and test the sample basket as normal per the Burn Procedure. Carefully observe the viewport on the side of the tube as well as the temperature data displayed by the LabVIEW control program. Timing the total burn time may prove very valuable as well. Take notes as necessary.
5. Compare the observations from Step 4) to the pre-burns and known behaviors of the non-coal containing fuels mixtures to determine whether the amount of lighter fluid used is adequate.
6. Repeat Steps 2) through 5) as many times as necessary to find the specific amount or range of lighter fluid additions needed to initiate light-off in the coal. If the amount added is determined to be inadequate in Step 5), add to the next basket an additional 5 mL of fluid over the amount added to the previous basket. If the amount of fluid added is adequate in Step 5), then it may be reduced in further testing by some amount < 5 mL.
7. Be sure to record the volume of lighter fluid added to each test so that the proper amount of lighter fluid will always be added in future testing.

Part 2: Objective 3

Once Objectives 1 and 2 have been met, it may be beneficial to test fuel mixtures with varying percentages of coal to see if the amount of lighter fluid needed changes.

1. Follow the up-to-date Ash Measuring, Pellet Layering, and Burn Procedures to construct at least two test baskets of 50%/50% pine/coal pellets as well as several baskets of a X%/Y% pine/coal mixture (refrain from using algae to reduce variance). Do not forget to additionally mix two burn's worth of pre-burn fuel mixture in addition to the test baskets.
2. Conduct the pre-burns as normal and then prepare the first 50%/50% pine/coal sample basket for testing. After inserting the basket as per the Burn Procedure, carefully lift the mesh divider on top of the pellet layer. Add an amount of lighter fluid to the basket consistent with the findings of Part 1 before replacing the divider and reconstructing the combustor.

3. Conduct the burn of the basket in Step 2) according to the Burn Procedure and then repeat the set up from Step 2) for the second 50%/50% pine/coal basket before burning the material according to the Burn Procedure. For both tests, be sure to take notes on the thermocouple data presented in the LabVIEW control program, visual cues in the viewport of the combustor, and the total combustion time of the samples.
4. After the 50%/50% pine/coal samples have been burned, begin to set up the X%/Y% pine/coal samples with the same methodology as the 50%/50%. When adding the lighter fluid, begin by adding the same amount of fluid to the X%/Y% mixture as is prescribed for the 50%/50% mixture. The amount of fluid added is then varied similar to the process in Part 1, if necessary. Suggestions for adjustments (if necessary) are below.
    a. If the percentage of coal is higher than 50% in the new mixture, begin by adding 5 mL for the first test.
    b. If the percentage of coal in the mixture is less than 50%, lower the amount of fluid added, if possible. If the amount of fluid added cannot be lowered, consider adding no fluid or increasing the percentage of coal to ensure the test has purpose.
5. Proceed with testing of the new mixture using the same methodology of Steps 3) through 6) in Part 1, adjusting fluid addition amounts from test to test based on the recorded observations.
6. Once a specific amount or range of lighter fluid addition is found for the X%/Y% pine/coal mixture, record this value into the same reference as the lighter fluid amount for 50%/50% for ease of use.
7. If a relationship between coal percentage and the necessary lighter fluid addition is found, a simple linear interpolation can be used to approximate necessary additions for other mixtures as a function of coal percentage. If/when more specific ranges or values are found for these mixtures; make sure to record them for future reference.

Appendix B – Sample Calculation for Optimization Study Methodology

Fuel mass burned approximation procedure

The sample calculation for the fuel mass burned procedure outlined in Chapter 2 will use the CO_2 emissions from the first data point of the 100% pine test used as a normalizing baseline in the Results section of Chapter 3. This data point is measured in ppm by the FTIR and must be converted to a volume fraction in accordance with Eq. (1) from Chapter 2:

$$\varphi_{CO_2} = 282.230 \left(\frac{1}{10^6}\right) = 2.8223 \times 10^{-4} \tag{1}$$

Note that the volume fraction can immediately be converted into a mole fraction. Now, Chapter 2's Eq. (3) can convert from a mole fraction to a more useful mass fraction. It is necessary to determine the molar masses of CO_2 and the mixture before continuing this process. The CO_2 molar mass can be easily calculated as:

$$M_{CO_2} = M_C + 2M_{O_2} = 12 + 2(16) \tag{2}$$

$$M_{CO_2} = 44 \tag{3}$$

while the molar mass of the mixture first requires that the mole fraction of N_2 be calculated. Molecular nitrogen's mole fraction can be found by employing Eq. (6) from Chapter 2. Since there nearly a dozen individual emission species included in this calculation, it is not presented here, but for the first data point of the 100% pine emissions, X_{N_2} is found to be:

$$X_{N_2} = 0.7618 \tag{4}$$

Which is then applied to Eq. (4) from Chapter 2 to calculate the mixture's molar mass. Similarly to Eq. (4), this calculation is not included here due to spatial constraints, but the calculation yielded:

$$M_{mixture} = 28.888 \tag{5}$$

The mass fraction of CO_2 at the sample data point is then:

$$Y_{CO_2} = \varphi_{CO_2} \frac{M_{CO_2}}{M_{mixture}} = (2.8223 \times 10^{-4}) \left(\frac{44}{28.888}\right) \tag{6}$$

$$Y_{CO_2} = 4.298 \times 10^{-4} \tag{7}$$

Before Eq. (5) from Chapter 2 can be used, the density of the mixture under the conditions of the sample line must be determined via the ideal gas law as found in Eq. (11) in Chapter 2:

$$\rho_{mixture} = \frac{P M_{air}}{\bar{R} T} \tag{8}$$

From Chapter 2, it is known that P is 86 psi in the FTIR sample line while T is 191°C. For solving Eq. (7) above, it is useful to convert these values from psi to Pa and from °C to K. Thus, P becomes 592949.36 Pa and T is 464.15 K. Eq. (8) can now be solved to find the density of the overall mixture:

$$\rho_{\text{mixture}} = \frac{(592949.36)(28.888)}{(8314.5)(464.15)} = 4.4385 \tag{9}$$

Note that the solution of Eq. (9) will change at each data point, since the mole fraction of nitrogen will change as the composition of the exhaust changes. Now, Chapter 2's Eq. (7) can be solved at this data point:

$$C_{CO_2} = Y_{CO_2}\rho_{\text{mixture}} = (4.289 \times 10^{-4})(4.4496) \tag{10}$$

$$C_{CO_2} = 1.908 \times 10^{-3} \tag{11}$$

A baseline of the CO_2 emissions due to the steady flow of air from the Alicat flow controller is now estimated as the arithmetic mean of the masses of CO_2 per volume of mixture from the first thirty-five data points. These data points are measured before the start of combustion (during the fuel warming period) and are accurate estimates of ambient conditions during the test period. Due to the number of data points needed for the baseline calculation, it will not be given in its entirety here. It is calculated to be:

$$C_{CO_2,basline} = 3.5491 \times 10^{-3} \tag{12}$$

The baseline value are then subtracted from each mass flow rate calculated for the corresponding species at every data point. For the mass flow rate of CO_2 at the first data point, given in Eq. (10), this calculation yields:

$$C_{adjusted} = 1.908 \times 10^{-3} - 3.5491 \times 10^{-3} \tag{13}$$

$$C_{adjusted} = -1.6411 \times 10^{-3} \tag{14}$$

Since the result in Eq. (14) is less than zero, the mass of CO_2 per volume of mixture at this point is considered to be at ambient conditions and is set to zero for future calculations. The above method from Eq. (1) to here is repeated for all data points and for all species, using those species' baseline values in Eq. (12) to find adjusted values for C_{CO_2}.

Before using the instantaneous mass flow rate equation from Chapter 2, the volumetric flow rate of the air from the Alicat flow controller (an approximation of the total exhaust volumetric flow rate) is solved for using Eqs (11) and (12) from Chapter 2. Note that for all tests of 100% pine, the flow rate is held to a constant 70 sLpm and that the temperature and pressure of the air flow to the bed needs to be used. Hence, the air flow temperature is assumed as approximately the temperature of the room air, around 297.039 K (75°F), and the flow pressure is estimated as 14.8 psia (slightly higher than atmospheric pressure) making the calculation:

$$\dot{V}_{Lpm} = (70)\left(\frac{297.039}{294.26}\right)\left(\frac{14.696}{14.8}\right) = 70.165 \tag{15}$$

$$\dot{V}_{air} = (70.165)\left(\frac{10^{-3}}{1}\right)\left(\frac{1}{60}\right) = 1.169 \times 10^{-3} \tag{16}$$

Now the instantaneous mass flow rate of CO_2 due to fuel combustion can be estimated at the first data point of the 100% pine test as:

$$\dot{m}_{CO_2} = C_{\text{adjusted}}\dot{V}_{air} = (0)(1.169 \times 10^{-3}) \tag{17}$$

$$\dot{m}_{CO_2} = 0 \tag{18}$$

Eqs (17) and (18) are repeated at all data points to find the mass flow rate of CO_2 due to combustion at these points.

Once the adjusted mass flow rate values have been calculated at all data points, the trapezoid rule is applied to the mass flow rate data in order estimate the total integral of the mass flow rates for each species, which provides an estimate for the total mass emission for each species over the total combustion time. These values are then converted to gm from kg, for a more direct comparison to fuel weight measurements, which are made in gm. Since this calculation involves more data points that the baseline estimation calculation, it will likewise not be provided in its entirety here. For CO_2, however, this value is found to be:

$$m_{CO_2,total} = 37.1885 \tag{19}$$

The mass fraction of carbon in CO_2 is then calculated using the molar mass of the atomic constituents assuming 1 mol of CO_2:

$$y_{C \text{ in } CO_2} = \frac{(1)(12)}{(1)(12)+(2)(16)} \tag{20}$$

$$y_{C \text{ in } CO_2} = 0.2727 \tag{21}$$

Multiplying the result in Eq. (19) with the result in Eq. (21) then yields the total mass emission of carbon in the form of CO_2 from fuel combustion:

$$m_{C \text{ from } CO_2} = 0.2727(37.1885) = 10.1413 \tag{22}$$

The methodology from Eqs (20) to (22) is repeated for all carbon containing emissions and the results summed into a total carbon mass emission due to fuel combustion. The result for the current test is found to be:

$$m_C = 10.446 \tag{23}$$

With the total mass of fuel carbon emitted as products of combustion known in Eq. (19), the total mass of fuel burned can now be estimated using Eq. (23) and the fuel mass fraction of carbon. The fuel mass fraction of carbon can be found in Chapter 3. The estimated total mass of fuel combusted during the example test is:

$$m_f = \frac{10.446}{0.514} = 20.323 \tag{24}$$

Note that although the result of Eq. (24) is within 0.2 gm of the average fuel mass in a basket during a combustion test, this similarity may not throw the accuracy of the above procedure's final results into a negative light. Comparisons with predicted ash masses, the procedure for which is outlined in the next section, place this deficit within an expectable range. But the difference between the total fuel mass and the estimated mass of fuel burned is still close enough to warrant concerns regarding rounding error and statistical errors. Regardless of the accuracy of

the individual estimates, the trends produced by this analysis across multiple fuel blend and flow rate combinations match well with real world results and observations. Hence, credence is lent to the accuracy and usefulness of the model's estimates in predicting overall trends.

Ash content estimation procedure for Table 2 in Chapter 2

The %wt ash content will be determined for each fuel mixture through a weighted sums process:

$$y_{ash,mixture} = y_{pine}y_{ash,pine} + y_{algae}y_{ash,algae} \tag{25}$$

where $y_{ash,mixture}$ is the estimated ash content of the total mixture in mass fraction, y_{pine} and y_{algae} are the mass fraction of pine and algae in the fuel mixture (respectively), and $y_{ash,pine}$ is the mass fraction ash content in the pine while $y_{ash,algae}$ is the mass fraction ash content of the algae. Since the ash contents of both pine and algae are given as a range of values, it is desirable to do the same for their mixtures. To this, Eq. (25) will be applied to each fuel mixture twice: once in an estimated minimum ash content value and a second time for an estimated maximum value.

To accomplish this, the corresponding pine and algae ash contents are substituted in to Eq. (25); i.e., the minimum pine ash content and minimum algae ash content are used in Eq. (25) to calculate the mixture's minimum ash content. Thus, Eq. (25) becomes:

$$y_{min.\ ash,mixture} = y_{pine}y_{min.\ ash,pine} + y_{algae}y_{min.\ ash,algae} \tag{26}$$

for the minimum ash content case and:

$$y_{max.\ ash,mixture} = y_{pine}y_{max.\ ash,pine} + y_{algae}y_{max.\ ash,algae} \tag{27}$$

for the maximum ash content case. As an example, consider the estimated low ash content case for the 90%/10% pine algae mixture. The low value of ash contents for pine and algae are 0.5% and 3.5%, by weight, respectively [46]. Note that %wt values are simply mass fractions multiplied by one hundred. Thus, Eq. (27) can be solved as:

$$y_{min.\ ash,mixture} = (0.9)(0.005) + (0.1)(0.035) \tag{28}$$

$$y_{min.\ ash,mixture} = 0.0045 + 0.0035 \tag{29}$$

$$y_{min.\ ash,mixture} = 0.008 \tag{30}$$

Thus, the low estimate of the %wt ash content for the 90%/10% mixtures is 0.8%. With an ash content estimate now made, an estimate for the mass of ash produced during a combustion test can be found using the relation:

$$m_{ash} = y_{ash,mixture}m_{fuel} \tag{31}$$

where m_{fuel} is the average mass of fuel in a fuel basket during a single test in gm. Therefore, for the minimum ash estimate case of the 90%/10% mixture, Eq. (31) yields an ash mass estimate of:

$$m_{ash} = (0.008)(23.5) = 0.188 \tag{32}$$

Thus, the 90%/10% mixtures are theoretically capable of combusting nearly all of their fuel mass. Practically, this will likely not be the observed result and the ash mass estimates will be closer to the average case, which will use the averaged %wt ash content calculated from the mean of the maximum and minimum ash content cases for each mixture.

Flow validation analysis procedure

For this sample calculation procedure, the Alicat and manometer values for a flow validation test at 50 sLpm are used to demonstrate the process. Beginning with Eq. (15) in Chapter 2, the standardized flow rate as set on the Alicat is converted from sLpm to Lpm. Note that the air flow is assumed to be at 295.37 K (72°F) with a pressure of 14.8 psia:

$$\dot{V}_{Lpm} = (50)\left(\frac{297.37}{294.26}\right)\left(\frac{14.696}{14.8}\right) = 50.1734 \tag{33}$$

The solution of Eq. (33) is then converted into ft^3 min^{-1} using Chapter 2's Eq. (19):

$$\dot{V}_{Alicat,Imp.} = 50.1734(0.0353147) = 1.7716 \tag{34}$$

With the set flow rate of the Alicat solved for, the measured flow rate must now be calculated for before comparisons can be drawn.

Eq. (20) is a relatively simple Equation to solve, however, one variable remains unknown: the air density. The flow stream is assumed to follow ideal gas law characteristics and is found via Eq. (11) from Chapter 2. The molar mass in this Equation remains the molar mass of air while the temperature and pressure are assumed to be the values used in Eq. (34) above (converted to the proper units). Thus:

$$\rho = \frac{PM_{air}}{\bar{R}T} = \frac{(102042.4)(28.96)}{(8314.5)(297.37)} = 1.1952 \tag{35}$$

and the air velocity measured by the Pitot-static tube becomes:

$$v_{airflow} = \sqrt{\frac{2(P_d - P_s)}{\rho}} = \sqrt{\frac{2(24)}{1.1952}} = 6.3372 \tag{36}$$

Since the calculated flow rate is in terms of m s^{-1}, it is converted in ft min^{-1} for future calculations:

$$v_{airflow,Imp} = 6.3372(3.28084)(60) = 1247.4887 \tag{37}$$

The solution to Eq. (38) can be used to solve for a "measured" volumetric flow rate that can be compared to the set flow rate calculated from the Alicat settings.

Before the measured volume flow rate can be calculated, however, the cross-sectional area of at the point of measurement must be known. Since the pipe used has a circular cross-section, its cross-sectional area can be found using the pipe's interior diameter. The section holding the Pitot-static tube is constructed of 3" Sch 40 pipe, with an inner diameter of 3.068".

Thus, using the equation for the area of a circle, listed in Chapter 2's Eq. (22), the cross-sectional area becomes:

$$A_C = \pi \left(\frac{3.068}{2}\right)^2 = 7.393 \left(\frac{1}{(12)^2}\right) = 0.05134 \tag{38}$$

Finally, Eq. (23) from Chapter 2 is applied to solve for the measured volume flow rate:

$$\dot{V}_{measured} = (1247.4887)(0.05134) = 64.0461 \tag{39}$$

Eq. (39) does not match Eq. (34), so Chapter 2's Eq. (24) must be applied to determine an effective cross-sectional area:

$$A_{C,equivalent} = \frac{\dot{V}_{Alicat,Imp.}}{v_{airflow,Imp}} = \frac{1.7716}{1247.4887} = 0.001420 \tag{40}$$

The result of Eq. (40) can now be compared to the cross-sectional areas of the large pipe and the Alicat outlet in order to draw conclusions regarding the state of the air flow inside the flow validation set up.

Appendix C – Energy Release Logic and Process

Note: The Tables A through D referenced in this section can be found in Appendix D

Estimation of the heat of formation of a fuel can be accomplished using the generalized heating value relationship:

$$\overline{Q}_{HV} = \sum_R \overline{n}_i \, \overline{h^0_{f,\iota}} + \sum_P \overline{n}_i \, \overline{h^0_{f,\iota}} \tag{1}$$

where $\overline{Q}_{HV}$ is the molar heating value of the combusted fuel, $\overline{n}_i$ is the mole fraction of species i in the reaction, $\overline{h^0_{f,\iota}}$ is the molar heat of formation of species i, R represents the reactant species, and P represents the product species. The moles of product species can be estimated from the emissions measurements by the FTIR; however, another method of evaluation must be employed for the fuel composition. The individual species mass fraction information (i.e., carbon, hydrogen, oxygen, and nitrogen aka CHON) obtained from combustion analysis studies will be used for this purpose. Combining the mass composition information from Chapter 3's Table 1 with the molar mass data provided in Table A can allow for solution of the molar composition of the fuel using the Equation:

$$X_i = \frac{\frac{m_i}{M_i}}{\frac{m_C}{M_C}+\frac{m_H}{M_H}+\frac{m_O}{M_O}+\frac{m_N}{M_N}} \tag{2}$$

which solves for X_i, the molar fraction of species i in the fuel, by using the mass fraction of that species from Chapter 3 Table 1 (m_i) divided by the molar mass of the species (M_i), all divided by the sum of that calculation for all of the species in the fuel. As an example, consider the carbon content of the 90%/10% fuel mixture. Using the mass fraction data from Chapter 3 and the molar mass data of each species, Eq. (2) becomes:

$$X_C = \frac{\frac{m_C}{M_C}}{\frac{m_C}{M_C}+\frac{m_H}{M_H}+\frac{m_O}{M_O}+\frac{m_N}{M_N}} \tag{3}$$

$$X_C = \frac{\frac{0.499}{12}}{\frac{0.499}{12}+\frac{0.061}{1}+\frac{0.417}{16}+\frac{0.002}{14}} \tag{4}$$

$$X_C = 0.3229 \tag{5}$$

The calculated molar mass fractions for all mixtures are provided with the molar mass of each species in Table A. Next, looking at the generalized stoichiometric combustion reaction for one mole of fuel:

$$C_xH_yO_zN_a + f(O_2 + 3.76N_2) \rightarrow bCO_2 + cH_2O + dN_2 \tag{6}$$
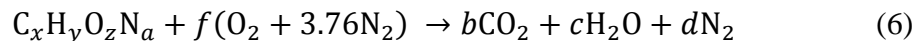
the next step is to translate the calculated mole fractions to moles. To do this, the following relationship is established:

$$\frac{X_i}{X_C} = \frac{x_i}{x} \tag{7}$$

where X_i is the fuel molar fraction of the species of interest, x_i is the moles of the species in Eq. (6), and x is the number of moles of fuel carbon. Eq. (7) can be rearranged as:

$$x_i = x\left(\frac{X_i}{X_C}\right) \tag{8}$$

to solve for the moles of any fuel elemental species in Eq. (6) given a known value for x. Thus, an estimate for the moles of carbon in a mole of biomass fuel is then made. One source points towards 1.64 as a reasonable estimate of x; however, testing of this procedure in MATLAB has shown that the actual value of x has little impact on the final result [76]. Thus, for the 90%/10% mixture, the moles of hydrogen, oxygen, and nitrogen become, respectively:

$$y = x\left(\frac{X_H}{X_C}\right) = (1.64)\left(\frac{0.4736}{0.3229}\right) = 2.405 \tag{9}$$

$$z = x\left(\frac{X_O}{X_C}\right) = (1.64)\left(\frac{0.2024}{0.3229}\right) = 1.028 \tag{10}$$

$$a = x\left(\frac{X_N}{X_C}\right) = (1.64)\left(\frac{0.0011}{0.3229}\right) = 0.006 \tag{11}$$

With the moles of individual elements per mole of fuel determined, the molar mass of the fuel can be estimated through the relation:

$$M_{fuel} = x \cdot M_C + y \cdot M_H + z \cdot M_O + a \cdot M_N \tag{12}$$

The calculations for fuel molar mass for all tested blends are provided in Table B. Also included in Table B are the molar higher heating values calculated from the Equation:

$$\overline{Q}_{HV} = Q_{HHV} M_{fuel} \tag{13}$$

where Q_{HV} is the higher heating value of the fuel. Note that the energy content determined via calorimetry and presented in Chapter 3 Table 1 is a "gross heating value" which is Equivalent to the higher heating value. Eq. (13) can then be applied to the 90%/10% fuel to find:

$$\overline{Q}_{HV} = (17496.98)(0.04149) = 725.95 \tag{14}$$

The next step is then to determine the moles of air and products in Eq. (6).These values are determined via an element balance, starting with the carbon balance:

$$b = x = 1.64\ mol \tag{15}$$

followed by the hydrogen balance:

$$2c = y \tag{16}$$

$$c = \frac{y}{2} = \frac{2.4054}{2} = 1.703 \tag{17}$$

then the oxygen balance:

$$z + 2f = 2 \cdot b + c \tag{18}$$

$$f = b + \frac{c}{2} - \frac{z}{2} = 1.64 + \frac{1.703}{2} - \frac{1.028}{2} \tag{19}$$

$$f = 1.978 \tag{20}$$

and finally the nitrogen balance:

$$a + 3.76 \cdot 2 \cdot f = 2 \cdot d \tag{21}$$

$$d = 3.76 \cdot f + \frac{a}{2} = 3.76 \cdot 1.978 + \frac{0.0056}{2} \tag{22}$$

$$d = 7.440 \tag{23}$$

The calculated moles for Eq. (6) can now be combined with the heat of formation data for each species so that Eq. (1) can be solved for the heat of formation of the fuel. Before this, however, it is useful to expand the summations in Eq. (1) in application to Eq. (6). This yields the relation:

$$\overline{Q}_{HV} = \left(n_f \cdot \overline{h}^0_{f,fuel} + f \cdot \overline{h}^0_{f,O_2} + 3.76 \cdot f \cdot \overline{h}^0_{f,N_2}\right) - \left(b \cdot \overline{h}^0_{f,CO_2} + c \cdot \overline{h}^0_{f,H_2O_g} + d \cdot \overline{h}^0_{f,N_2}\right) \tag{24}$$

which can be rearranged into:

$$\overline{h}^0_{f,fuel} = \overline{Q}_{HV} - f \cdot \overline{h}^0_{f,O_2} + (d - 3.76 \cdot f)\overline{h}^0_{f,N_2} + b \cdot \overline{h}^0_{f,CO_2} + c \cdot \overline{h}^0_{f,H_2O_g} \tag{25}$$

Solutions for Eq. (25) for each of the fuels are given in Table C. The stoichiometric combustion reaction Equation is useful for estimating several parameters of the fuel itself but is not an accurate portrayal of the in situ conditions inside the combustion bed. As evidenced by the O_2 emissions figures in the results sections of Chapters 3 and 4, there is excess oxygen in the bed, and a lean combustion reaction is more accurate. The lean combustion reaction Equation is written as:

$$n_f C_x H_y O_z N_a + g(O_2 + 3.76N_2) \rightarrow x_{CO_2}CO_2 + x_{CO}CO + x_{H_2O}H_2O + x_{NO}NO$$

$$+ x_{NO_2}NO_2 + x_{N_2O}N_2O + x_{THC}THC + x_{O_2}O_2 + x_{N_2}N_2 \tag{26}$$
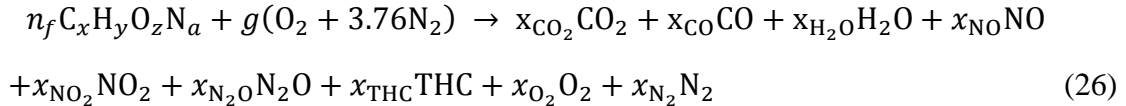
where x_i is the moles of product species i per mole of exhaust, n is the moles of fuel, and g is the moles of air available for combustion. Note that Eq. (26) is in a per mole exhaust basis since the moles of product species are calculated from the emissions measurements provided by the FTIR. These measurements are in ppm, which are directly convertible into molarity ($mol \times mol_{exhaust}^{-1}$); thus, on a per mole exhaust basis. Also of interest is the total hydrocarbon (THC) emissions measurement. This measurement is useful for calculations because it accounts for several chemical species that individually have almost negligible values but together represent a significant portion of the reacted carbon. The only value that is not known is x_{N_2} since nitrogen is used as a purging medium in the FTIR and is, therefore, not measured by the device. However, assuming ideal gas behavior allows for the relation:

$$\sum x_i = 1 \tag{27}$$

allows x_{N_2} to be calculated from the known exhaust species via:

$$x_{\text{N}_2} = 1 - x_{\text{CO}_2} - x_{\text{CO}} - x_{\text{H}_2\text{O}} - x_{\text{NO}} - x_{\text{NO}_2} - x_{\text{N}_2\text{O}} - x_{\text{THC}} - x_{\text{O}_2} \quad (28)$$

With all of the exhaust mole fractions now known in addition to the fuel molar composition, the values of n and g can be found via the appropriate element balances. The carbon balance works well for n:

$$n \cdot x = x_{\text{CO}_2} + x_{\text{CO}} + 3 \cdot x_{\text{THC}} \quad (29)$$

$$n = \frac{x_{\text{CO}_2} + x_{\text{CO}} + 3 \cdot x_{\text{THC}}}{x} \quad (30)$$

while the oxygen balance finds g with relative ease:

$$n \cdot z + 2 \cdot g = 2 \cdot x_{\text{CO}_2} + x_{\text{CO}} + x_{\text{H}_2\text{O}} + x_{\text{NO}} + 2 \cdot x_{\text{NO}_2} + x_{\text{N}_2\text{O}} + 2 \cdot x_{\text{O}_2} \quad (31)$$

$$g = x_{\text{CO}_2} + x_{\text{NO}_2} + x_{\text{O}_2} + \frac{x_{\text{CO}} + x_{\text{H}_2\text{O}} + x_{\text{NO}} + x_{\text{N}_2\text{O}} + n \cdot z}{2} \quad (32)$$

Note that x_{THC} in Eqs. (29) and (30) must be multiplied by three because the THC measurements are presented in a moles of propane basis (and propane has three carbon atoms). From the first data point of the FTIR data file for the normalized 90%/10% test, this yields:

$$n = \frac{(4.591 \times 10^{-5}) + (1.120 \times 10^{-6}) + 3 \cdot (6.840 \times 10^{-6})}{1.64} \quad (33)$$

$$n = 4.119 \times 10^{-5} \quad (34)$$

$$g = \frac{(1.120 \times 10^{-6}) + 0.0087 + 0 + (1.400 \times 10^{-7}) + (4.119 \times 10^{-5})(1.0280)}{2}$$

$$+ (4.591 \times 10^{-5}) + (3.700 \times 10^{-7}) + 0.225 \quad (35)$$

$$g = 2.347 \quad (36)$$

The next step in the solution is to convert the air flow rate from a normalized volume flow rate (sLpm) to a molar flow rate so that it can be used to calculate a molar rate of fuel combustion.

As a first step, the normalized volume flow rate must be converted into a non-normalized volume rate. The standard liter per minute (sLpm) normalizes the volume flow rate measurement to standard temperature and pressure via the Equation:

$$\dot{V}_{sLpm} = \dot{V}_{Lpm} \left(\frac{294.26\ K}{T_{gas}} \right) \left(\frac{P_{gas}}{14.696\ psia} \right) \quad (37)$$

where $\dot{V}_{sLpm}$ is the normalized flow rate in sLpm, $\dot{V}_{Lpm}$ is the actual volume flow rate in liters per minute (Lpm), T_{gas} is the air flow's temperature in Kelvin (K), and P_{gas} is the average absolute flow pressure in pounds per square inch (psia). For all tests, the flow temperature and pressure is assumed to roughly Equivalent to the ambient conditions inside of the test area with T_{gas} around 297.039 K and P_{gas} at standard atmospheric pressure (14.696 psia). Eq. (37) is then rearranged into:

$$\dot{V}_{Lpm} = \dot{V}_{sLpm} \left(\frac{T_{gas}}{294.26 \, K} \right) \left(\frac{14.696 \, psia}{P_{gas}} \right) \tag{38}$$

and the sLpm flow rate of the tests of interest is then substituted for $\dot{V}_{sLpm}$ to find $\dot{V}_{Lpm}$. For the normalized 90%/10% test used in sample calculations thus far, this yields:

$$\dot{V}_{Lpm} = (67) \left(\frac{297.039}{294.26} \right) \left(\frac{14.696}{14.696} \right) \tag{39}$$

$$\dot{V}_{Lpm} = 67.6 \tag{40}$$

The volume flow rate is converted to a mass flow rate by multiplying it by the density of air at standard temperature and pressure:

$$\dot{m}_{air} = \rho_{air} \dot{V} = (1204.1)(67.6)\left(1.\overline{6} \times 10^{-5}\right) \tag{41}$$

$$\dot{m}_{air} = 1.357 \tag{42}$$

Now, this mass flow rate of air needs to be converted into a molar flow rate before it can be used to find the molar combustion rate of the fuel.

To begin, the mole fractions of air's constituent molecules are found. As can be seen in Eqs. (6) and (26), the number of moles of both O_2 and N_2 in air are known, and their mole fractions can be calculated similarly to the fuel CHON balance in Eqs. (2) through (5):

$$X_{air,O_2} = \frac{1}{1+3.76} = 0.21 \tag{43}$$

$$X_{air,N_2} = \frac{3.76}{1+3.76} = 0.79 \tag{44}$$

From Eqs. (43) and (44), the molar mass data from Table A can be used to calculate the molar mass of air:

$$M_{air} = X_{air,O_2} \cdot 2 \cdot M_O + X_{air,N_2} \cdot 2 \cdot M_N \tag{45}$$

$$M_{air} = 0.21 \cdot 2 \cdot 16 + 0.79 \cdot 2 \cdot 14 \tag{46}$$

$$M_{air} = 28.84 \tag{47}$$

and from the results of Eqs. (42) and (47), the molar flow rate can be found:

$$\dot{n}_{air} = \frac{\dot{m}_{air}}{M_{air}} = \frac{1.357}{28.84} = 0.047 \tag{48}$$

The molar combustion rate of the fuel can then be obtained at each time step from the Equivalency:

$$\frac{\dot{n}_{fuel}}{\dot{n}_{air}} = \frac{n}{g} \tag{49}$$

which can be rearranged to isolate $\dot{n}_{fuel}$. With $\dot{n}_{air}$ found through Eq. (48) and n and g known for each time step from Eqs. (34) and (36), respectively, Eq. (49) can be used to find $\dot{n}_{fuel}$ as:

$$\dot{n}_{fuel} = \dot{n}_{air}\frac{n}{g} = (0.047)\left(\frac{4.119\times10^{-5}}{2.347}\right) \tag{50}$$

$$\dot{n}_{fuel} = 8.249 \times 10^{-7} \tag{51}$$

Multiplying the molar fuel combustion rate by the estimated fuel molar mass yields:

$$\dot{m}_{fuel} = \dot{n}_{fuel}M_{fuel} = (8.249 \times 10^{-7})(0.0415) \tag{52}$$

$$\dot{m}_{fuel} = 3.423 \times 10^{-8} \tag{53}$$

At the first data point in the FTIR emissions file, the glow plug would have just been activated, and only small particles of biomass may be sufficiently heated to ignition. Thus, the relatively small result of Eq. (53) is expected. The same process described for Eq. (26) through (53) should now be applied for all time steps of the emissions results files to find the fuel mass flow rates at these time points. To find the total mass burned (m_{burned}), the integral of this fuel mass flow rate curve is estimated via the trapezoid rule:

$$m_{burned} = \int_0^t \dot{m}_{fuel}(t)dt = \sum_0^{t-\Delta t}\frac{1}{2}\left(\dot{m}_{fuel,k} + \dot{m}_{fuel,k+1}\right)\Delta t \tag{54}$$

where t is the time in seconds of the final data point, Δt is the time step between data points (which is 1 sec for all FTIR emissions files), k is the current data point, and $k + 1$ is the next data point. Since there are hundreds of data points per emissions file, a sample calculation for Eq. (54) will not be provided, but the results of Eq. (54) for the 70 sLpm and normalized tests of 100% pine, 90%/10% pine/algae, and 75%/25% pine/algae are provided in Table D.

The total burned mass of fuel calculated from Eq. (54) can now be used to estimate the total energy release ($Q_{release}$) during a test:

$$Q_{release} = m_{burned}Q_{LHV,fuel} \tag{55}$$

where $Q_{LHV,fuel}$ is the lower heating value (LHV) of the fuel. As stated above, only the higher heating value (HHV) of the fuel mixtures has been directly determined through experimentation. However, the LHV can be estimated from the HHV by removing the energy gained through the condensation of water vapor:

$$Q_{LHV,fuel} = Q_{HHV,fuel} - H_v\left(\frac{m_{H2O,out}}{m_{burned}}\right) \tag{56}$$

In Eq. (56), H_v is the heat of vaporization of water, which is the energy addition required for water to change state from liquid to vapor or the energy removal required for water to change state from vapor to liquid. The total mass of water produced by combustion is represented by $m_{H2O,out}$ and is found by applying the trapezoid rule in Eq. (53) to the molar water emissions data and then multiplying the result by water's molar mass (twice hydrogen's molar mass plus oxygen's molar mass). For the 90%/10% mixture, Eq. (56) is calculated as:

$$Q_{LHV,fuel} = 17796.48 - (451.9)\left(\frac{127.7679}{25.7603}\right) \tag{57}$$

$$Q_{LHV,fuel} = 15555.112 \tag{58}$$

Thus, Eq. (55) can be calculated:

$$Q_{release} = (25.7603)(15555.112)\left(\frac{1}{1000}\right) \tag{59}$$

$$Q_{release} = 400.704 \tag{60}$$

The $Q_{release}$ results from Eq. (60) are provided in Chapters 3 and 4 for the fuel blends, but the results for the primary test blends of Chapter 3 are additionally provided alongside the results of Eq. (54) in Table D.

Without experimental data that can confirm these results, the $Q_{release}$ calculations for all tested fuels cannot be taken as absolutely accurate to real life and have a relative uncertainty. However, the described model in this Appendix is consistent between all tests, and can be used to find trends between different fuel mixtures and air flow rates. Thus, this heat release model is a relative analysis tool for the work contained in the Chapters of this report.

Appendix D – Data Tables for Appendix C
Table R Molar masses of C, H, O, and N and their mole fractions in different fuel mixtures.

	Carbon	Hydrogen	Oxygen	Nitrogen
Molar Mass [gm mol^{-1}]	12	1	16	14
Mole Fraction (100% pine mixture)	0.3199	0.4854	0.1942	0.0005334
Mole Fraction (90%/10% pine/algae mixture)	0.3229	0.4736	0.2024	0.0011
Mole Fraction (75%/25% pine/algae mixture)	0.3161	0.4731	0.2080	0.0029

Table S Calculated fuel molar mass and molar higher heating values from the process in Appendix C.

	Calculated Molar Mass of Fuel [gm mol^{-1}]	Molar Higher Heating Value [kJ mol^{-1}]
100% pine	38.1359	703.3354
90%/10% pine/algae	41.4946	725.9497
75%/25% pine/algae	39.6118	636.8841

Table T Calculated fuel heat of formation values for several fuel mixtures corresponding to Eq. (25) in Appendix C.

Estimated heat of formation of fuel mixtures [kJ mol^{-1}]		
100% pine	90%/10% pine/algae	75%/25% pine/algae
-297.71	-406.22	-359.30

Table U MATLAB calculated total mass burned and total heat release figures.

	100% Pine @ 70 sLpm	90%/10% @ 67 sLpm	75%/25% @ 82 sLpm	90%/10% @ 70 sLpm	75%/25% @ 70 sLpm
Total Mass Burned [gm]	23.57	25.76	28.34	26.76	19.64
Total Energy Release [kJ]	398.70	392.99	391.49	413.39	250.22

Appendix E – Example MATLAB code developed from Appendix B

```matlab
%Brian Gessler
%Energy Release And Fuel Estimate
%5/24/17

clear
clc

%Define known values
filename = '9010_Norm.xlsx'; %file name of test data
raw_data = xlsread(filename); %emissions in ppm (O2 in Vol %)
[len,wid] = size(raw_data);
raw_data(:,(wid+1)) = zeros(len,1);
raw_data(:,1:(wid-1)) = raw_data(:,1:(wid-1))*(10^(-4)); %all emissions in
Vol%
raw_data = raw_data*(10^(-2)); %all emissions in Volume fraction/mole
fraction
[len1, wid1] = size(raw_data);
t_step = 1; %time step in sec of data

%mpellets = 20; %mass of pellets placed in basket for 100%
mpellets = 23.5; %mass of pellets placed in basket for 90-10
%mpellets = 27.5; %mass of pellets placed in basket for 75-25
%Comp = [0.514 0.065 0.001 0.416]; %fractional CHNO composition of 100% Pine
Comp = [0.499 0.061 0.002 0.417]; %fractional CHNO composition of 90-10 Pine
%Comp = [0.465 0.058 0.005 0.408]; %fractional CHNO composition of 75-25 Pine
M_CHON = [12 1 16 14]; %Molar masses of C, H, O, & N [g/mol]

X_CHON = zeros(1,4); %preallocate matrix for mole fractions of C, H, O, & N
in fuel
denom =
(Comp(1)/M_CHON(1))+(Comp(2)/M_CHON(2))+(Comp(4)/M_CHON(3))+(Comp(3)/M_CHON(4
));
X_CHON(1) = (Comp(1)/M_CHON(1))/denom;
X_CHON(2) = (Comp(2)/M_CHON(2))/denom;
X_CHON(3) = (Comp(4)/M_CHON(3))/denom;
X_CHON(4) = (Comp(3)/M_CHON(4))/denom;

%For CxHyOzNa, find y, z, and a in terms of x
%Assume a number of moles for C
x = 1.64; %Assumed number of moles of C
y = x*(X_CHON(2)/X_CHON(1));
z = x*(X_CHON(3)/X_CHON(1));
a = x*(X_CHON(4)/X_CHON(1));

%QHHV_fuel = 18442.87; %HHV [kJ/kg] energy content of 100% Pine fuel from
calorimetry tests and/or estimates
QHHV_fuel = 17496.98; %HHV energy content of 90-10
%QHHV_fuel = 16078.14; %HHV energy content of 75-25

sLpm_air = 67; %sLpm flow rate of air for test
%convert from sLpm to Vdot
T_amb = 297.039; %ambient temperature in Rankine
p_amb = 14.696; %atmospheric pressure in psia
```

```matlab
Vdot_air = sLpm_air*(T_amb/294.26)*(14.696/p_amb); %volume flow rate of air
in Lpm
Vdot_air = Vdot_air*1.66667*(10^(-5)); %Vdot of air [(m^3)/sec]
%convert from Vdot to mdot for air
rho_air = 1.2041; %density of air @ STP [kg/(m^3)]
mdot_air = Vdot_air*rho_air*1000; %mdot of air [g/sec]

hfo_CO2 = -393.522; %heat of formation of CO2 [kJ/kmol]
hfo_H2O = -285.840; %heat of formation of H2O (gaseous) [kJ/kmol]
hfo_O2 = 0; %heat of formation of O2 [kJ/kmol]
hfo_N2 = 0; %heat of formation of N2 [kJ/kmol]

ash_content = 0.30; %estimated fractional ash content of fuel
mburned = (1-ash_content)*mpellets;

%Determine molar mass of fuel
M_fuel = (x*M_CHON(1)+y*M_CHON(2)+z*M_CHON(3)+a*M_CHON(4))/1000;

%Determine Qbar_HHV of fuel
QbarHHV_fuel = QHHV_fuel*M_fuel;

%Use soichiometric combustion reaction
b = x; %Carbon balance
c = y/2; %Hydrogen balance
f = b+(c/2)-(z/2); %Oxygen balance
d = (a/2)+3.76*f; %Nitrogen balance

%Use Qbar_HV Equation from ME 636 notes to calculate hfo_fuel
hfo_fuel = QbarHHV_fuel+b*hfo_CO2+c*hfo_H2O+d*hfo_N2-3.76*f*hfo_N2-f*hfo_O2;

%Use full lean combustion Equation to convert from ppm to energy released
%Nitrogen balance
raw_data(:,wid1) = 1-raw_data(:,2)-raw_data(:,1)-raw_data(:,3)-raw_data(:,4)-
raw_data(:,(wid1-1));

%Calculate n and g using the calculated fuel molar composition
n = (raw_data(:,2)+raw_data(:,3)+3*raw_data(:,(wid1-2)))/x;
g = raw_data(:,(wid1-
1))+(raw_data(:,3)/2)+(raw_data(:,4)/2)+raw_data(:,2)+(raw_data(:,1)/2);

%Use mdotair to find ndotair
XairO2 = 1/(1+3.76);
XairN2 = 3.76/(1+3.76);

Mair = M_CHON(3)*2*XairO2+M_CHON(4)*2*XairN2;
ndot_air = mdot_air/Mair;

ndot_fuel = ndot_air*n./g;

%Determine mass of fuel burnt
mdot_fuel = ndot_fuel*(M_fuel*1000); %[gm/s]
traps = zeros((len1-1),1);
traps_H2O = zeros((len1-1),1);
for j = 1:(len1-1)
```

```matlab
    traps(j) = (0.5)*(mdot_fuel(j)+mdot_fuel(j+1))*t_step;
    traps_H2O(j) = (0.5)*(raw_data(j,1)+raw_data((j+1),1))*t_step;
end
mfuel_burnt = sum(traps); %[gm]
%mfuel_burnt = median(mdot_fuel)*len1;
n_H2O = sum(traps_H2O); %[mol]
m_H2O = n_H2O*(2*1+16); %[gm]

disp('Mass of fuel burned [gm]: ')
disp(mfuel_burnt)

Hv = 0.4519; %latent heat of vaporization of water [kJ/gm]
Q_LHV = (QHHV_fuel/1000)-Hv*(m_H2O/mfuel_burnt); %estimated lower heating
value [kJ/gm]
Q_release = mfuel_burnt*Q_LHV; %[kJ]

disp(' ')
disp('Total estimated heat release [kJ]: ')
disp(Q_release)
```

Appendix F – Material Safety Data Sheet for Kingsford Lighter Fluid

THE CLOROX COMPANY

SAFETY DATA SHEET

1. IDENTIFICATION OF THE SUBSTANCE/PREPARATION AND OF THE COMPANY/UNDERTAKING

Product identifier

Product Name   Kingsford® Odorless Charcoal Lighter

Other means of identification

Synonyms   None

Recommended use of the chemical and restrictions on use

Recommended use   Fuel for lighting charcoal

Uses advised against   No information available

Details of the supplier of the safety data sheet

Supplier Address
The Clorox Company
1221 Broadway
Oakland, CA 94612

Phone: 1-510-271-7000

Emergency telephone number

Emergency Phone Numbers   For Medical Emergencies, call: 1-800-446-1014
                                    For Transportation Emergencies, call Chemtrec: 1-800-424-9300

2. HAZARDS IDENTIFICATION

Classification

This chemical is considered hazardous by the 2012 OSHA Hazard Communication Standard (29 CFR 1910.1200).

Aspiration toxicity	Category 1
Flammable liquids	Category 3

GHS Label elements, including precautionary statements

Emergency Overview

Signal word	**Danger**	

Hazard Statements
May be fatal if swallowed and enters airways
Flammable liquid and vapor

Appearance Clear, colorless	**Physical State** Liquid	**Odor** Petroleum solvent

Precautionary Statements - Prevention
Keep away from heat/sparks/open flames/hot surfaces.   - No smoking
Keep container tightly closed
Ground/bond container and receiving equipment
Use explosion-proof electrical/ventilating/lighting equipment
Use only non-sparking tools
Take precautionary measures against static discharge
Wear eye protection such as safety glasses.

Precautionary Statements - Response
If swallowed: Immediately call a poison control center or doctor.
Do NOT induce vomiting.
If on skin (or hair):   Take off immediately all contaminated clothing.   Rinse skin with water.
In case of fire: Use dry chemical, carbon dioxide (CO_2), foam, or water fog to extinguish.

Precautionary Statements - Storage
Store locked up.
Store in a well-ventilated place.   Keep cool.

Precautionary Statements - Disposal
Dispose of contents in accordance with all applicable federal, state, and local regulations.

Hazards not otherwise classified (HNOC)
Vapors may cause irritation to the nose, throat, and respiratory tract.   Repeated or prolonged exposure to concentrations above the Worker Exposure Limit may cause central nervous system depression (e.g. dizziness, weakness, nausea, headaches and/or unconsciousness).

Solvents similar to those contained in this product have caused adverse kidney effects in male rats after prolonged and repeated inhalation exposure.   Reports have associated repeated and prolonged occupational exposure to solvents with permanent brain and nervous system damage.

__Unknown Toxicity__
None of the mixture consists of ingredients of unknown toxicity.

__Other information__
Preexisting eye, skin, and respiratory disorders may be aggravated by exposure to this product.

Intentional misuse by deliberately concentrating and inhaling contents may be harmful or fatal

__Interactions with Other Chemicals__
Reacts with strong oxidizers.

3. COMPOSITION/INFORMATION ON INGREDIENTS

Chemical Name	CAS-No	Weight %	Trade Secret
Petroleum distillates, hydrotreated light	64742-47-8	100	No

* The exact percentage (concentration) of composition has been withheld as a trade secret.

4. FIRST AID MEASURES

__First aid measures__

General Advice	Show this safety data sheet to the doctor in attendance.
Eye Contact	Hold eye open and rinse slowly and gently with water for 15 - 20 minutes. Remove contact lenses, if present, after the first 5 minutes, then continue rinsing eye. Call a poison control center or doctor for treatment advice.
Skin Contact	Wash skin with soap and water. If irritation persists, call a doctor.
Inhalation	Move to fresh air. If irritation or breathing problems develop, call a doctor.
Ingestion	DO NOT INDUCE VOMITING. Call a doctor or poison control center immediately. Aspiration hazard if swallowed - can enter lungs and cause chemical pneumonitis. If vomiting occurs, lean victim forward to reduce the risk of aspiration.
Protection of First-aiders	Avoid contact with skin, eyes, and clothing. Use personal protective equipment as required. Wear personal protective clothing (see section 8).

__Most important symptoms and effects, both acute and delayed__

Most Important Symptoms and Effects	Vapors may cause irritation to the nose, throat, and respiratory tract. Inhalation of high concentrations of vapors may cause central nervous system depression (e.g. dizziness, weakness, nausea, headaches, and/or unconsciousness).

__Indication of any immediate medical attention and special treatment needed__

Notes to Physician	Treat symptomatically.

148

5. FIRE-FIGHTING MEASURES

Suitable Extinguishing Media
Use dry chemical, carbon dioxide (CO_2), foam, or water fog to extinguish.   Do not use a direct stream of water.

Unsuitable Extinguishing Media
Use of water spray may be inefficient.

Specific Hazards Arising from the Chemical
Flammable.

Explosion Data

Sensitivity to Mechanical Impact   None.

Sensitivity to Static Discharge   Yes.

Protective equipment and precautions for firefighters
As in any fire, wear self-contained breathing apparatus pressure-demand, MSHA/NIOSH (approved or equivalent) and full protective gear.

6. ACCIDENTAL RELEASE MEASURES

Personal precautions, protective equipment and emergency procedures

Personal Precautions	Avoid contact with skin, eyes, and clothing. Ensure adequate ventilation. Use personal protective equipment as required. Eliminate all potential sources of ignition. Take precautionary measures against static discharges.
Other Information	Refer to protective measures listed in Sections 7 and 8.

Environmental precautions

Environmental Precautions	Prevent entry into waterways, sewers, basements, and confined areas.

Methods and material for containment and cleaning up

Methods for Containment	Prevent further spillage if safe to do so. Absorb with non-combustible absorbent material. Keep out of drains, sewers, ditches, and waterways.
Methods for Cleaning Up	Remove heat and ignition sources. Absorb and containerize. Do not wash down to sanitary sewer.

7. HANDLING AND STORAGE

Precautions for safe handling

Handling	Handle in accordance with good industrial hygiene and safety practice. Avoid contact with eyes, skin, and clothing. Avoid breathing vapors. Keep away from heat, sparks, open flames, and hot surfaces. Do not eat, drink, or smoke when using this product. To avoid vapor ignition by static electricity discharge, all metal parts of equipment must be grounded.

Conditions for safe storage, including any incompatibilities

Storage	Store in accordance with NFPA 30B for Class II combustible liquids. Store locked up in a well-ventilated and dry area away from open flames, heat sources, and other ignition sources.
Incompatible Products	Strong oxidizers.

149

8. EXPOSURE CONTROLS/PERSONAL PROTECTION

Control parameters

Exposure Guidelines

Chemical Name	ACGIH TLV	OSHA PEL	NIOSH IDLH
Petroleum distillates, hydrotreated light 64742-47-8	TWA - 100 ppm[b] [b]Based on TWA for Stoddard solvent	TWA - 500 ppm[d] [d]Based on TWA for Stoddard solvent	IDLH* - 20000 mg/m³ Ceiling* - 1800 mg/m³ (15 min) TWA* - 350 mg/m³ *Based on limits for Stoddard solvent

ACGIH TLV: American Conference of Governmental Industrial Hygienists - Threshold Limit Value.   OSHA PEL: Occupational Safety and Health Administration - Permissible Exposure Limits.   NIOSH IDLH: Immediately Dangerous to Life or Health.

Appropriate engineering controls

Engineering Measures	Showers Eyewash stations Ventilation systems

Individual protection measures, such as personal protective equipment

Eye/Face Protection   Wear safety glasses.   None required for consumer use.

Skin and Body Protection   Wear rubber or neoprene gloves if there is the potential for repeated or prolonged skin contact.

Respiratory Protection   No protective equipment is needed under normal use conditions.   If exposure limits are exceeded or irritation is experienced, NIOSH/MSHA approved respiratory protection should be worn.   Respiratory protection must be provided in accordance with current local regulations.

Hygiene Measures   Handle in accordance with good industrial hygiene and safety practice.   Do not eat, drink, or smoke when using this product.   Do not wear product-contaminated clothing for prolonged periods.   Wash hands after handling product.

150

9. PHYSICAL AND CHEMICAL PROPERTIES

Physical and Chemical Properties

Physical State	Liquid		
Appearance	Clear	**Odor**	Petroleum solvent
Color	Colorless	**Odor Threshold**	No information available

Property	**Values**	**Remarks/ Method**
pH	Not applicable	None known
Melting/freezing point	No data available	None known
Boiling point / boiling range	No data available	None known
Flash Point	~40°C	None known
Evaporation rate	No data available	None known
Flammability (solid, gas)	No data available	None known
Flammability Limits in Air		
Upper flammability limit	~5.6%	None known
Lower flammability limit	~0.8%	None known
Vapor pressure	~2 mm Hg) at 20°C	None known
Vapor density	~4.9 at 101 kPa (Air = 1)	None known
Specific Gravity	~0.78 @ 15°C	None known
Water Solubility	Insoluble in water	None known
Solubility in other solvents	No data available	None known
Partition coefficient: n-octanol/water	No data available	None known
Autoignition temperature	No data available	None known
Decomposition temperature	No data available	None known
Kinematic viscosity	No data available	None known
Dynamic viscosity	No data available	None known
Explosive Properties	Not explosive	
Oxidizing Properties	No data available	

Other Information

Softening Point	No data available
VOC Content (%)	No data available
Particle Size	No data available
Particle Size Distribution	No data available

10. STABILITY AND REACTIVITY

Reactivity
Reacts with strong oxidizers.

Chemical stability
Stable under recommended storage conditions.

Possibility of Hazardous Reactions
None under normal processing.

Conditions to avoid
Flames, heat sources, and ignition sources.

Incompatible materials
Strong oxidizers.

Hazardous Decomposition Products
Oxides of carbon.

11. TOXICOLOGICAL INFORMATION

Information on likely routes of exposure

Product Information   .

| Inhalation | Inhalation may irritate nose, throat, and respiratory tract.   Inhalation of high concentrations of vapors may cause central nervous system depression (e.g. dizziness, weakness, nausea, headaches, and/or unconsciousness). |

Eye Contact   May cause temporary eye irritation.

Skin Contact   Repeated exposure may cause skin dryness or cracking.

Ingestion   Small amounts of liquid aspirated into lungs can cause chemical pneumonitis, which can be fatal.

Component Information

Chemical Name	LD50 Oral	LD50 Dermal	LC50 Inhalation
Petroleum distillates, hydrotreated light 64742-47-8	>5 g/kg (Rat)	>2 g/kg (Rabbit)	>5.2 mg/L (Rat, 4 h)

Information on toxicological effects

Symptoms   Vapors may cause irritation to the nose, throat, and respiratory tract.   Liquid may irritate eyes and skin.   Inhalation of high concentrations of vapors may cause central nervous system depression (e.g. dizziness, weakness, nausea, headaches and/or unconsciousness).

Delayed and immediate effects as well as chronic effects from short and long-term exposure

Sensitization   No information available.

Mutagenic Effects   No information available.

Carcinogenicity   Contains no ingredient listed as a carcinogen.

Reproductive Toxicity   No information available.

STOT - single exposure   No information available.

STOT - repeated exposure   No information available.
Chronic Toxicity   No information available.
Target Organ Effects   Respiratory system, central nervous system, eyes.

Aspiration Hazard   Risk of serious damage to the lungs by aspiration.   May be harmful or fatal if swallowed.

Numerical measures of toxicity - Product Information

The following values are calculated based on chapter 3.1 of the GHS document
No information available.

152

12. ECOLOGICAL INFORMATION

Ecotoxicity
The environmental impact of this product has not been fully investigated.

Persistence and Degradability
No information available.

Bioaccumulation
No information available.

Other adverse effects
No information available.

13. DISPOSAL CONSIDERATIONS

Disposal methods
Dispose of in accordance with all applicable federal, state, and local regulations.

Contaminated Packaging
Dispose of in accordance with all applicable federal, state, and local regulations.

14. TRANSPORT INFORMATION

DOT   Not restricted in non-bulk containers less than 119 gallons.

TDG   Exempt from TDG regulations in containers less than 454 liters per TDG regulations, Part 1, Section 1.33.

ICAO
  UN-No   UN1268
  Proper Shipping Name   PETROLEUM DISTILLATES, N.O.S.
  Hazard Class   3
  Packing Group   III
  Description   UN1268,PETROLEUM DISTILLATES, N.O.S., 3, PG III

IATA
  UN-No   UN1268
  Proper Shipping Name   PETROLEUM DISTILLATES, N.O.S.
  Hazard Class   3
  Packing Group   III
  Description   UN1268,PETROLEUM DISTILLATES, N.O.S., 3, PG III

IMDG/IMO
  UN-No   UN1268
  Proper Shipping Name   PETROLEUM DISTILLATES, N.O.S.
  Hazard Class   3
  EMs No.   F-E, S-E
  Packing Group   III
  Description   UN1268,PETROLEUM DISTILLATES, N.O.S., 3,PG III

15. REGULATORY INFORMATION

Chemical Inventories

TSCA	All components of this product are either on the TSCA 8(b) Inventory or otherwise exempt from listing.
DSL/NDSL	All components are on the DSL or NDSL.

TSCA - United States Toxic Substances Control Act Section 8(b) Inventory
DSL/NDSL - Canadian Domestic Substances List/Non-Domestic Substances List

U.S. Federal Regulations

SARA 313
Section 313 of Title III of the Superfund Amendments and Reauthorization Act of 1986 (SARA).   This product does not contain any chemicals which are subject to the reporting requirements of the Act and Title 40 of the Code of Federal Regulations, Part 372

SARA 311/312 Hazard Categories
Acute Health Hazard	Yes
Chronic Health Hazard	Yes
Fire Hazard	Yes
Sudden Release of Pressure Hazard	No
Reactive Hazard	No

Clean Water Act
This product does not contain any substances that are regulated pollutants pursuant to the Clean Water Act (40 CFR 122.21 and 40 CFR 122.42).

CERCLA
This material, as supplied, does not contain any substances regulated as hazardous substances under the Comprehensive Environmental Response Compensation and Liability Act (CERCLA) (40 CFR 302) or the Superfund Amendments and Reauthorization Act (SARA) (40 CFR 355).   There may be specific reporting requirements at the local, regional, or state level pertaining to releases of this material.

US State Regulations

California Proposition 65
This product does not contain any Proposition 65 chemicals.

U.S. State Right-to-Know Regulations
This product does not contain any chemicals subject to state right-to-know regulations.

International Regulations

Canada
WHMIS Hazard Class
B3 - Combustible liquid
D2A - Very toxic material

154

16. OTHER INFORMATION			
NFPA Health Hazard 1	Flammability 2	Instability 0	Physical and Chemical Hazards -
HMIS Health Hazard 1	Flammability 2	Physical Hazard 0	Personal Protection A

Prepared By　　　　　Product Stewardship
23 British American Blvd.
Latham, NY 12110
1-800-572-6501

Revision Date　　　　New

Revision Note　　　　New

Reference　　　　　1010304/020300.016

General Disclaimer
The information provided in this Safety Data Sheet is correct to the best of our knowledge, information and belief at the date of its publication.　The information given is designed only as a guidance for safe handling, use, processing, storage, transportation, disposal, and release and is not to be considered a warranty or quality specification.　The information relates only to the specific material designated and may not be valid for such material used in combination with any other materials or in any process, unless specified in the text.

End of Safety Data Sheet

155